Molecular Characterization of Trim E3 Ubiquitin Ligases in Early Neurogenesis of *Xenopus laevis*

Dissertation

zur Erlangung des
Doktorgrades der Naturwissenschaften (Dr. rer. nat.)
der Naturwissenschaftlichen Fakultät I – Biowissenschaften –
der Martin-Luther-Universität Halle-Wittenberg,

Vorgelegt von

Herrn MSc. Ashwin Lokapally

Halle/Saale, 2019

Reviewers

1. Prof. Dr. Thomas Hollemann, MLU Halle-Wittenberg
2. Prof. Dr. Gunter Reuter, MLU Halle-Wittenberg
3. Prof. Dr. Michael Kühl, Ulm Universität

Defense: 13th June 2019

Table of Contents

Table of Figures

Abbreviations

AD	Alzheimers Disease
APC	Anaphase-promoting complex
ATP	Adenosine triphosphate
BACE1	Beta-secretase 1
bHLH	basic helix loop helix
BMP	Bone morphogenic protein
CNS	Central nervous system
CRL	Cullin RING ligase
dkk	dickkopf
DNA	deoxyribonucleic acid
DUBs	Deubiquitinases
EGF	Epidermal growth factor
fgf	fibroblast growth factor
GLI3	GLI Family Zinc Finger 3
HECT	Homologous to the E6-AP carboxyl terminus
HES	Hairy and enhancer of split
ISG15	Interferon-stimulated gene 15
LAP	Leukaemia-associated protein
MAPK	Mitogen-activated protein kinase
Met1	N-terminal methionine
MID1	Midline1
mTOR	mechanistic Target of Rapamycin
NEDD8	Neural precursor cell expressed developmentally downregulated 8
NEFL	neurofilament light chain
OS	Opitz BBB/G syndrome
PHD	Plant homeodomain
PP2A	Protein phosphatase 2A
RING	Really interesting new gene
RNA	ribonucleic acid
SHH	Sonic hedgehog
Skp1	S-phase phase kinase-associated protein 1
SoxB	Sry-related HMG box B
SUMO	Small ubiquitin like modifier
SVZ	subventricular zone
TGFβ	Transforming growth factor-β
TORC1	Target of rapamycin complex 1
TRIM	Tripartite motif
TRK	Tyrosine receptor kinase
UPS	Ubiquitin proteasome system
Wnt	Wingless/Integrated

1 Introduction

1.1 The Ubiquitin Proteasome System

The ubiquitin proteasome system (UPS) - an enzymatic cascade that marks a protein and tags with ubiquitin for proteolytic degradation[1]. Proteolysis in eukaryotes is mainly mediated by the UPS and the autophagous endo-lysosomal system. Central to both the UPS and autophagy is ubiquitination i.e., the conjugation of ubiquitin to substrate proteins through the lysine residues[2]. Conjugation of ubiquitin to a target protein or to itself is regulated by a sequential activity in three main steps. These three steps are characterized by the action of three different types of enzymes, namely E1 - ubiquitin activating enzymes, E2 – ubiquitin conjugating enzymes, and E3 - ubiquitin-ligase enzymes (Fig.1-1). E3-ubiquitin-ligases are crucial components in the UPS because they provide the substrate specificity. The first step in ubiquitination, is a two-step reaction catalysed by E1 enzyme, wherein E1 binds to ATP and ubiquitin and catalyses ubiquitin C-terminal acyl-adenylation. Ubiquitin is then transferred to the catalytic cysteine of the E1 enzyme forming a thioester bond[3]. Only two human E1 genes that have been so far identified, namely Uba1 and Uba6[4]. E1s collaborate with multiple E2s, the ubiquitin-conjugating enzymes to catalyse the transfer of the activated ubiquitin from E1 to its own catalytic cysteine residue through a thioester bond. In humans, 35 E2 enzymes have been identified[5]. Each E2 can activate a palette of E3 ligases producing multiple different but specific E2–E3 combinations. The final step of ubiquitination is catalysed by E3 ligases forming an isopeptide bond between the C-terminal glycine of ubiquitin and primary ε-amino group of another ubiquitin/substrate lysine[6]. The number of ubiquitin moieties added on a protein and the lysine residues involved in the binding confer activity, localization, protein-protein interactions, participation in different signalling pathways, and degradation either by the 26S proteasome or by endo-lysosome system[7,8]. While any of the 7 ubiquitin lysine's (K6, K11, K27, K29, K33, K48, or K63) or alternatively, the N-terminal methionine (Met1) may involve to create a polyubiquitin chain. The K-48 and K-63 chains are the most characterized polyubiquitin chains involving at least four ubiquitin moieties that constitute the signal for 26S proteasome mediated recognition and degradation of protein substrates.

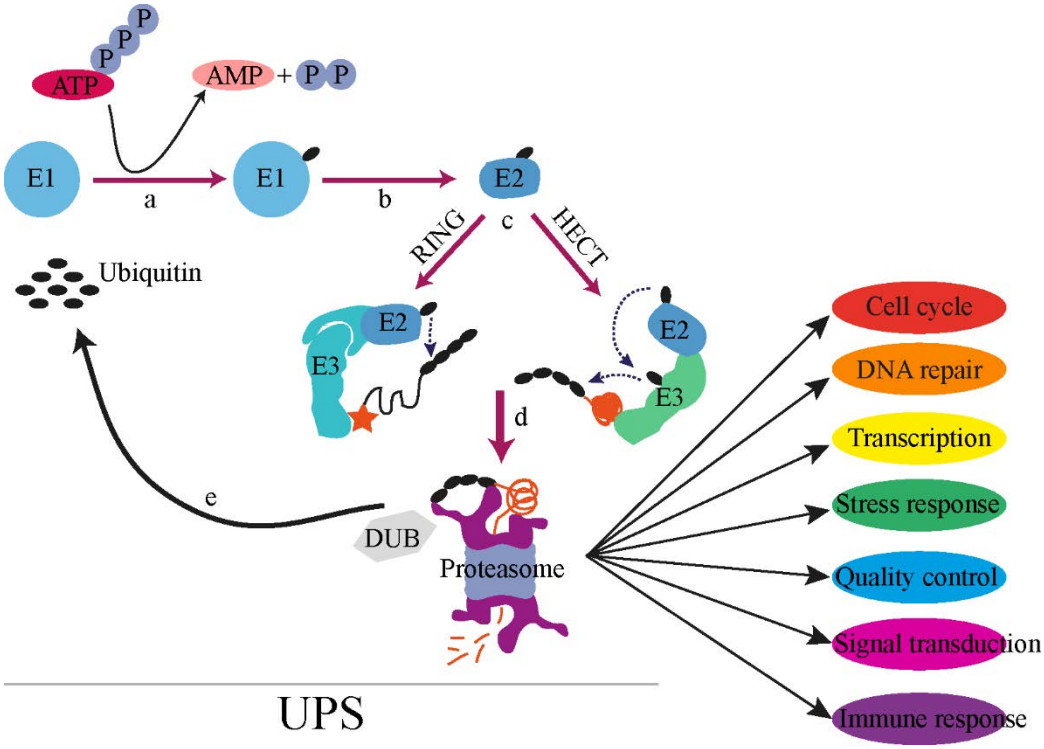

Figure 1-1. The ubiquitin-proteasome system (UPS). (a) Ubiquitin activation through ubiquitin-activating enzyme (E1). (b) Activated ubiquitin is transferred to ubiquitin-conjugating enzyme (E2). (c) RING domain ligase: the ubiquitin charged E2 binds to the E3 ligase that carries the substrate for degradation and ubiquitin is directly transferred to the substrate. HECT domain ligase: ubiquitin is first transferred from E2 to the E3 ligase that carries the substrate for degradation and then to the substrate. All three steps are repeated to result in substrate polyubiquitination. (d) Ubiquitinated protein is recognized by the proteasome, captured and processed for degradation. Short peptides (3–22 aa) are released at the end of the process. (e) Following substrate recognition, polyubiquitin chain is cleaved off through deubiquitinases (DUB) and free ubiquitin is released to be reused.

The most prominent polyubiquitination via proteasome is the K48-linked signal, while K-63 chains often directs the endo-lysosomal degradation of proteins[9]. Interestingly, although primarily modifying Lys residues, ubiquitin can also attach to the amino group at the N-terminus of the substrate[10], as well as to Cys, Ser, and Thr residues of target proteins[11,12]. Other forms of mono- or polyubiquitination have been shown to regulate protein processing, activity, or localization, rather than destruction. To prevent energy loss, once the tagged substrate is recognized by the proteasome for degradation, specific deubiquitinases (DUBs) remove the polyubiquitin chains for ubiquitin molecules to be reused[13]. In addition to ubiquitin, other ubiquitin-like modifiers with diverse functions have also been identified, eg. the small ubiquitin-like modifier (SUMO) that plays a role in nuclear transport. Similarly,

interferon-stimulated gene 15 (ISG15), which acts in immune responses and neural precursor cell expressed developmentally downregulated 8 (NEDD8) that activates specific E3 ligases[14]. All these different modifiers have different and distinct sets of E1, E2 and E3 enzymes.

1.1.1 The Ubiquitin E3 ligases

The ubiquitin E3 ligase proteins are responsible for target recognition in developing, maintaining, as well as degrading the cellular components. Developing roles include processes such as, cell division, stem cell differentiation and organogenesis, among others[15–17]. Maintenance responsibilities include, cell signalling, metabolism, transcriptional control, protein sorting, trafficking, cell to cell communication and modulation of inflammatory responses, etc[18–23]. However, E3 ubiquitin ligases are commonly associated with the establishment of cellular proteostasis by regulating the turnover of cellular proteins, using degradatory pathways of UPS and autophagy[24,25]. Since past few years, several E3 ubiquitin ligases have been reported to play critical roles in diverse aspects of neuronal development, including axon, dendrite, and synapse morphogenesis[26–28]. Neurogenesis requires the precise and sophisticated coordination of signaling events for the controlled progression of neuron formation[29].

The two main classes of E3 ligases, classified based on the domain structure are the homologous to the E6-AP carboxyl terminus (HECT) domain proteins and the really interesting new gene (RING) domain proteins[30]. The RING group of E3 ligases along with the RING-related E3s, such as the U-box family, the plant homeodomain (PHD), and the leukaemia-associated protein (LAP) form the largest group of E3 ligases[31]. HECT domain E3 ligases first accept the ubiquitin moiety through a thioester linkage and then they transfer it to the protein substrate, whereas RING domain E3 ligases bind to the cooperating E2 and they mediate the direct transfer of ubiquitin from E2 to the target protein[30] (Fig.1-1). More than 600 E3 ligases have been annotated in humans[32]from which approx. 30 are HECT domain E3 ligases. Most of the multi subunit RING E3 ligases belong to the cullin RING ligase (CRL) superfamily[33] with SCF complex consisting of S-phase phase kinase-associated protein 1/Skp1, cullin , F-box protein and anaphase-promoting complex (APC/C) being the most studied complexes that ensure the correct progression of cell cycle[34].

The discovery of the ubiquitin C-terminal hydrolase protein gene product 9.5 (PGP 9.5) in somata and dendrites of differentiating neurons, first indicated that ubiquitination and UPS may play a key part in brain development[35,36]. In developing central nervous system, the diverse neuronal processes subjected to regulation by the UPS range from the regulation of neural progenitor proliferation, cell specification, neuronal differentiation, maturation and migration, neuritogenesis and synapse formation[37,38]

1.2 Neurogenesis

The important aspects of the structure and function of the central nervous system (CNS), including the number and placement of neurons, as well as individual neuronal attributes are all controlled by processes during early development.

1.2.1 *Xenopus laevis* as a model organism to study neurogenesis

One of the widely used tractable model systems to answer the fundamental questions of biology and medicine and is the South African clawed frog, *Xenopus laevis*. It offers experimental advantage over other vertebrates in particular due to availability of large and robust eggs, its ease of handling and breeding. Likewise, its ease of manipulability and availability of large quantity of material makes it a choice model organism. For example, large size of the oocytes/embryos and their accessibility allows for manipulation of gene specific loss-of- or gain-of-function through RNA/DNA, morpholino oligonucleotide microinjection. This is easily performed by injecting one/two blastomeres of a two/four cell staged embryo with the un-injected side serving as inner control. Furthermore, microscopy and histology of *in vivo* expression and localization of RNA and proteins can be easily studied through whole mount *in situ* hybridization and immunofluorescence.

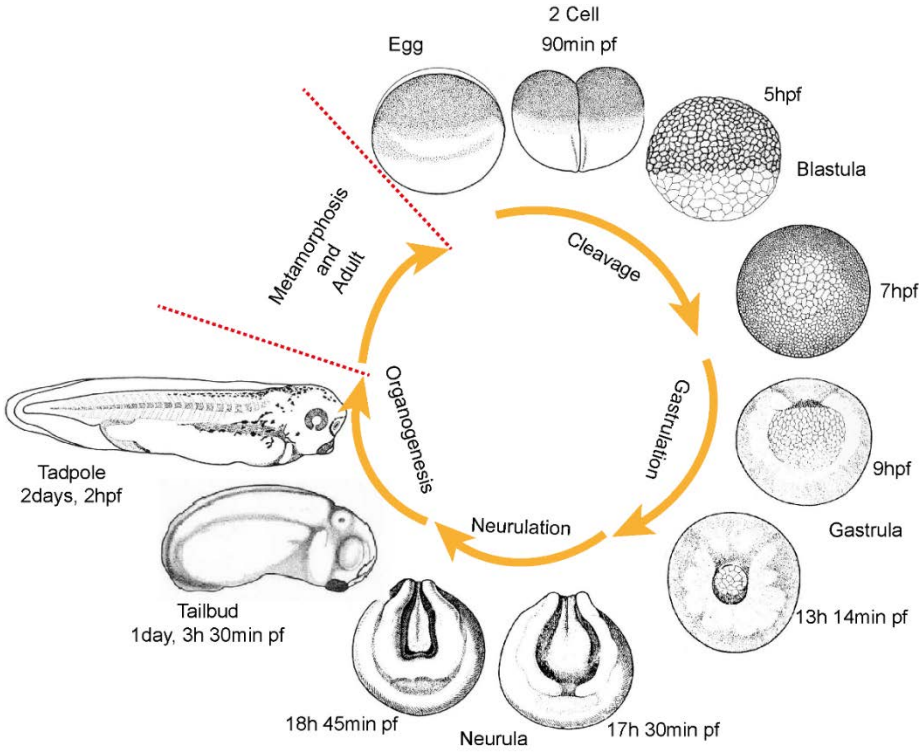

Figure 1-2. Xenopus laevis developmental cycle through different stages at room temperature (23°C). hpf – hours post fertilization.

Most importantly, the high degree of conservation of essential cellular and molecular mechanisms and genomic synteny with mammals provides significant link to understand human development and disease[39]. Other important applications include procedures such as transplantation of single cell to tissue cut-paste. The large size and robust nature of the embryos has specific advantages in studying early neurogenesis in *Xenopus laevis*. It is also worth noting that some of the earliest studies on molecular mechanisms underlying early vertebrate neurogenesis were first described in *Xenopus*[40–42]. But in addition, from an evolutionary point of view *Xenopus* provides key clues as amphibians represent the only anamniote tetrapod's that accomplish fast development through embryonic to larval and juvenile stages, along with a metamorphic process in which the neurogenic capabilities vary, thus allowing a very interesting scenario for such analysis (Fig.1-2).

1.2.2 Vertebrate Embryonic Neurogenesis

In vertebrates, the foundation for the nervous systems is laid during embryonic patterning, involving the generation and movement of neural progenitors and their progeny, which are

controlled by diverse conserved factors. The initial step during the foundation of the vertebrate nervous system is the decision of the ectodermal cells to adopt a neural fate at the expense of an epidermal. The first signals of neural induction are triggered by the organizing (Spemann Organizer) region of the early embryo during gastrulation. As dorsal mesoderm is formed at gastrulation, a series of molecular growth factor antagonists such as *noggin*, *chordin*, *follistatin*, *dkk*, *Cerberus* are secreted by the Spemann Organizer[43,44] (Fig.1-3). Here, these antagonist along with *fgf* share the ability to inhibit bmp signalling and thereby inducing the neural fate of the ectodermal tissue[45].This newly formed vertebrate neuro-ectoderm, which is restricted to the dorsal side, invaginates to form a hollow cylinder called the neural tube (Fig.1-4). Expression of neurogenic factors such as SoxB, BMP, Wnt and Fgf signalling are involved in setting up of the neuro-ectoderm[46–48].

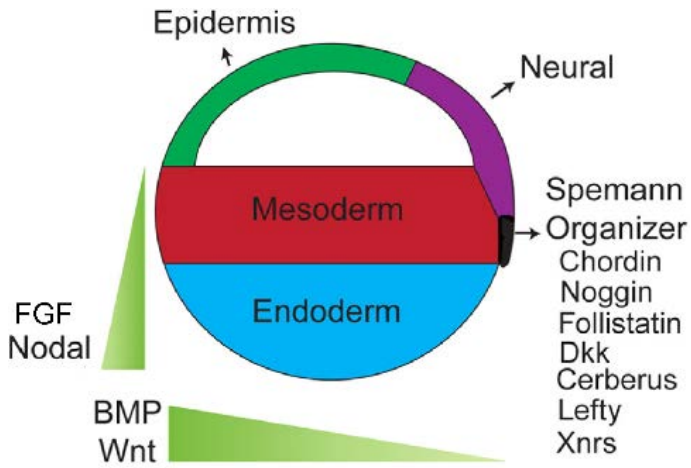

Figure 1-3. Neural induction in vertebrates. The dorsal organizer in Xenopus express factors that protect the ectodermal domain. It gives rise to neural fates from activators of the BMP, Nodal and Wnt pathways. The combined functions of secreted agonists of these pathways and the inhibitors produced by the dorsal organizer give rise to gradients that both pattern the embryo and specify the domain of neural induction. Adapted and modified from Gaulden J and Reiter JF 2008[45]

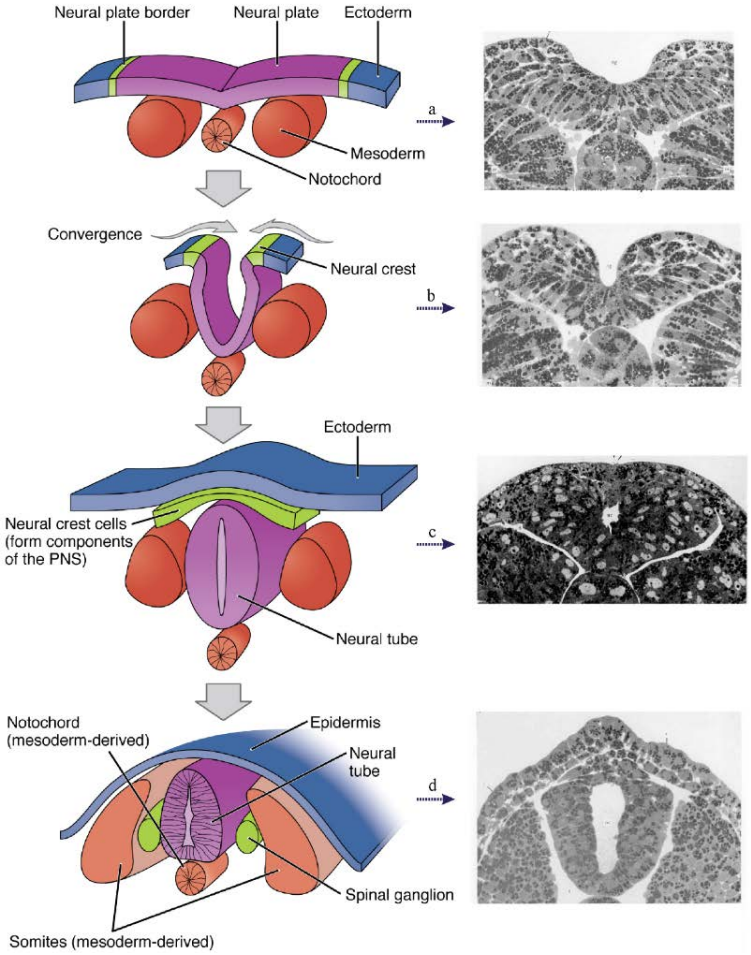

Figure 1-4. Neurulation in Xenopus laevis. Transverse sections that show the progression of neurulation form neural plate to neural tube. a) Neuroectoderm differentiates and thickens to form neural plate. b) Neural plate converges dorsally, eventually joining at the neural plate border. c) Neural tube closure disconnects neural crest from epidermis. d) Notochord degenerates while mesodermal cells differentiate into somites and the skeletal muscle. Adapted and modified from Wikipedia (Neurulation), and Shroeder 1970[49]

Cells of the neural tube possess neurogenic factors and undergo diverse patterns of proliferation to produce neurons and glia. These proliferating cells generally consists of apical and basal progenitors[29,50,51] (Fig.1-5). At early stage, apical progenitors undergo symmetric division, resulting in expansion of the neural tube. Whereas at later stages, apical progenitors increasingly switch towards an asymmetric, self-renewing mode of division, where one cell remains mitotically active, and the other one delaminates and differentiates as a neuron, oligodendrocyte, or basal progenitor. At this point, apical progenitors transition molecularly, expressing markers of radial glial cells[29]. These radial glials produce mostly neurons until late stage in embryogenesis, where most of these cells differentiate as astroglia;

a smaller fraction becomes the ependymal lining of the ventricle, while some radial glia remains undifferentiated, which give rise to adult neural stem cells[52] (Fig.1-5). Distinct to apical progenitors, basal progenitors do not self-renew, but undergo typically a single symmetrical division before differentiating[53,54]. Basal progenitors are found predominantly in the anterior part of the neural tube, in the telencephalon, where they form the massive subventricular zone (SVZ) from late embryonic stages onward. Self-renewal of progenitor cell populations and their transition into neurogenic and gliogenic stages are controlled by a set of extracellular cues and cell-intrinsic signalling pathways of five major types: WNT signalling, Notch signalling, Hedgehog signalling, receptor type serine/threonine kinase signalling — for example, through transforming growth factor-β (TGFβ) receptors — and signalling through receptor-type tyrosine kinases (for example, through high affinity nerve growth factor receptor (TRK), fibroblast growth factor (FGF) receptor family members or the epidermal growth factor (EGF) receptor[55].

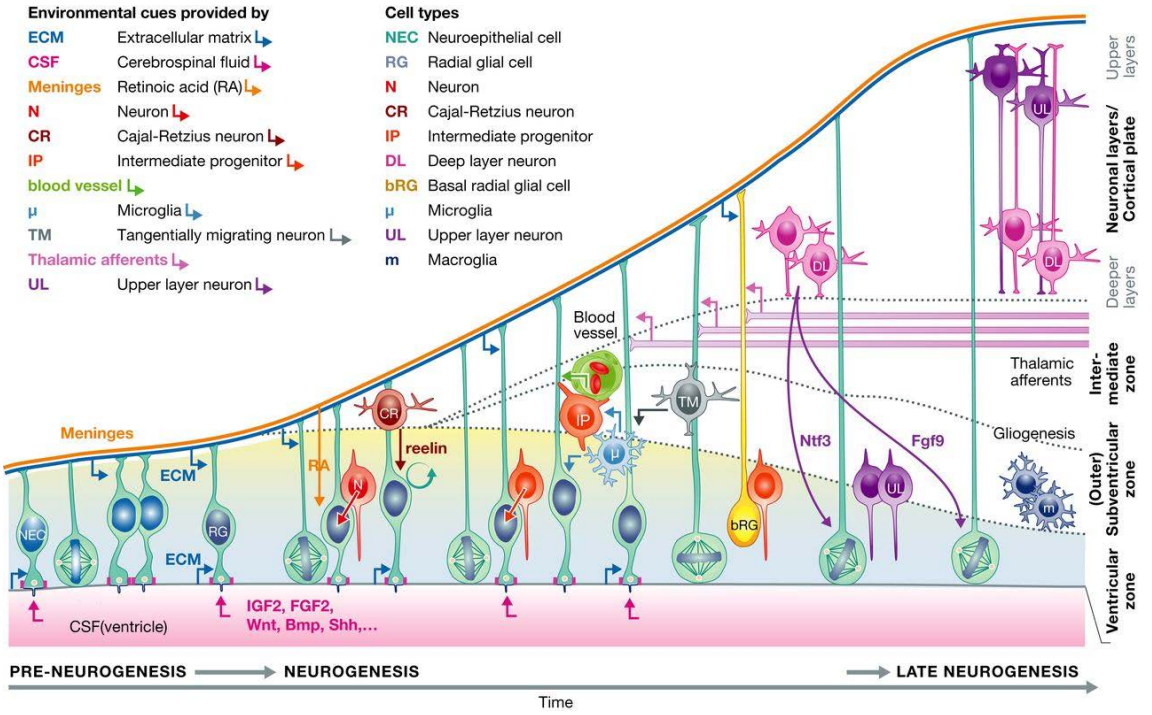

Figure 1-5. Regulation of neural progenitor cells proliferation and differentiation upon various cues from the environment. Adapted from Paridaen and Huttner 2014[56]

These successive steps of neurogenesis are characterized by dynamic changes in cellular protein profiles. Failure to properly regulate these changes in protein levels disrupts the

balance of proliferating progenitors and differentiated neurons and can be detrimental to the development of the central nervous system (CNS)[57–59]. Many conserved features such as SoxB transcription factors[60,61] and Snail zinc-finger proteins[62,63] play vital role in the neuroepithelium to promote neural progenitor delamination and proliferation and prevent cell death. The proneural bHLH genes define proneural domains from which precursors of primary neurons are selected. These domains are surrounded by territories where primary neurogenesis is inhibited by expression of the HES genes[48,64] and become active after hatching-, a source for secondary neurogenesis. Within the embryonic proneural domains, Notch signalling defines the differential fate of asymmetrically dividing apical progenitors; the daughter cell ending up with lower Notch activity loses its progenitor fate and differentiates as a neuron or becomes an intermediate progenitor. The ability of the Notch signaling pathway to exert these opposite functions is made possible by tight regulation of a variety of molecular mechanisms, including the UPS.

1.3 Trim Ubiquitin E3 ligases

Tripartite motif (TRIM) proteins also referred to as RBCC proteins, represent one of the largest family of highly conserved RING E3 ligases. TRIM proteins are characterized by an N-terminus tripartite or RBCC motif that consists of a RING-finger domain, one or two zinc finger domains, so-called B boxes, and a coiled-coil domain followed by a highly variable C-terminal domain[65,66]. To date, more than 70 TRIM family members have been identified in humans. Based on the type of C-terminal domains these proteins have been classified into 11 subgroups (CI-CXI)[67,68] (Fig. 6). Most TRIM family members have been proposed to function as E3 ubiquitin ligases due the presence of their RING-finger domain[69]. The RING-type E3 ligases operate as scaffolds to recruit both ubiquitin coupled E2 and substrate, thereby facilitating ubiquitination[70,71]. Despite their overall similar structural organization, TRIM proteins regulate a wide variety of cellular processes. Recent insights, demonstrated on the role of Trim E3 ligases in neurogenesis. Tuoc et al. showed Trim11 mediated proteasomal degradation of Pax6 protein levels in cortical progenitors[72]. Similarly, Schwamborn, et al., demonstrated that another member of the TRIM E3 ligase, Trim32 interacts with C-Myc and mediates C-Myc degradation, leading to suppression of progenitor proliferation and induction of premature neuronal differentiation[73].

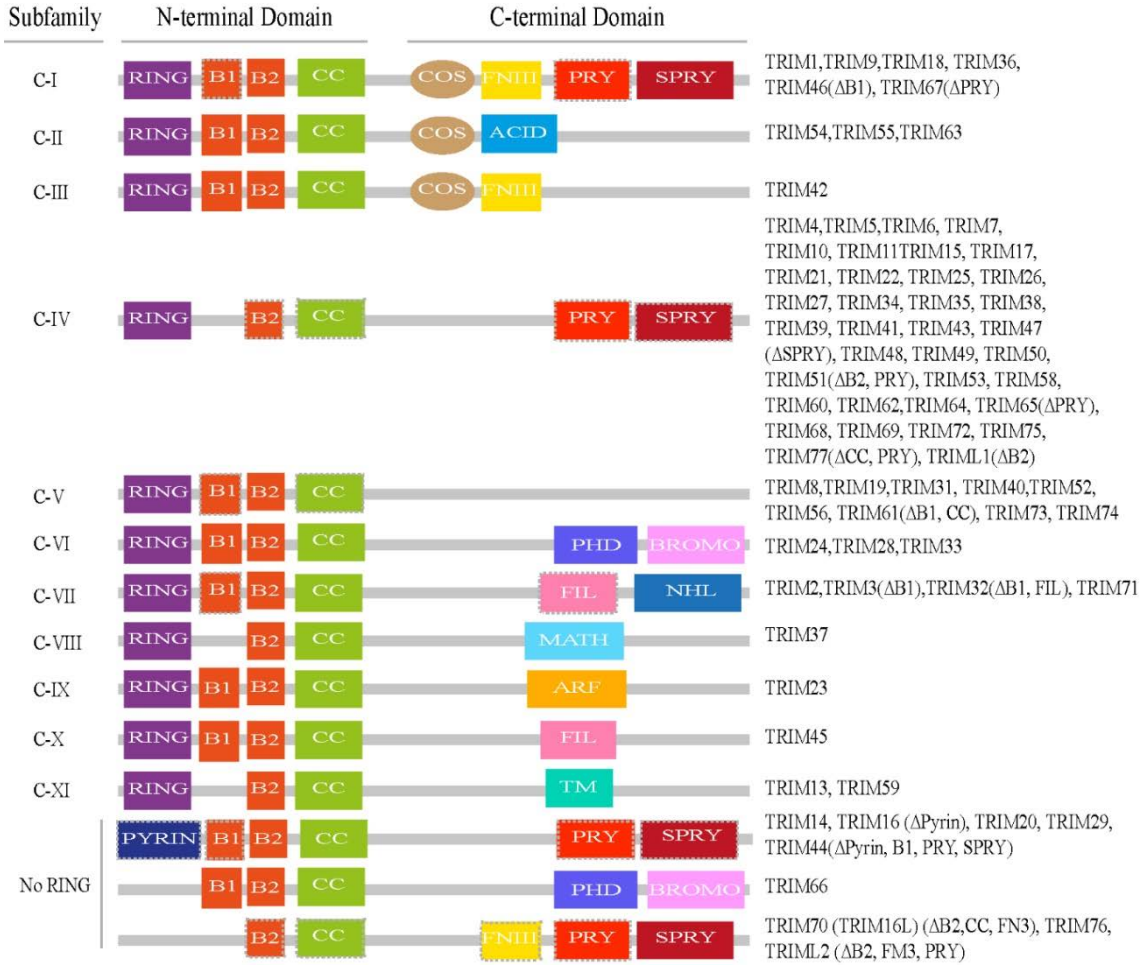

Figure 1-6. Structural classification of human TRIM proteins. The TRIM family members are classified into 11 subfamilies (C-I to C-XI) and 3 TRIM like subfamily. Majority of the TRIM proteins possess an N-terminal RING finger (R), one or two B-boxes (B1, B2), and a coiled coil (CC) domain. Abbreviations: ACID – acid-rich region, ARF – ADPribosylation factor family domain, BROMO – bromodomain, COS – cos-box, FIL – filamin-type I G domain, FN3 – fibronectin type III repeat, MATH – meprin and TRAF-homology domain, NHL – NCL1, HT2A and LIN41 domain, PHD - PHD domain, PRY – PRY domain, SPRY – SPRY domain, TM – transmembrane region.

1.3.1 Midline1/Trim18 Ubiquitin E3 ligase

MID1 (midline1/Trim18), a member of the TRIM E3 ligase family was first identified in 1997 to be perturbed in patients with Opitz BBB/G syndrome (OS)[74]. OS patients suffer from the malformations of the ventral midline including hypertelorism, hypospadias, structural abnormalities in the brain, heart defects and cleft lip and palate. *Xenopus* Mid1 is a 76 kDa protein, containing a RING domain, two B boxes, a coiled-coil domain, a fibronectin type III domain and a large C-terminal B30.2 domain (Figure 7a). The E3 ubiquitin ligase activity of MID1 was first described for its target protein PP2A. Here, MID1

binds to the alpha4 regulatory subunit of PP2A with its B-Box1 domain[75,76] and mediates the proteasomal degradation via polyubiquitination of the catalytic subunit of PP2A (PP2Ac)[76]. By inhibiting PP2A activity MID1 enhances the activity of another central enzyme: the mTOR/ TORC1 complex. Perturbations of the MID1-PP2A complex affect mTORC1 signalling at the level of mTOR-Raptor complex formation. Depletion of MID1 increases PP2A levels, which in turn leads to the disruption of the mTOR-Raptor complex, leading to down regulation of mTORC1 signalling[77]. Furthermore, MID1 mediates the ubiquitination of alpha4 in two distinct ways: either catalysing polyubiquitination, which targets alpha4 for degradation via the proteasome[78], or catalysing monoubiquitination, which promotes calpain cleavage[79]. Another substrate of the MID1 E3 ubiquitin ligase is the kinase Fused (Fu), which is involved in the Sonic hedgehog-signalling (SHH) pathway. Mid1 interacts with the GLI regulator Fu, leading to a cytoplasmic retention of GLI3 in cancer cells[80]. Additionally, MID1 has also been implicated in the pathogenesis of neurodegenerative Alzheimer's (AD) and Huntington's disease (HD). In AD, MID1 is shown to regulate the translation of BACE1 mRNA[81], causative in the generation of amyloid plaques through enhancement of Tau phosphorylation[82]. Similarly, in HD MID1 specifically binds to and enhances translation of the mutant Huntingtin mRNA carrying an expanded CAG repeat[83].

1.3.2 Trim2 Ubiquitin E3 ligase

TRIM2, a member of Trim ubiquitin E3 ligase family has been shown to exclusively express in the mouse brain[84,85]. *Xenopus* Trim2 has a molecular mass of 85 kDa and contains a RING domain, a B box, large coiled-coil and Filamin/ABP280 domain, and six C-terminal NHL repeats (Figure 7b). In mouse, TRIM2 expression is most predominant within the cytoplasm of hippocampal neurons, where it interacts with motor protein myosin V via its NHL domain[84]. Moreover, *Trim2*-deficient mice showed accumulation of neurofilament light chain (NEFL) in neuronal structures, which causes axonopathy, progressive neurodegeneration, and juvenile onset of tremor and ataxia. Re-expression of TRIM2 prevented neurodegeneration via UbcH5a-dependent degradation of NEFL[85]. Similarly, cultured hippocampal neurons from mice lacking *Trim2* showed loss of axons and neuronal polarity, whereas overexpression of TRIM2 induced specification of multiple axons[86]. In mouse embryonic fibroblasts, p42/p44 MAPK-dependent ubiquitination of cell death-

promoting factor Bim (Bcl-2-interacting mediator of cell death) by TRIM2 conferred neuroprotection during rapid ischemia[87]. Consistent with its neuroprotective functions in mice, alterations of TRIM2 function have been linked to neural diseases in humans. Here, specific miRNAs (miR-9 and miR-181c) are involved in deregulation of *Trim2* expression which are in turn down-regulated by amyloid-β and has been linked to the onset of neurodegenerative Alzheimer's disease[88]. Furthermore, mutations in the *TRIM2* gene have been associated with childhood onset of axonal neuropathy[89]. Together, these findings implicate TRIM2 as a key regulator in differentiated neurons, while its function during neurogenesis and neurodevelopment remains enigmatic.

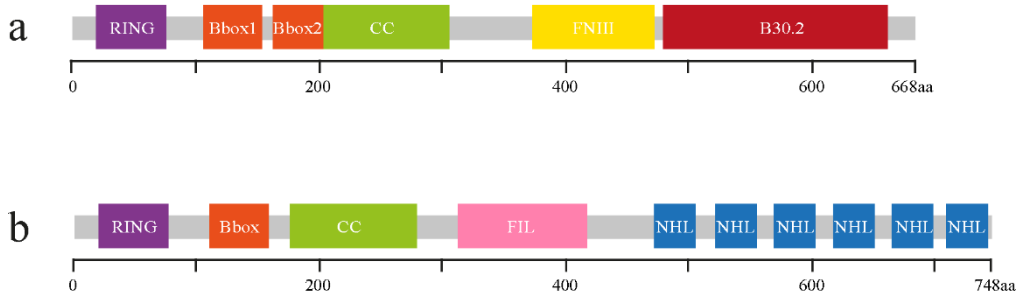

Figure 1-7. Mid1 and Trim2 protein domain structures. (a) Xenopus Mid1 protein consists of 668 amino acids and is organized in domains containing a single RING zinc finger, two B-box zinc finger, a single coiled-coiled, FNII and a B30.2 domain. (b) Xenopus Trim2 protein consists of 748 amino acids and is organized in domains containing a single RING zinc finger, a B-box zinc finger, a single coiled-coiled, Filamin/ABP 280 and six NHL repeats

2 Aim of the Work

To date, there have been over 70 TRIM E3 ligases identified in humans and extensive work both in humans and mouse has given answers to various fundamental mechanisms. Most of these studies addressed physiological functions but were rarely characterized during early development. As demonstrated in the previous sections, Trim E3 ligases Mid1 and Trim2 are essential for early neurogenesis during CNS development. Although, there have been studies showing physiological and clinical pathological effects due to mutations in these genes during development, but still there is lack of data on the functional and mechanistic aspects of these proteins during early development. Therefore, the major aim of the thesis was to characterize novel functions of these proteins during vertebrate embryonic neurogenesis. Towards this, to further fundamental mechanistic clarification, the following questions were addressed.

1. Whether there are other Trim E3 ligases present in the Xenopus genome, their expression during early development compared to other species and their homology towards human orthologues?
2. Whether *mid1*, which is associated with OS is involved in the functional and mechanistic regulation of the proteins expressed during early neurogenesis?
3. The molecular characterization of *trim2* during early development of CNS in *Xenopus laevis*.

3 Short Summary of Published Manuscripts

3.1 Manuscript 1: Interplay of Trim2 E3 ubiquitin ligase and Alix/ESCRT complex: Control of developmental plasticity during early neurogenesis

Ashwin Lokapally, Herbert Neuhaus, Juliane Herfurth and Thomas Hollemann

Manuscript under 2nd review process!

TRIM2 drives neurite outgrowth and polarization, is involved in axon specification, and confers neuro-protective functions during rapid ischemia. Here we show that in *Xenopus, trim2* knock down affects primary neurogenesis and neural progenitor cell survival. Embryos also suffer from severe craniofacial malformation, reduction in brain volume, and loss of gross motor sensory function. Using a high throughput LC-MS/MS approach with GST-Trim2 as bait, we identified the ALG-2 interacting protein X (Alix) from *Xenopus* embryonic lysates as a novel interacting partner of Trim2. We demonstrate at that expression of *trim2* and *alix* overlap during embryogenesis as well as at cellular level in the cellular cytoplasm. Alix is involved in bending and fission of endosomal and cell surface membranes. Interestingly, *trim2*-morphants showed loss of cellular polarity and clustering and apoptosis of neural progenitors, phenotypic hallmarks also observed in *Alix* KO mice. Therefore, we propose that interaction of Alix and Trim2 plays a key role in the determination and differentiation of neural progenitors via modulation of cell proliferation/apoptosis during neurogenesis

3.2 Manuscript 2: Hedgehog-dependent E3-ligase Midline1 regulates ubiquitin-mediated proteasomal degradation of Pax6 during visual system development

Thorsten Pfirrmann, Enrico Jandt, Swantje Ranft, ***Ashwin Lokapally***, Herbert Neuhaus, Muriel Perron and Thomas Hollemann

PNAS (2016), 113 (36) 10103-10108. https://doi.org/10.1073/pnas.1600770113

The manuscript describes Mid1 regulated ubiquitination and proteasomal degradation of Pax6 protein in the forming optic stalk. Pax6 an evolutionarily conserved transcription factor, plays a key role in the cell fate determination during development of eyes, brain and pancreas. In humans, heterozygous mutation in *PAX6* cause a wide variety of ocular defects, whereas the homozygous loss results in the anophthalmia. Moreover, spatio-temporal and quantitative expression levels of Pax6 is indispensable and is a key regulator for the normal development of eye. Mid1, a member of the TRIM/RBCC E3 ligase family, was first identified in patients with X-chromosome-linked Opitz BBB/G (OS) syndrome. Expression analysis of Mid1 in *Xenopus* showed early expression in the neural tube and optic vesicle a eye, especially in the forming eye stalk. Misexpression of the morphogen sonic hedgehog (*shh*) strongly induced *mid1* expression in the optic cup, whereas as *pax6* was repressed. Furthermore, suppression of *mid1* function resulted in large eyes with loss of sharp boundaries of retinal layers, but still expressed *pax6*. At cellular level, Mid1 interacts with Pax6 *in vivo* in the nucleus. Lysates from cells co-transfected with *pax6* and *mid1* showed a clear reduction in Pax6 protein levels in the presence of Mid1 and Pax6 served as a substrate for the E3 ligase mediated proteasomal degradation.

3.3 Manuscript 3: *Xenopus laevis* neuronal cell adhesion molecule (*nrcam*): plasticity of a CAM in the developing nervous system

Ashwin Lokapally, Sanjeeva Metikala, Thomas Hollemann

Development Genes and Evolution (2017), 227: 61-67. https://doi.org/10.1007/s00427-016-0569-9

The manuscript describes expressional characterization of neuronal cell adhesion molecule (*nrcam*) of the L1 immunoglobulin superfamily during *Xenopus* neural development and as a marker for differentiated neurons. NRCAM plays diverse roles during the formation of the nervous system including axon growth and guidance, synapse formation and formation of the myelinated sheath. Sequence analysis and evolutionary relationship among vertebrates showed a high conservation with >85% homology against human NRCAM. Similarly, the spatio-temporal expression using semiquantitative-RT-PCR and whole-mount *in situ* hybridization (WMISH) showed mRNA expression along the entire axis of the developing CNS from forebrain extending into the spinal cord. However, primary expression in the brain was mainly observed in regions where cells differentiate into various cell types such as motor neuron region, dorsal intermediate and longitudinal neuron, the trigeminus and the radial glial. Likewise, in the lens epithelium and retinal outer nuclear layer, where neural progenitors differentiate into various cell types based on the cues from the surrounding environment, *nrcam* transcripts were also highly enriched. These findings establish *Xenopus nrcam* as a marker for neuronal determination and differentiation.

3.4 Manuscript 4: Expressional characterization of mRNA (guanine-7) methyltransferase (*rnmt*) during early development of *Xenopus laevis*

Ashwin Lokapally, Sanjeeva Metikala, Thomas Hollemann

International Journal of Developmental Biology (2016), 60: 65-69. https://doi.org/10.1387/ijdb.150409th

The manuscript describes the expression of (guanine-7) methyltransferase (*rnmt*) during *Xenopus* neural development. Recent insights into the function of mammalian cap methyl transferase revealed that RNMT along with its activating subunit RAM is highly expressed in embryonic stem cells and is important for pluripotency associated genes. Thus, the repression of RAM during neural differentiation is essential for the expression of neural associated genes. Amino acid sequence comparison among vertebrates revealed 100% conservation within the methyltransferase activity region. Moreover, spatial expression using whole-mount *in situ* hybridization (WMISH) during early neurulation showed expression in the anterior neural plate, neural folds and in the eye anlage, regions where neural stem cells arise. Similarly, at later stages, mRNA transcripts were observed throughout the developing CNS i.e. the brain, eye, and the spinal cord as well as in the glial cells of the otic vesicle. These observations further strengthen the evidence for an involvement of *rnmt* in the regions of increased translation. Here, RNMT seems to play a role for the formation of theses neuronal structures and at the same time instructs changes in gene expression profile to allow differentiation and reprogramming in these cells.

3.5 Manuscript 5: SOMA: A Single Oligonucleotide Mutagenesis and Cloning Approach

Thorsten Pfirrmann, ***Ashwin Lokapally***, Claes Andréasson, Per Ljungdahl, Thomas Holleman

PLoS ONE (2013), 8(6): e64870. https://doi.org/10.1371/journal.pone.0064870

The manuscript describes a new mutagenesis and cloning approach: Single Oligonucleotide Mutagenesis and Cloning Approach (SOMA) that is independent of restriction sites and only requires a single mutagenic oligonucleotide to modify a plasmid. The broad application spectrum of SOMA is demonstrated with the help of three examples. First, a novel plasmid that in a standardized and rapid fashion can be used as a template for SOMA to generate GFP-reporters. We successfully use such a reporter to assess the *in vivo* knock-down quality of morpholinos in *Xenopus laevis* embryos. In a second example, we show how to use a SOMA-based protocol for restriction-site independent cloning to generate chimeric proteins by domain swapping between the two human hRMD5a and hRMD5b isoforms. Last, we show that SOMA simplifies the generation of randomized single-site mutagenized gene libraries. As an example we random-mutagenize a single codon affecting the catalytic activity of the yeast Ssy5 endoprotease and identify a spectrum of tolerated and non-tolerated substitutions. Thus, SOMA represents a highly efficient alternative to classical cloning and mutagenesis strategies.

4 Published Manuscripts

4.1 Manuscript 1: Interplay of Trim2 E3 ubiquitin ligase and Alix/ESCRT complex: Control of developmental plasticity during early neurogenesis

Ashwin Lokapally, Herbert Neuhaus, Juliane Herfurth and Thomas Hollemann*

Manuscript under 2nd review process

Abstract: TRIM2 drives neurite outgrowth and polarization, is involved in axon specification, and confers neuro-protective functions during rapid ischemia. The mechanisms controlling neuronal cell fate determination and differentiation are fundamental for neural development. Here we show that in *Xenopus*, *trim2* knock down affects primary neurogenesis and neural progenitor cell survival. Embryos also suffer from severe craniofacial malformation, reduction in brain volume, and loss of motor sensory function. Using a high throughput LC-MS/MS approach with GST-Trim2 as bait, we pulled down ALG-2 interacting protein X (Alix) from *Xenopus* embryonic lysates. We demonstrate that expression of *trim2*/TRIM2 and *alix*/ALIX overlap during larval development and on cellular level in cell culture. Interestingly, *trim2*-morphants showed loss of cellular polarity and clustering and apoptosis of neural progenitors, phenotypic hallmarks also observed in *Alix* KO mice. Therefore, we propose that interaction of Alix and Trim2 plays a key role in the determination and differentiation of neural progenitors via modulation of cell proliferation/apoptosis during neurogenesis.

Introduction

Tripartite motif (TRIM) proteins represent a large family of proteins, with more than 80 family members in humans. TRIM proteins are characterized by a similar domain structure at the N-terminus that consists of a RING-finger domain, one or two zinc finger domains, so-called B boxes, and a coiled-coil domain. Most TRIM family members have been proposed to function as E3 ubiquitin ligases due the presence of their RING-finger domain. The RING-type E3 ligases operate as scaffolds to recruit both ubiquitin coupled E2 and

substrate, thereby facilitating ubiquitination[1,2]. Despite their overall similar structural organization, TRIM proteins regulate a wide variety of cellular processes.

One such ubiquitin ligase, TRIM2, is expressed in the mouse brain, predominantly within the cytoplasm of hippocampal neurons, where it interacts with motor protein myosin V via its NHL domain[3]. Moreover, *Trim2*-deficient mice showed accumulation of neurofilament light chain (NEFL) in neuronal structures, which causes axonopathy, progressive neurodegeneration, and juvenile onset of tremor and ataxia. Re-expression of TRIM2 prevented neurodegeneration via UbcH5a-dependent degradation of NEFL[4]. Similarly, cultured hippocampal neurons from mice lacking *Trim2* showed loss of axons and neuronal polarity, whereas overexpression of TRIM2 induced specification of multiple axons[5]. In mouse embryonic fibroblasts, p42/p44 MAPK-dependent ubiquitination of cell death-promoting factor Bim (Bcl-2-interacting mediator of cell death) by TRIM2 conferred neuroprotection during rapid ischemia[6]. Consistent with its neuroprotective functions in mice, alterations of TRIM2 function have been linked to neural diseases in humans. In this respect miRNAs (miR-9 and miR-181c) had been described, which are down-regulated by amyloid-β in Alzheimer's disease. In particular, miR-181c was found to suppress Trim2 expression providing a link to progressive neurodegeneration accompanied by juvenile-onset tremor and ataxia[4,7]. Furthermore, mutations in the *TRIM2* gene have been associated with childhood onset of axonal neuropathy[8]. Together, these findings implicate TRIM2 as a key regulator in differentiated neurons, while its function during neurogenesis and neurodevelopment remains enigmatic.

Our present study strongly suggests that in *Xenopus*, Trim2 associates with Pdcd6ip/Alix (Programmed cell death 6 interacting protein/Apoptosis-linked gene-2 interacting protein X) and regulates neural development. Alix is a multimodular adaptor protein involved in the sorting of cargo proteins of multivesicular bodies for incorporation into vesicles and the endo-lysosome system[9-12]. Alix plays a role in the regulation of apoptosis, cell adhesion, and cytomorphology[13,14]. Overexpression of *Alix* can promote apoptosis[15,16] or tumor cell proliferation[17], whereas a truncated form prevents apoptosis[15]. Numerous studies have linked Alix to the modulation of apoptosis in neurons and neurodegenerative diseases[15,16,18-20]. A recent study from Laporte et al. (2017) showed that the lack of *Alix* expression at the

beginning of neurogenesis induces a transient wave of apoptosis in neural progenitors and results in the development of smaller brains in mice[21].

We could show that Trim2 physically interacts with Alix and is possibly involved in a Trim2-Alix/ESCRT-dependent modulation of early neurogenesis. We observed overlapping expression of *trim2* and *alix* during *Xenopus* development and in cell culture. At early and late tailbud stages, *alix* and *trim2* are both expressed in the central nervous system, olfactory placode, otic vesicle, cement gland, and pronephros. Suppression of *trim2* function led to a reduction in brain size caused by increased apoptosis in the head region, phenocopying *Alix* KO mice. These findings provide evidence that Alix and Trim2 E3 ligase are possibly involved in the timing of determination and differentiation of neural progenitors by the control of cell proliferation and cell survival during early neural development.

Results

During *Xenopus* development, *trim2* is expressed in neural and non-neural ectoderm

Trim2 expression was first described in the adult mouse brain[4]. However, its expression during development has not been reported. At first, we examined the temporal expression, sequence analysis and evolutionary relationship of *Xenopus trim2*. Temporal analysis showed gradual decrease of maternal expression. First zygotic expression was detected at low levels at the onset of gastrulation and was maintained throughout early development with an increase at the onset of neurulation. A comparison of amino acid sequences revealed that the known domains of Trim2 are fully conserved between mammalian and *Xenopus*. Moreover, analysis of synteny and phylogeny showed a high conservation of Trim2/*trim2* particularly in tetrapods (Suppl. fig. 1). To analyze the spatial expression of *trim2* during early neural development, we performed a series of whole-mount *in situ* hybridizations (Wmish) on *Xenopus* embryos (Fig. 1). In accordance with the temporal analysis, maternal transcripts of *trim2* were detected in the animal hemisphere of the embryo. At the onset of neurulation, neural plate and forming neural folds showed weak *trim2* expression (not shown). During early neurulation, this expression was more prominent in the prospective head region, where we detected *trim2* transcripts in the neural folds, forming eye vesicles, the prospective brain, olfactory and otic placodes, and the cement gland. At tailbud stages, expression of *trim2* was detected in the eye, brain, otic vesicle, spinal cord, olfactory placodes, and the trigeminal ganglion (Fig. 1, h-m).

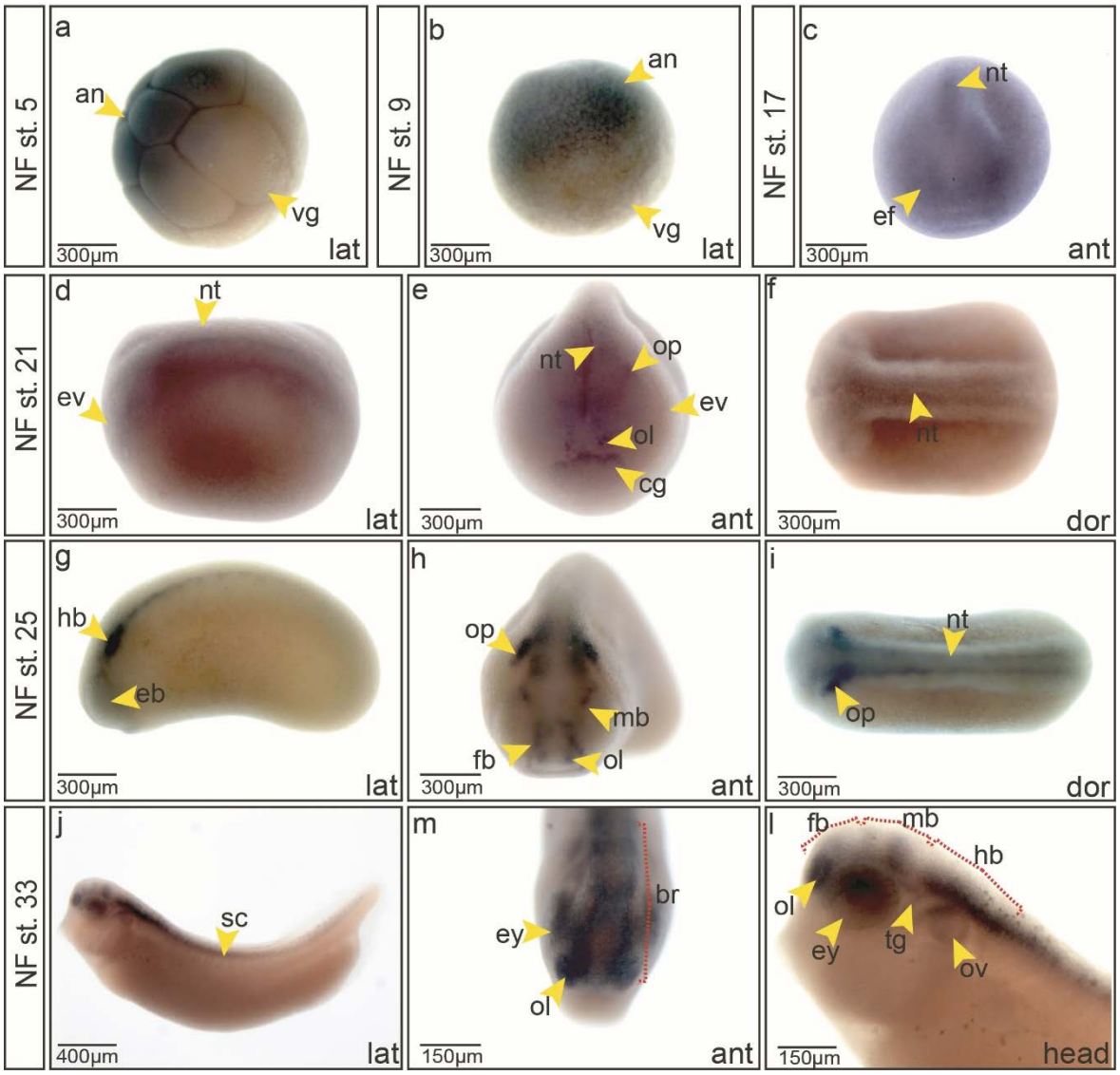

Figure 1. Expression of *trim2* during neurogenesis. (a-i) *trim2* expression was assessed by whole-mount in situ hybridization (Wmish) at different developmental stages. (a-b) Maternal *trim2* transcripts were detected in the animal (an) and vegetal (vg) hemisphere of *Xenopus* embryos. (c) NF stage 17, anterior view, *trim2* transcripts were evident in the eye field (ef) and in the forming neural tube. (e-g) NF stage 21, lateral, anterior and dorsal views. *trim2* transcripts were detected in eye vesicle (ev), neural tube (nt), olfactory (ol), and otic placode (op), as well as cement gland anlage (cg). (h-j) At NF stage 25, *trim2* expression became more distinct in eye bulb (eb), forebrain (fb), midbrain (mb), olfactory placode (ol), otic placode (ot) and neural tube (nt). (k-m) NF stage 33, *trim2* in fore- (fb), mid- (mb), and hindbrain (hb), eye (ey), otic vesicle (ov), spinal cord (sc), and trigeminal ganglion (tg). Scales as indicated.

To investigate whether the timing and appearance of mRNA and protein expression correlate, we compared whole-mount *in situ* detection of *trim2* mRNA and immunohistochemical detection of Trim2 protein in late tailbud stage embryos (Fig. 2A, B). Histological analysis of sectioned embryos revealed that temporal and spatial expression of *trim2* transcripts and Trim2 protein overlap. We observed elevated expression of *trim2*/Trim2 in the region of prospective motor neurons, crossing fibers of the floor plate, and cells of the medial and lateral ganglionic eminences (Fig. 2A, e-g; 2B, e-g. Lower levels of expression were detected throughout the forebrain (Fig. 2A, d; 2B, d). At the level of diencephalon, Trim2 expression was also observed in the ventral midline region, where radial glial cells[22] are present (Fig. 2B, e). Furthermore, *trim2/*Trim2 was found in the hypothalamus, prethalamus, radial glial, as well as in ganglion cells of the retina and in the lens epithelium (Fig. 2A, e; 2B, e). Double whole-mount in situ with *n-ß-tubulin* revealed, that *trim2* was expressed at particularly high levels in secondary neurons of the hindbrain, the inner otic vesicle, dorsal root entry zone, and in dorso-lateral sensory neurons of the spinal cord (Suppl. fig. 2). Generally, *trim2*/Trim2 were highly expressed in committed and differentiated neuronal cells, whereas the expression level in neural progenitors was almost absent. Outside the forming neural system, we observed weak *trim2* expression only in somites, notochord, and the ventral blood island. The localization of *trim2* transcripts and protein suggest a functional role of Trim2 during the formation of the central nervous system.

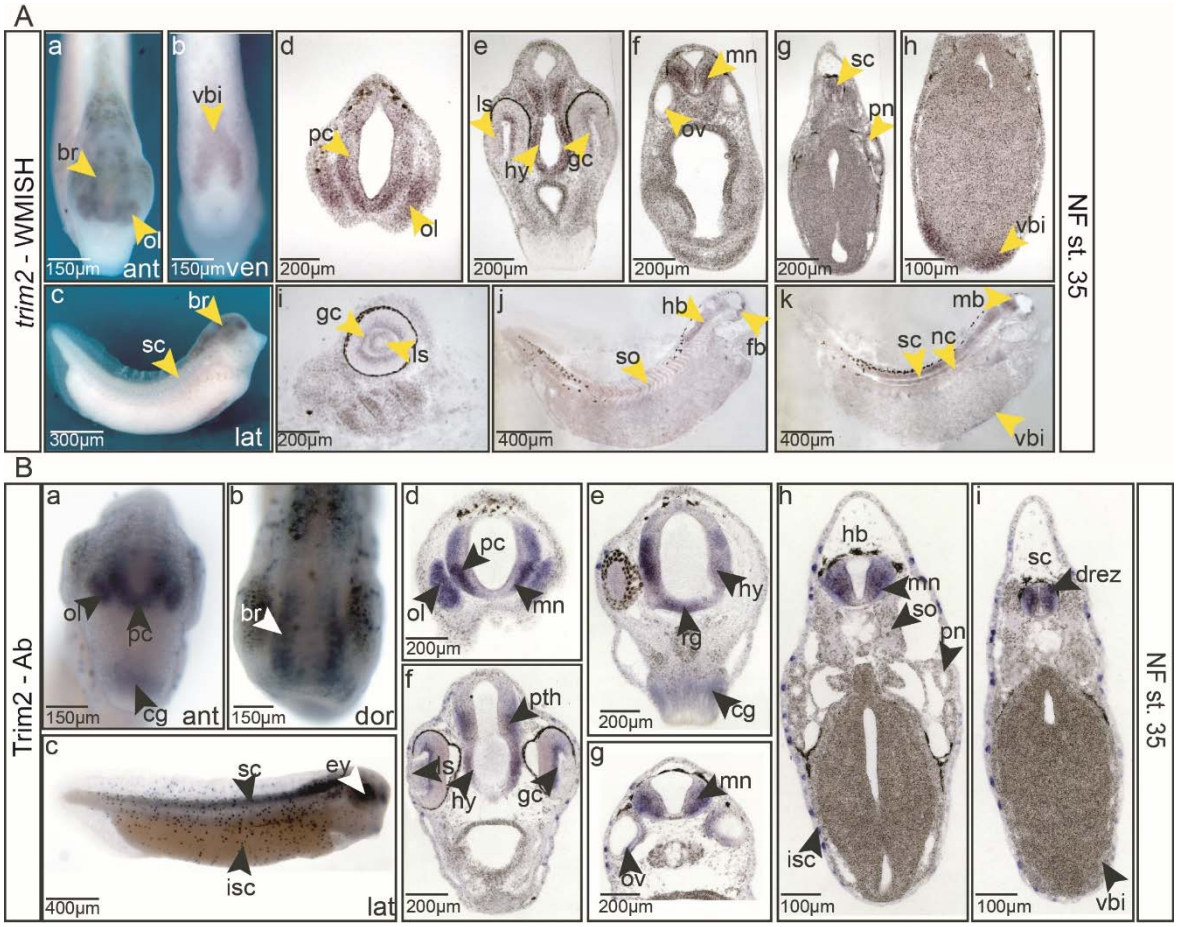

Figure 2. Trim2/*trim2* is expressed in differentiated neurons of the forming central nervous system at tailbud stage. **(A)** (a-c) Expression *trim2* mRNA at NF stage 35, anterior, ventral and lateral views, *trim2* transcripts were detected in the forming brain (br), olfactory placode (ol), spinal cord (sc) and the ventral blood island (vbi). (d-h) Twenty-micrometer gelatin/albumin sections at the level of fore-, mid-, hindbrain, and spinal cord. *trim2* is expressed prosencephalon (pc), olfactory placode (ol), ganglion cell layer (gc), lens epithelium (ls), hypothalamus (hy), motor neurons (mn), inner otic vesicle (ov), and spinal cord (sc), Faint expression was observed in pronephros (pn) and ventral blood island (vbi). (i-k) Sagittal sections reveal *trim2* expression in the ganglion cells layer, lens epithelium, brain, spinal cord, notochord, somites, and ventral blood island. **(B)** Whole-mount immunochemistry. (a-c) At NF stage 35 (anterior, dorsal and lateral views), Trim2 protein expression corresponding highly to that of *trim2* mRNA. (d-i) Twenty-micrometer gelatin/albumin transverse sections along fore-, mid-, hindbrain, and spinal cord region. Trim2 protein was detected in the developing CNS, cement gland, dorsal root entry zone (drez), ganglion cells, hindbrain, hypothalamus, ion secreting cells (isc), motor neurons, olfactory placode, otic vesicle, prosencephalon (pc), prethalamus (pth), presumptive radial glial cells (rg), somites (so), and ventral blood island. Scales as indicated.

trim2 knock down leads to smaller head and affects cranial axis positioning

In order to understand the function of Trim2, we utilized antisense morpholino oligonucleotides to block translation of *trim2*. Synthetic *egfp*-RNA was co-injected as a tracer into one cell of two-cell stage *Xenopus* embryos. The specificity of the morpholino was confirmed by injecting a GFP-tagged complimentary sequence as a morpholino reporter as reported earlier[23] and by immunohistochemistry (Fig. 3). A scrambled morpholino was injected as control. A first inspection of *trim2*-morphants equivalent to NF stage 35 revealed that on the injected side the prospective head was smaller and that the pigmentation particularly of the eye was suppressed (Suppl. fig. 3). Immunohistochemistry of *trim2*-morphants at NF stage 17 revealed complete absence of Trim2 within the neural plate territory (Fig. 3, a). Tadpoles at NF stage 35 showed a strong reduction of Trim2 expression in the eye, brain, and spinal cord on the *trim2*-morpholino-injected side of the embryo (Fig. 3b-b'', b1-b3). Moreover, a structural disorganization of presumptive brain tissue towards the non-injected side was also observed (Fig. 3, b1). Cells were found dissociated, misaligned, and clustered all over the presumptive brain and in the forming eye (*strd*-mo N=20 embryos; *trim2*-mo N=16 embryos (E); P=1.97E-09, unpaired χ^2 test, $\chi^2 = 36$, df =1, phenotype occurrence (po) =16, $P<0.001$).

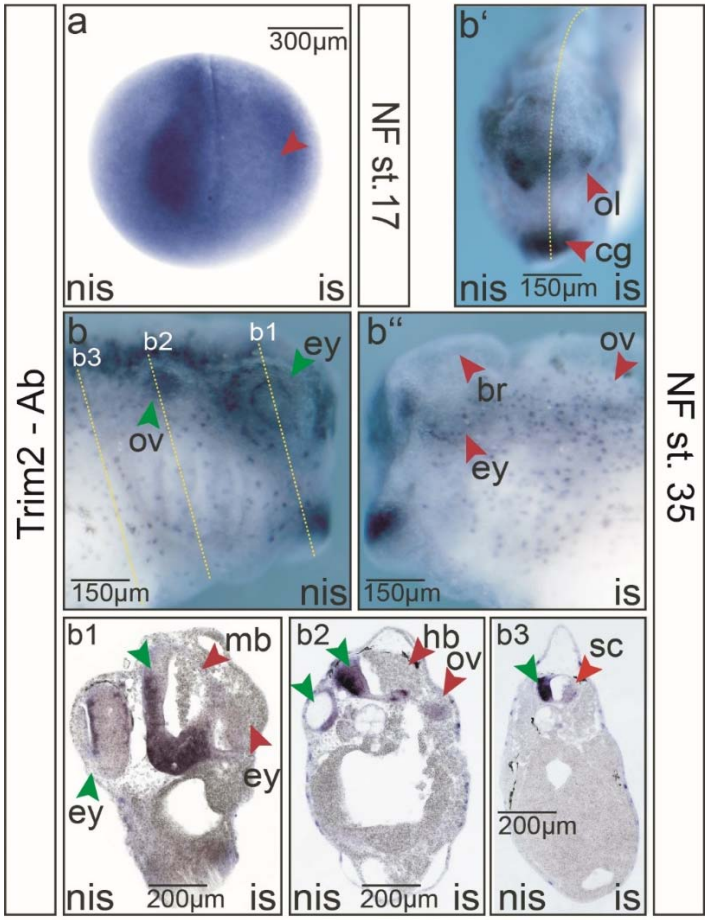

Figure 3. Suppression of *trim2* function interferes with embryonic CNS development. Micro-injections of *trim2* morpholino was performed in one cell of a two-cell stage embryo. Trim2-morphants were analysed by whole-mount immunochemistry using a commercial Trim2 antibody at (a) NF stage 17 and (b) NF stage 35. (b) non-injected side (nis), (b‘) anterior view, (b‘‘) injected side (is). Forming brain (br), cement gland (cg), eye (ey), olfactory vesicle (ol), and otic vesicle (ov), showed loss of Trim2 expression. (b1-b3) Twenty-micrometer gelatin/albumin transverse sections of the cranial region. The embryonic brain appeared smaller and disorganized upon *trim2* morpholino injection. Midbrain (mb), cement gland (cg), eye (ey), hindbrain (hb), otic vesicle (ov), and spinal cord (sc). Red arrow heads represent the affected region in the injected side. Green arrow heads indicate complementary regions on the control side (nis). Scales as indicated.

Suppression of *trim2* function impairs neural tube closure

To investigate whether knock down of *trim2* affects neural tube closure, we looked at different embryonic stages during neural tube formation. Indeed, *trim2*-morphants showed a marked delay in neural tube closure as compared to control embryos (Fig. 4A). The injected side of the embryos showed a widened neural plate and delayed convergent extension of the neural folds at NF stage 20 (Fig. 4a’’). Interestingly, already at the onset of neural tube formation at NF stage 15, *trim2*-morphants showed an impaired invagination movement of epithelial cells. Accumulation of phalloidin on the injected side of *trim2*-morphants indicated a high proportion of F-actin and thus a disturbed dynamic of actin assembly/disassembly in *trim2*-deficient cells. In contrast, the neuroepithelial cells on the injected side showed normal apicobasal elongation and apical constriction (Fig. 4B).

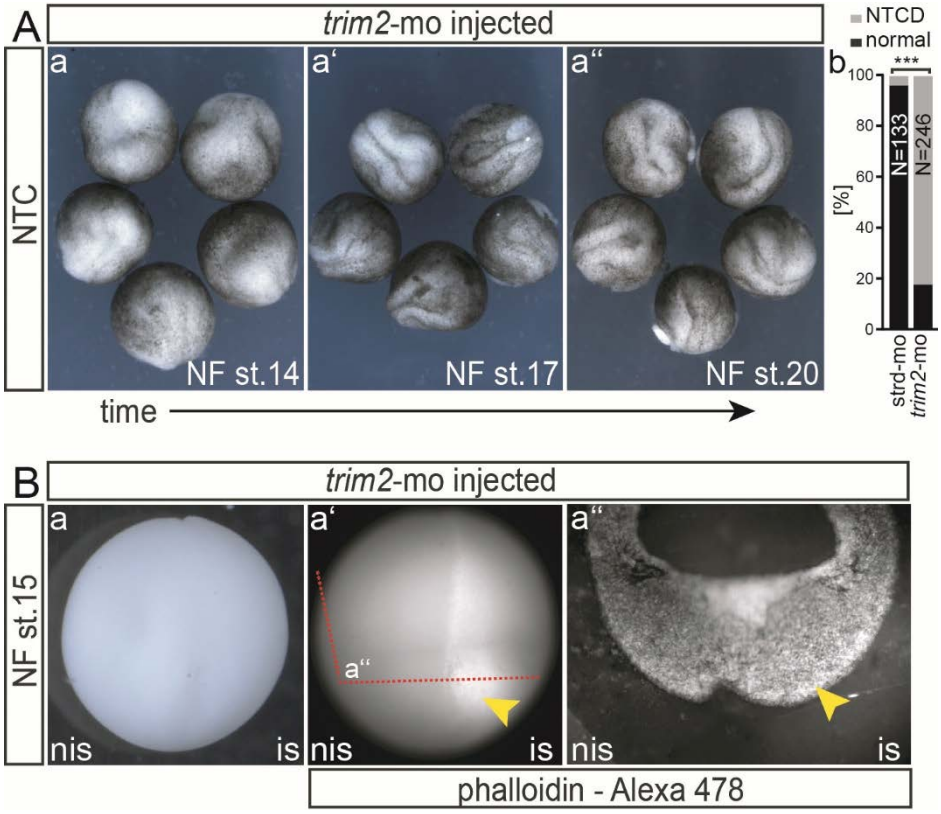

Figure 4. (A) Suppression of *trim2* function affects neural tube closure. (a-a'') Three developmental stages equivalent to (Aa) open neural plate, (Ab) closing neural tube, (Ac) closed neural tube stage. Embryos were injected with *trim2* morpholino in one cell at the 2-cell stage and were grown until neural plate stage. At NF stage 14, the neural plate appeared widened on the injected side. Similarly, at NF stage 17, the convergence of neural folds was impaired and irregular in particular at the anterior end. At NF stage 20, embryos show aberrant closure of the neural tube with the anterior axis of the embryo bending towards the *trim2*-mo injected side. Bar plot: percentage embryos affected by neural tube closure defects (standard-mo injected embryos N=133, *trim2*-mo N=246 embryos, *p*=*** (2.9E-79), unpaired χ^2 test. (B) Whole-mount staining of *trim2*-morphants with phalloidin dye conjugate (Alexa 488) at NF stage 15. (a', a'') Suppression of *trim2* function led to an accumulation of F-actin on the injected side, accompanied by a delayed invagination of the neuroectoderm to form the neural groove.

Suppression of *trim2* function affects neurogenesis, proliferation and cell survival

Suppression of *trim2* function resulted in smaller heads, affecting the developing brain and eyes. To investigate whether early forebrain development is impaired in *trim2*-morphants, we investigated the expression of early forebrain markers in those embryos. Expression of *pax6* appeared widened at stage 15 in the prospective eye field (Fig. 5A, b; strd-mo N=12E;

trim2-mo N=20E; *P*=2.1E-06, unpaired χ^2 test, χ^2 =22.5, df =1, po=18, *P*<0.001). A similar effect was observed for *fb1* and *otx2* genes (Fig. 5A, a, b; *fb1*: strd-mo N=10E; *trim2*-mo N=12E; *P*=2.73E-06, χ^2 =22, df =1, po=12; *otx2*: strd-mo N=10E; *trim2*-mo N=12E; *P*=1.85E-05, unpaired χ^2 test, χ^2 =18.33, df =1, po=11, *P*<0.001). The appearance of a broader expression of forebrain markers on the *trim2*-deficient side was presumably a result of impaired convergent and extension movements of the neural plate as shown in Fig. 4 and not an expansion of the neural plate itself. However, we wanted to know whether the suppression of *trim2* affected cell proliferation and/or survival (Fig. 5A, d-h''). Cell proliferation assay identified only half the number of mitotic cells on the injected side compared to the non-injected side (Fig. 5, f-h''; nis: N=384 cells/E; is: mean N=202 cell/E; *P*=0.0074, paired t-test, percentage error set at 5%, *P*<0.01). TUNEL assay revealed a profound increase in apoptotic cells at early neuronal (NF stage 15) as well as at early organogenesis stages (NF stage 27). The block of *trim2* translation led to an increased number of apoptotic cells within the brain, eye, and cement gland (Fig. 5A, d-e'', red arrow heads), and all other territories of *trim2* gene expression. As observed in the cranial transverse section of an NF stage 27 embryo, we often observed aggregation of apoptotic cells in the presumptive brain and eye on the injected side (Fig. 5A, e''). To further characterize the *trim2*-deficient phenotype during early neural development, we monitored the expression of three key markers of neural differentiation (Fig. 5B, a, d, g). Neural precursor cells express the pan-neural marker *sox3* throughout the neural plate at NF stage 15 and appeared with a clearly expanded band on the *trim2* morpholino-injected side as was shown for *pax6* (Fig. 5B, a, upper left, strd-mo N=30E; *trim2*-mo N=28E; *P*=1.88E-13, unpaired χ^2 test, χ^2 =54, df =1, po=27, *P*<0.001) indicating regular induction of neural fate in *trim2*-deficient cells. However, neural specification and differentiation markers such as *myt1* and *n-ß-tubulin*, which are expressed in medial, intermediate and longitudinal stripes and in the trigeminal placode within the neural plate, were clearly reduced upon suppression of *trim2* function (Fig. 5B, d, g; *myt1*: strd-mo N=30E; *trim2*-mo N=28E; *P*=1.88E-13, χ^2 = 54, df =1, po=27; *n-ß-tubulin*: strd-mo N=30E; *trim2*-mo N=29E; *P*=7.17E-13, unpaired χ^2 test, χ^2 =51, df =1, po=27, *P*<0.001). Correspondingly, at tailbud stage, expression of *sox3*, *myt1*, and *n-ß-tubulin* was significantly reduced (Fig. 5B, b-c, e-f, h-i). Here, as observed in transverse sections of *trim2*-morphants, *sox3* expression was strongly reduced in the dorsal regions of forebrain and midbrain (Fig. 5B, b-c; *sox3*: strd-mo N=34E; *trim2*-

mo N=41 embryos; *P*=2.24E-16, unpaired χ^2 test, χ^2 = 67, df =1, po=39, *P*<0.001). Similarly, expression of the neural specification and differentiation marker *myt1* and the differentiation marker *n-ß-tubulin* was strongly reduced in the prospective dorsal brain, eyes and secondary neurons at the lateral side of the neural tube (Fig. 5B, e-f, h-i; *myt1*: strd-mo N=28E; *trim2*-mo N=39E; *P*=2.03E-15, χ^2=63, df=1, po=38; *n-ß-tub*: strd-mo N=29E; *trim2*-mo N=40E; *P*=4.85E-15, unpaired χ^2 test, χ^2=61, df =1, po=38, *P*<0.001). In placodal structures such as olfactory, otic and trigeminal placodes the expression of *myt1* and *n-ß-tubulin* was also reduced (5B). These results showed that suppression of *trim2*-function affects cell proliferation and cell survival during early neurogenesis and consequentially led to a loss of primary and secondary neurons.

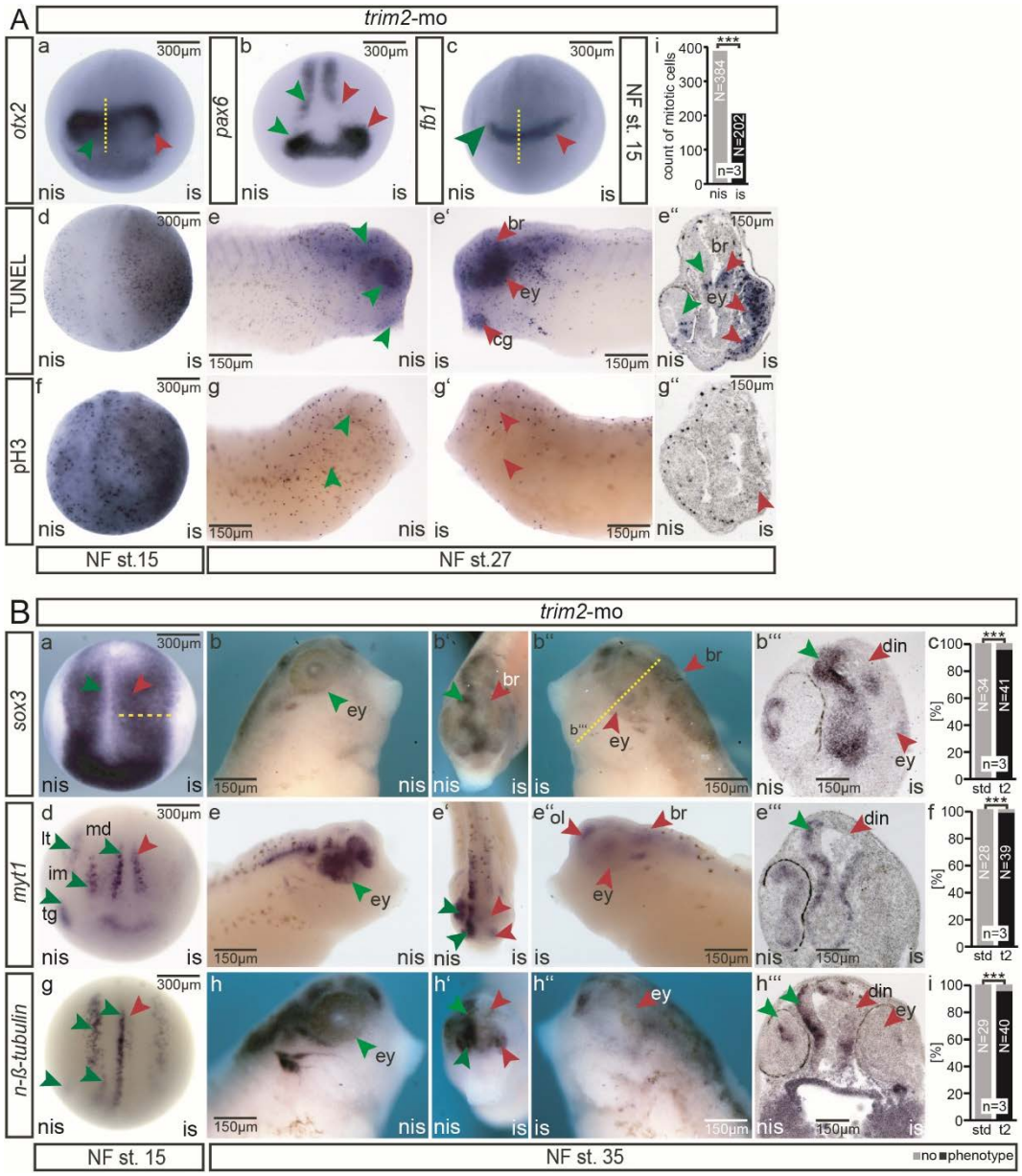

Figure 5. (A) Suppression of *trim2* function affected cell proliferation and cell survival within the forming CNS in tadpoles. (a-c) At NF stage 15, early forebrain marker gene expression (*otx2*, *pax6*, and *fb1*) appeared expanded apparently (red arrow heads), accompanied by a mild increase in apoptotic cells (d, TUNEL), while proliferation (f, pH3) was not affected at this early stage. In early tadpole stages, the rate of apoptosis was highly increased in the brain region including the eye (e'-e'') and the number of mitotic cells was strongly reduced (g-g''). (i) Bar plot: cranial region counted for pH3 positive cells (n=3 embryos; *nis* mean N=384 cells/embryo, *is* mean N=202 cell/embryo, *P*=0.0074, paired t-test, percentage error 5%, *p*>0.001). **(**B) Suppression of *trim2* function interfered with primary and secondary neurogenesis. (a, d, g) A comparison of early neuronal marker gene (*sox3*, *myt1*, and *n-ß-tubulin*) expression at NF stage15 of *trim2* morphants revealed that primary neurogenesis was impaired. An apparent, widened expression of *sox3* positive neural progenitors and the suppression of primary neuron formation was observed. (b-c, e-f, h-i) At NF stage 35, *trim2*-morphants showed reduced *sox3* expression in the lens epithelium and the dorsal intermediate neurons (din) (b-c). Similarly, *myt1* and *n-ß-tubulin* expression was absent in the morphant brain territory (br), particularly in dorsal intermediate neurons (din), eye (ey), olfactory placode (op) (e-f, h-i). Red arrowheads indicate the affected regions. Green arrow heads represent the corresponding region in the control side. (c) *sox3* (*p*=*** (2.24E-16)); (f) *myt1* (*p*=*** (2.03E-15)), (i) *n-ß-tub* (*p*=*** (4.85E-15), unpaired χ^2 test). Scales as indicated. (b''', e''', h''') Twenty-micrometer gelatine/albumin transverse sections.

trim2-morphants show loss of motor sensory function

Recently, a human patient with a heterozygous missense mutation in TRIM2 was reported to exhibit loss of gross motor neuron development that resulted in early onset of axonal neuropathy, muscle hypotonia, and sarcopenia[8]. *Trim2*-depleted mice displayed tremors with episodes of spontaneous seizures[4]. Since *Xenopus* tailbud embryos and tadpoles respond to poking/touching by escaping with a rapid beating movement, we performed motility-escape assays on late tailbud stage embryos to investigate whether *trim2* knock down affects this motor-sensory function. The analysis revealed loss of motor and sensory function in *trim2*-morphants injected into one cell at the 2-cell stage (Movie 1). After several attempts of poking/stimulating the embryos on the injected side, embryos moved in circles with one sided-beating against stimulation on the non-injected side, indicative of non-spontaneous response to sensory stimulation (control embryos N=100; *trim2*-mo N=298E; *P*=2.90E-79, unpaired χ^2 test, χ^2 =355, df =1, po=298, *P*<0.001). A complete loss of motor sensory function accompanied by severe developmental defects and high mortality was observed upon injection of *trim2*- morpholino into both blastomeres of a two-cell stage embryo (Movie 3; control N=20E; *trim2*-mo N=12E; *P*=1.54E-08, unpaired χ^2 test, χ^2=32, df=1, po=12, *P*<0.001). We were able to rescue this phenotype as well as marker gene

expression of primary neurogenesis (Suppl. fig. 4) by injecting synthetic mutated *Xenopus trim2* RNA (Δ*trim2*) resistant to the *trim2*-morpholino (Movie 2; control N=50E; *trim2*-mo+Δ*trim2* N=47E; *P*=4.64E-21, unpaired χ^2 test, χ^2 =87, df =1, po (rescued) =47, p<0.001).

Trim2 interacts with Alix physically

Previous studies have shown that NEFL is a substrate for TRIM2-catalysed ubiquitination and that NEFL accumulates in the cerebellum of *Trim2* mutant mice[4]. However, using a GST-Trim2 protein as bait, we were unable to pull down NEFL from *Xenopus* embryonic lysates or over-expressed NEFL from cultured cells. To identify proteins that interact with *Xenopus* Trim2, we applied GST-pulldown along with high throughput LC-MS/MS screening (Fig. 6A). We identified the Alix protein in very high abundance as a prominent candidate for a Trim2 interacting protein (Table 1). We confirmed the interaction of Trim2 with Alix, by a GST-pulldown assay using GST-Trim2 and lysates of flag-Alix transfected HEK293T cells (Fig.6B).

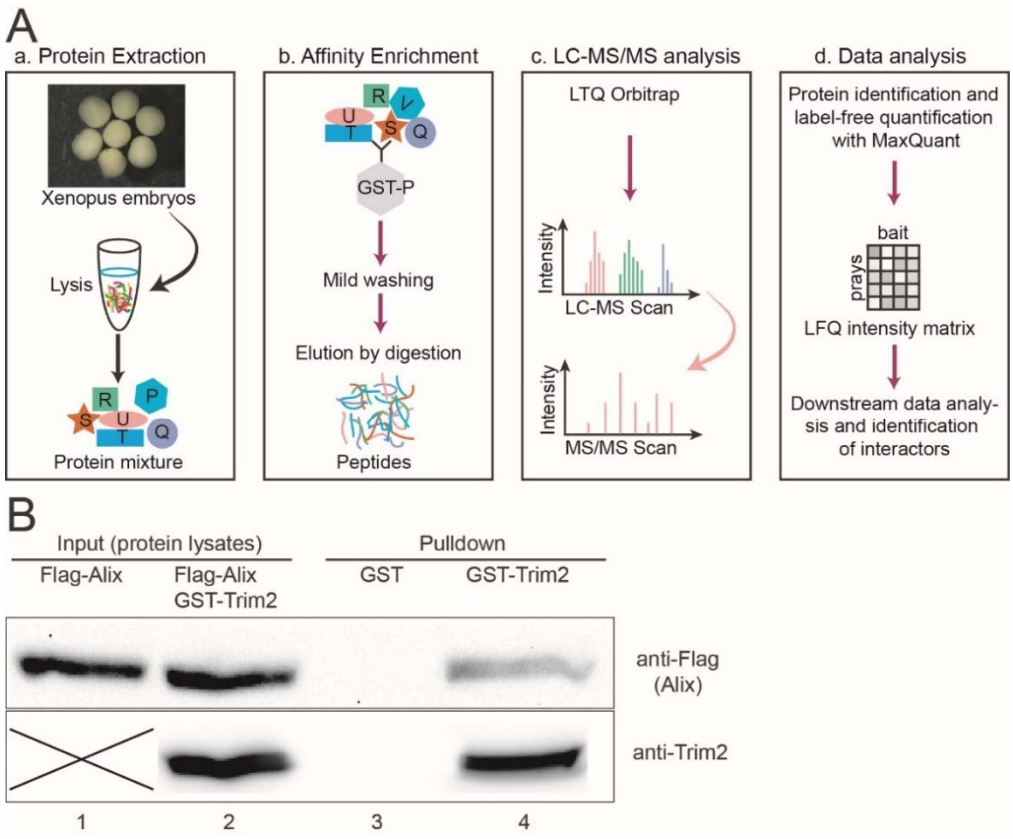

Figure 6. (A) Schematic representation of LC-MS/MS analysis for identification of interaction partners, modified after[32]. (a) Protein lysates were extracted from NF stage 30-36 embryos using mild non-denaturing conditions, (b) GST tagged bait protein and protein interactors from the embryo lysates were enriched by GSH-

Sepharose. Subsequently, bound proteins were digested into peptides. (c) The peptide mixture was analysed by single-shot liquid chromatography tandem mass spectrometry (LC-MS/MS) on an Orbitrap instrument (see acknowledgement). (d) Raw data were processed with MaxQuant to identify and quantify proteins and to identify interacting proteins. (B) Interaction of Trim2 and Alix was verified by GST pull down assay using GST-Trim2 as bait and lysates of HEK293T cells transfected with Flag-Alix by Western blot. Cell lysates with input proteins (Lane 1 & 2). GST alone serves as a control (Lane 3). Eluted flag-tagged Alix after binding GST-Trim2 (lane 4, upper blot). Note: images of the blots are cropped accordingly to the area of exposed protein bands. Two different gels/bolts were used to show the eluted flag-tagged Alix and precipitated GST-Trim2 of the same sample. Uncropped blots in supplementary figure 5.

Expression of *alix* overlaps with *trim2* in *Xenopus* embryos

Direct interactions between Trim2 and Alix suggests that both genes are either expressed in overlapping or at least adjacent domains of the embryo. Indeed, we observed an overlapping pattern of expression for *alix* and *trim2*. During early neurulation, *alix* transcripts were detected in the neural tube, eye bulb, and the cement gland (Fig. 7). At late tailbud stages, expression of *alix* appeared strongly within the forming CNS and cranial placodes. High level of expression was further detected in the pronephros, which did not show *trim2* expression (Fig. 2Ag, 2Bh), indicating additional Trim2 independent functions of Alix. Moreover, we tested by immunofluorescence whether endogenous TRIM2 and ALIX do show overlapping expression in a human neuroblastoma cell line SH-SY5Y. The specificity of both commercial antibodies employed was confirmed by blocking the respective signals in Western blot using specific siRNAs for each transcript (Suppl. fig. 5). Signals for endogenous TRIM2 and ALIX overlapped strongly and showed a filamentous pattern including some vesicular-like or granular structures within the cytoplasm (Fig. 7B).

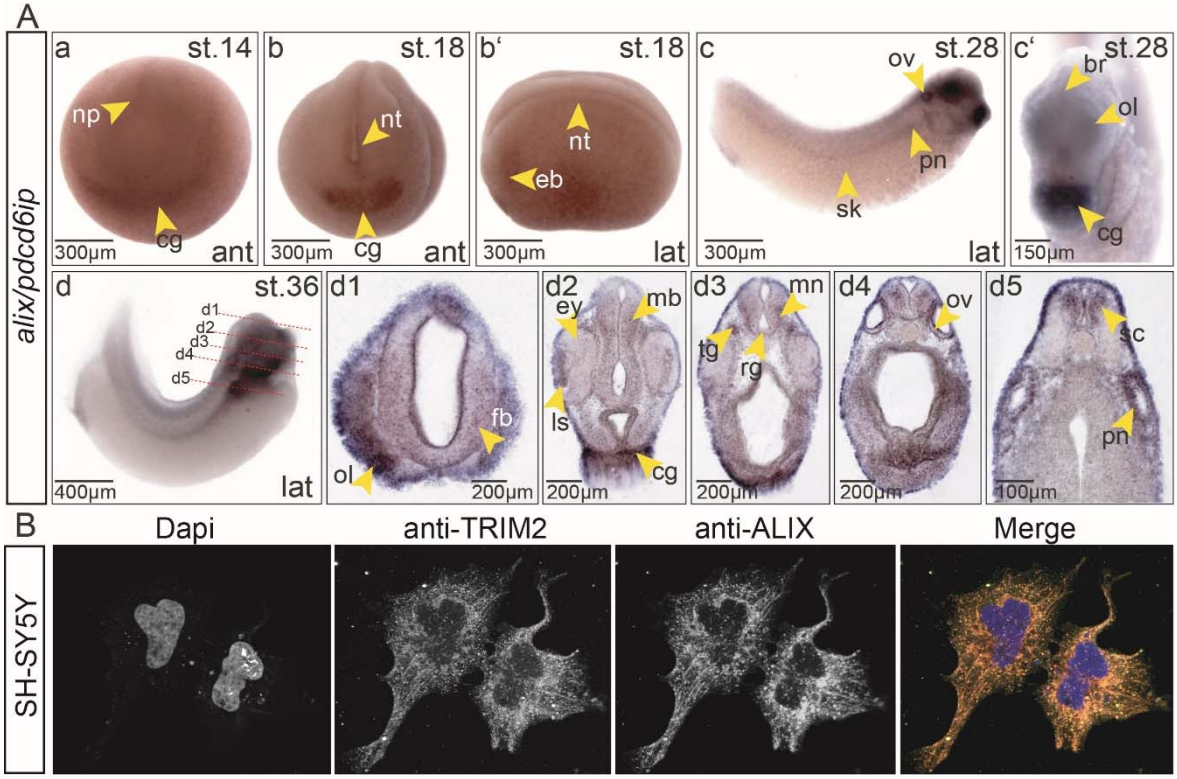

Figure 7. (A) Expression of *alix* during neurogenesis overlaps strongly with *trim2* in *Xenopus*. (a) At NF stage 14, *alix* expression was observed within the neural plate (np) and cement gland Anlage (cg). (b-b', anterior (ant) and lateral (lat) views) At NF stage 18, *alix* transcripts were detected in the neural tube (nt), eye bulb (eb), and forming cement gland (cg). (c-c') At NF stage 28, the presumptive brain (br), olfactory placode (ol), otic vesicle (ov), cement gland (cg), pronephros (pn) and skin cells (sk) reveal *alix* transcripts. (d) At NF stage 36, a lateral view showed strong expression in eye, embryonic brain, spinal cord (sc), otic vesicle, and pronephros (pn). (d1-d5) Twenty-micrometer transverse gelatine/albumin sections taken at the level of fore-, mid-, hindbrain, otic vesicle, and spinal cord. Transcripts of *alix* were detected in the eye (ey), forebrain (fb), midbrain (mb), hindbrain, lens epithelium (ls), motor neuron (mn), olfactory placodes (ol), otic vesicles (ov), radial glial cells (rg), spinal cord (sc) and trigeminal nerve (tg). (B) Endogenous Alix and Trim2 were detected by fluorescence immunohistochemistry in a strongly overlapping pattern within the cytoplasm of SH-SY5Y glioblastoma cells. Pictures were taken in greyscale. Merge in false colours. Nuclei were stained with DAPI (blue).

Functional interactions of Trim2 and Alix

To provide first insight into the functional relationship of Trim2 and Alix, we performed single and co-suppression experiments of *trim2* and *alix* and compared the expression of early neural marker genes. The injection of both morpholinos at a combined dose equal to the final dose of a single *trim2*-morpholino (see figure 5) injection resulted in similar

alterations of marker gene expression compared to *trim2*-morphants (Fig. 8). At NF stage 15, *sox3* expression within the neural plate appeared widened upon injection of alix alone or in combination (Fig. 8a and fig. 5 for *trim2-mo*) as ; strd-mo, N=10E; *co-inj. trim2/alix*-mo, N=20E; *P*=9.47E-06, unpaired χ^2 test, χ^2 =19.6, df =1, po=17, *P*<0.001). The expression of *myt1* and *n-ß-tubulin* in intermediate and longitudinal stripes and the trigeminal placode were again reduced in trim2/alix morphants (Fig. 8e-f, h-i; *myt1*: strd-mo N=10E; *trim2/alix*-mo N=12E; *P*=1.85E-05, χ^2 =18, df =1, po=11; *n-ß-tubulin*: strd-mo, N=10E; *trim2/alix*-mo, N=13E; *P*=1.12E-05, unpaired χ^2 test, χ^2 =19, df = 1, po=12, *P*<0.001). Moreover, at early tail bud stage (NF stage 32), *alix*-morphants showed a similar loss of motor-sensory function as observed for *trim2*-morphants (Movie 4). Since Trim2 and Alix physically interacted and either-or combined suppression resulted in an almost identical phenotype, we asked whether an epistatic relationship exits or whether both act interdependent. To this end, we performed rescue experiments for co-injected morphants with synthetic *trim2* RNA or with human *ALIX* mRNA. However, we were unable to rescue the morphants with either *trim2* or *ALIX* mRNA, which suggests that Trim2 and Alix act or interact in the same pathway in parallel (data not shown).

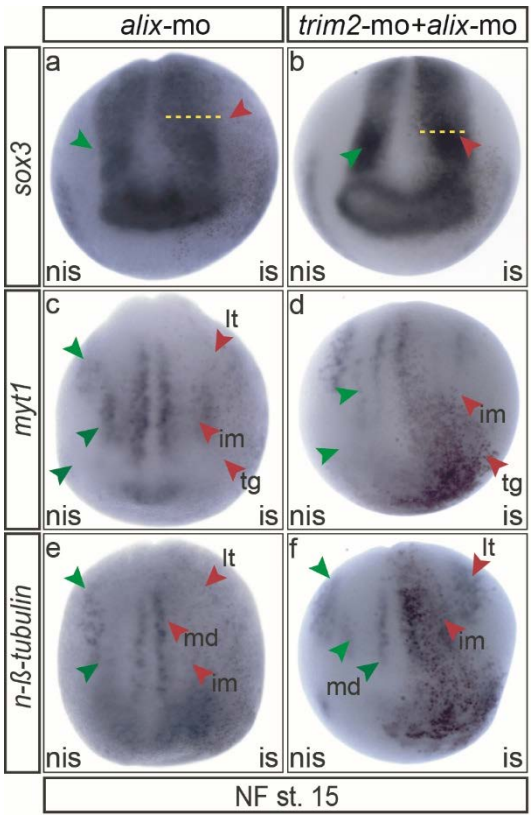

Figure 8. *trim2* and *alix* act in parallel on the formation of primary neurons in *Xenopus*. A comparison of early neuronal marker gene (*sox3*, *myt1*, and *n-ß-tubulin*) expression at NF stage15 of *trim2* (see fig.5), *alix* and combined morphants revealed that primary neurogenesis is likewise impaired. (a-b) An apparent, widened expression of *sox3* positive neural progenitors in the neural plate region on the injected side (red arrowheads and dotted lines). (c-f) The expression of the neural specification marker *myt1* and the differentiation marker *n-ß-tubulin* were repressed or lost upon suppression of *trim2*, *alix*, and *trim2/alix* function. Primary neurons revealed as medial (md), intermediate (im), longitudinal (lt) stripes, and trigeminal placode (tg).

Discussion

Our present work provides insight into the differential expression and function of Trim2 during vertebrate embryogenesis. Trim2 is a conserved member of the TRIM-NHL family of E3 ligases[24]. Evolutionarily, Trim2 is highly conserved across species; the amino acid sequence of the human orthologue shows 96% homology to *Xenopus* Trim2 (Suppl. fig. 1). Analysis of *trim2*/Trim2 mRNA and protein expression revealed that *trim2*/Trim2 is predominantly expressed in the developing neural system of *Xenopus laevis* embryos. By suppression of function experiments, we demonstrated that *trim2* affects proliferation, determination, and differentiation of neural progenitors during embryonic neurogenesis but not primary neural induction and also affects motor sensory function at later stages. We also provide evidence that Trim2 interacts with Alix using pulldown techniques, mass spectroscopic and functional analysis.

In adult mice, *Trim2* expression was reported in regions of the cerebellum, hippocampus, retina, and the spinal cord[4]. In *Xenopus* embryos, we found *trim2* expression in the presumptive ventral brain and spinal cord, including the floor plate, otic vesicles, and olfactory placodes. Both, Trim2 protein and *trim2* mRNA levels were high in committed and differentiated neuronal cell layers of the future central nervous system. Thus, *Trim2/trim2* expression appeared highly similar in the CNS of *Xenopus* tadpoles and adult mice. In non-neural tissues, only weak expression like in head mesenchyme, notochord, somites and in the ventral blood island was observed.

Recent insights into the mechanisms of neuronal polarization during axon specification revealed TRIM2-dependent post-translational regulation of NEFL[4,5,25]. First reported in the molluscan *Lymnaea stagnalis*, the orthologue L-Trim is up-regulated during neurite outgrowth of central neurons and in the postnatal brain during neuronal regeneration. Strong inhibition of neurite outgrowth was observed upon knock-down of *l-trim* mRNA as well[25]. Similarly, cultured hippocampal neurons and motor neurons from mice showed a hyperpolarization-like phenotype upon TRIM2 overexpression and a hypopolarization-like phenotype after *trim2* knockdown. Likewise, proteasomal degradation of NEFL by TRIM2 is necessary for neural polarization of the hippocampal neurons. All data thus far indicate a functional role for TRIM2 in secondary neurogenesis. Our findings complement this previous work, providing further evidence of *trim2* function in embryonic neurogenesis. We

showed that in *trim2*-morphants, determination and differentiation of proneural genes is impaired at the open neural plate stage, while the precursor cell pool was unaffected or appeared even enlarged. This was also the case as observed for early forebrain markers. Presumably, suppression of *trim2* function inhibited the cells from exiting the cell cycle properly, thereby resulting in an accumulation of precursor cells with a higher frequency of apoptotic cells. The apparent expansion of the neural precursor territory upon suppression of *trim2* was most likely due to a delayed invagination movement of neural plate cells. In later stages, we also observed severe gross morphological malformations and loss of structural organization within the craniofacial region, in contrast to findings in *Trim2*^{GT} mice. However, this may be due to integration of gene trap vector inside the Trim2 locus between exons 6 and 7, which may result in a partially active protein (since the catalytically active RING domain of Trim2 is located on exon 2). In addition, the authors reported a residual expression of nearly 5% of WT mRNA due to an alternative splicing effect[4]. On the other hand, suppression of *trim2* function in *Xenopus* embryos resulted in defective motor neurons as seen by an ataxia-like phenotype of swimming tadpoles, similar to that reported in *Trim2*^{GT} mice.

Little is known about the direct interaction partners of TRIM2/Trim2. We identified Alix (originally described as a pro-apoptotic protein) as a candidate Trim2-interacting protein. First isolated from *Xenopus* oocytes, the *alix* homologue Xp95 is phosphorylated by src kinases[26]. In mice, ALIX has been described as a calcium-dependent interaction partner of apoptosis linked gene-2 (ALG-2)[27,28]. The overexpression of ALIX in cerebellar neurons of mice revealed activation of the caspase cascade leading to neuronal cell death, independent of the JNK or p38 MAPK signaling pathways. However, a C-terminal fragment of ALIX protected neurons from potassium withdrawal-induced cell death[16]. Our studies suggest a direct, functional interaction of Alix and Trim2 during embryonic neurogenesis and development. In a GST-pulldown/LC-MS/MS approach of *Xenopus* embryonic lysates using GST-Trim2 as bait, we identified the *Xenopus* homologue of Alix as a potential binding partner of Trim2. In general, expression of *alix* correlated strongly with *trim2* during *Xenopus* development. In tadpoles, both transcripts were found in an overlapping pattern in the developing central nervous system and particularly in the retina and lens, brain, spinal cord, and the olfactory and otic placodes. Moreover, loss of neural differentiation and the microcephalic-like phenotype observed in *trim2*-morphants mimics that of *Alix* deficient

mice[21]. To date, there is no evidence for a functional role of TRIM2 in the regulation of apoptosis or cell survival. However, there is clear evidence for ALIX in this respect[18,27,28]. We could show a significant decrease in cellular proliferation, most probably due to a high rate of apoptosis within the developing CNS of *trim2*-morphants. The proportion of phosphohistone-H3-positive cells decreased, while the number of TUNEL-positive cells increased significantly. Along similar lines, loss of neural progenitors was observed during the transient phase of apoptosis in *Alix* KO mice[21]. Alix is involved in the regulation of the endolysosomal system through binding to endophilins and to endosomal sorting complexes required for the transport (ESCRT) proteins TSG101 and CHMP4b. Since TRIM2 appear to localize to vesicular structures, this may provide a subcellular platform for functional interactions between these referred proteins[10-12,29].

Our results provide evidence for an important function of Trim2-Alix interaction during early neural development. In concert, they may link developmental cues to cellular proliferation/cell survival and thus may take an important function during neuronal determination and differentiation.

Materials and Methods

Experimental model, microinjections and plasmids

Albino *Xenopus laevis* frogs were purchased from Nasco (Ft. Atkinson, WI). Production, rearing and staging of embryos was performed according to Nieuwkoop and Faber, 1994[30]. All procedures were performed according to guidelines set by the German animal use and care laws (Tierschutzgesetz) and approved by the German state administration Saxony-Anhalt (Projekt/AZ: 42502-3-600 MLU). *trim2* antisense morpholino (5'-CTTCACTGGCCATCCTAGACCACTG-3') and *alix* antisense morpholino (5'-GTACCGAGATGAAGGTAGCCATCG-3') oligonucleotides were designed and purchased from Gene Tools, LLC, USA. For antisense microinjections 1.9 pmol of *trim2* morpholino and 2.5 pmol of *alix* morpholino together with 250 pg synthetic *egfp* or *ß-gal* RNA as a tracer, was injected into one cell of two-cell stage embryos. For epistatic analysis, a low concentration of 1pmol of each morpholino was used in co-injections. A control morpholino oligonucleotide designed by Gene Tools (USA) was injected as a control (5-CCTCTTACCTCAGTTACAATTTATA-3'). Embryos were raised until the desired stages

and fixed in MEMFA. *Xenopus trim2* (Acc. no.: NM_001092023) and *alix* (Acc. no.: NM_001088401) plasmid clones were purchased from Source Bioscience, UK.

Whole-mount *in situ* hybridization

To analyse the spatiotemporal expression of respective marker genes, whole-mount *in situ* hybridization was performed as described earlier[31]. Anti-sense RNA probes were transcribed in the presence of digoxigenin and/or fluorescein-labelled UTP (Roche) from plasmids. Chromogenic reactions were carried out using NBT/BCIP (Roche). For a more detailed analysis of gene expression 20µm thick sections were cut from embryos embedded in gelatine/albumin (Roth) using a microtome (Leica) and were mounted on glass slides. Antisense probes (cut, transcribe): pCS2+MT-*trim2*: *Bam*HI, T3; pBluescriptKS-*n-ß-tubulin*, *Bam*HI, T3; pCS107-*sox3*, *Hind*III, T7; pBluescriptKS-*myt1*, *Cla*I, T7; pGEM-T-*pax6*L, *Not*I, T7; pBluescriptKS+-*bf1*, *Bam*HI, T3; pCMVSport6-*pdcd6ip.L/alix*, *Sal*I, T7.

Immunostaining of *Xenopus* embryos

To analyse the protein expression, embryos injected with either morpholino or mRNA in one cell of a two-cell stage embryo and or non-injected embryos. Embryos grown until desired NF stage were fixed and left overnight in Dent's solution at -20°C for permeabilization. Next embryos were washed in a series of decreasing methanol concentration steps, blocked for ~6 hours in 20% horse serum/PBS and incubated with appropriate antibody (see Immunostaining and Western blotting) at 4°C overnight. Embryos were washed thoroughly in PBSTB twice, 2 hours each and in PBSTBN for 2 hours. Then 3 times 5 min wash and a wash step in PBSTB at 4°C overnight. Embryos are transferred to respective secondary antibody conjugated with either alkaline phosphate or fluorophores and incubated at 4°C overnight. This was followed by wash steps as above for 30 min and overnight. The staining of embryos was performed as described for Wmish. In case of fluorescence staining, embryos were washed twice for 5 min and left in PBS buffer for further analysis.

Apoptosis/proliferation assay in *Xenopus* embryos

Apoptotic cells were detected using the TUNEL assay (Hensey and Gautier, 1998). TdT (Terminal Deoxynucleotidyl Transferase, 20 u/µl) and Dig-11-dUTP were purchased from Roche. Proliferating cells were identified by detection of phosphorylated histone H3 (PH3)

as described (Saka and Smith, 2001). Rabbit polyclonal anti-phosphohistone H3 (Millipore) was used with a dilution of 1:400. Embryos were then subjected to plastic sections (5 μm) and the PH3-positive cells were counted on each section.

Cell culture and transfections.

HEK 293T cells were used for the Western blot analysis. For pull-down assay approximately $1.0*10^6$ cells were seeded in a 6-well plate and maintained in DMEM supplemented with 10% FCS and 100U/ml penicillin G and streptomycin. All media and sera were purchased from PAA laboratories. For transient transfection, 60% confluent cells were transfected with indicated plasmid DNA polyethyleneimine (3μg in 1μl) (PEI-Sigma Aldrich, 5mg/ml). After ~6h of incubation with the PEI/DNA complex, medium was replaced by fresh serum containing medium. 24h post transfection cells were harvested. The lysates were cooked in loading buffer and loaded on 10% SDS gels for further analysis.

Immunocytochemistry and Western blot

For immunofluorescence, approximately $1.1*10^6$ cells of NIH-3T3 and $1.6*10^6$ cells of SH-SY5Y were seeded on glass coverslips for 24h, fixed in 4% paraformaldehyde, permeabilized with 0.2% Triton X-100 for 5min, and blocked with 2% BSA for 30min. Following the incubation with the primary antibodies for 45min at 37°C, cells were blocked again for 30min and incubated with the secondary antibodies (anti-mouse-Alexa 488, anti–rabbit-Alexa 594, 1:200). Cells were washed three times with PBS after each step except after blocking and were finally desalted in water, dehydrated in 100% ethanol, and mounted on superfrost glass slides with Mowiol containing DAPI (1:1000). For antibody specificity approximately $1.5*10^5$ NIH-3T3 cells seeded, grown to confluency and transfected with different *trim2* and *alix* siRNAs to knockdown the endogenous protein levels. Cells grown overnight were collected and lysed with RIPA buffer containing appropriate inhibitors, cooked in Laemmli buffer and loaded on to SDS gels. The resolved proteins were transferred on to a PVDF membrane and the chemiluminescence reaction was observed on an X-ray film. Antibodies: anti-Trim2, Sigma-Aldrich, SAB4200206, rabbit, IHC 1:400, IF 1:200, WB 1:500; anti-Trim2, Novus Biologicals, NB100-1218, goat, IF 1:200, WB 1:500; anti-Alix (3A9), Santa Cruz Biotechnology, Inc., SC-53538, mouse, IF 1:200, WB 1:200; anti-Flag, Sigma-Aldrich, F1804, mouse, WB 1:5000; mouse *trim2* siRNA, 5-

GCACCUACGAGUUCUUGUA, mouse; *alix* siRNA, 5-GAACCUAGCAACUGCGUAU from Dharmacon, transfection by Lipofectamine "RNAi max", Invitrogen.

Total RNA extraction, cDNA preparation and semi-quantitative RT-PCR

Total RNA was extracted from snap frozen embryos. Embryos were homogenized in TRIZOL, and phase separated using chloroform. The mixture was centrifuged and re-extracted using chloroform. Total RNA was precipitated using isopropanol and re-suspended in RNase free water. 500 ng total RNA was used for cDNA synthesis using *Protoscript II RTase* (NEB) and random primers following manufacturer's protocol. Semi-quantitative RT-PCR was performed using intron spanning primer pairs (*trim2*-fwd, 5'-CCCGGACGGTAGTGTTACTG-3', *trim2*-rev, 5'-GTAGTTGACCTGGGGACCTG-3'). Annealing temperatures were 59 °C for both, 29 cycles respectively. *Histone h4* (*h4*-fwd, 5'-CGGGATAACATTCAGGGTATCACT-3', *h4*-rev, 5'-ATCCATGGCGGTAACTGTCTTCCT-3') was used to control the input mRNA (56 °C, 26 cycles).

GST-Pulldown and LC-MS/MS Mass Spectrometry

Xenopus trim2 was cloned into pGEX4-T1 vector. Fifty micrograms of bacterially expressed and purified GST or GST-Trim2 was added to 1mL (1 mg protein) lysate and after 1h at 4°C under continuous rotation, 50µL GSH-Sepharose beads were added to the mixture. Further 60min of incubation, the beads were washed three times with IP lysis buffer and once with 0.1mM Tris, pH7.4. Proteins were eluted with 2× Laemmli buffer, separated by SDS/PAGE, and analysed by Western blot. GST-Trim2 as a bait was applied on *Xenopus* embryonic lysates (NF stage 30-36) followed by affinity enriched LC-MS/MS on an LTQ Orbitrap instrument[32]. Three independent biological replicates were analysed. Proteins detected were evaluated based on the intensities of the MS signals and spectral counts to assess enrichment of protein interactions with GST-Trim2 relative to GST alone. First, proteins are required to be reproducibly present, detected by at least five spectral counts. Second, proteins showing less than 100-fold spectral count enrichment over proteins co-isolated with GST alone are deemed nonspecific and are excluded. Third, base value for student t-test with a significance of 10^{-5} is set as standard (Table 1).

Alignment, Phylogeny, Synteny

Fasta sequences for the protein families analysed were obtained by Blast tool (http://blast.ncbi.nlm.nih.gov) and aligned using T-Coffee and Box shade tool (http://tcoffee.vital-it.ch/apps/tcoffee/index.html). A phylogenetic tree of the proteins was generated through maximum-likelihood using one-click mode (http://phylogeny.lirmm.fr/phylo_cgi/index.cgi). The synteny analysis is based on data derived with the help of metazome v3.2 (https://metazome.jgi.doe.gov/pz/portal.html). The individual gene sequences and the corresponding information regarding *Xenopus laevis* gene loci were obtained from Xenbase (http://gbrowse.xenbase.org) and depicted accordingly.

Statistical Analysis

Chi square test of homogeneity examines the extent to which the occupied variables for a four-field table deviate from an expected, homogeneous distribution. Unpaired Chi square distribution of independence was used to test the null hypothesis. P-values were deduced from the abundance values of the replicates of independent biological samples. Significance of P value was set at $p<0.001$ and degrees of freedom (df) n-1. Null hypothesis is rejected, if the chi square is greater than the value in the chi-square table with $p \leq 0.001$ and 1 degree of freedom, then the null hypothesis of independence is rejected.

References

1 Borden, K. L. B. RING domains: master builders of molecular scaffolds? *Journal of molecular biology* **295**, 1103-1112 (2000).

2 Metzger, M. B., Pruneda, J. N., Klevit, R. E. & Weissman, A. M. RING-type E3 ligases: Master manipulators of E2 ubiquitin-conjugating enzymes and ubiquitination. *Biochimica et Biophysica Acta (BBA) - Molecular Cell Research* **1843**, 47-60, doi:10.1016/j.bbamcr.2013.05.026 (2014).

3 Ohkawa, N. *et al.* Molecular cloning and characterization of neural activity-related RING finger protein (NARF): a new member of the RBCC family is a candidate for the partner of myosin V. *Journal of Neurochemistry* **78**, 75-87, doi:10.1046/j.1471-4159.2001.00373.x (2001).

4 Balastik, M. *et al.* Deficiency in ubiquitin ligase TRIM2 causes accumulation of neurofilament light chain and neurodegeneration. *Proceedings of the National Academy of Sciences* **105**, 12016-12021 (2008).

5 Khazaei, M. R. *et al.* The E3-ubiquitin ligase TRIM2 regulates neuronal polarization: Function of TRIM2 for axon outgrowth. *Journal of Neurochemistry* **117**, 29-37, doi:10.1111/j.1471-4159.2010.06971.x (2011).

6 Thompson, S. *et al.* Identification of a Novel Bcl-2-interacting Mediator of Cell Death (Bim) E3 Ligase, Tripartite Motif-containing Protein 2 (TRIM2), and Its Role in Rapid Ischemic

Tolerance-induced Neuroprotection. *Journal of Biological Chemistry* **286**, 19331-19339, doi:10.1074/jbc.M110.197707 (2011).

7 Schonrock, N., Humphreys, D. T., Preiss, T. & Götz, J. Target Gene Repression Mediated by miRNAs miR-181c and miR-9 Both of Which Are Down-regulated by Amyloid-β. *Journal of Molecular Neuroscience* **46**, 324-335, doi:10.1007/s12031-011-9587-2 (2012).

8 Ylikallio, E. *et al.* Deficiency of the E3 ubiquitin ligase TRIM2 in early-onset axonal neuropathy. *Human Molecular Genetics* **22**, 2975-2983, doi:10.1093/hmg/ddt149 (2013).

9 Dikic, I. ALIX-ing phospholipids with endosome biogenesis. *BioEssays* **26**, 604-607, doi:10.1002/bies.20068 (2004).

10 Katoh, K. *et al.* The ALG-2-interacting Protein Alix Associates with CHMP4b, a Human Homologue of Yeast Snf7 That Is Involved in Multivesicular Body Sorting. *Journal of Biological Chemistry* **278**, 39104-39113, doi:10.1074/jbc.M301604200 (2003).

11 Martin-Serrano, J., Yaravoy, A., Perez-Caballero, D. & Bieniasz, P. D. Divergent retroviral late-budding domains recruit vacuolar protein sorting factors by using alternative adaptor proteins. *Proceedings of the National Academy of Sciences* **100**, 12414-12419, doi:10.1073/pnas.2133846100 (2003).

12 von Schwedler, U. K. *et al.* The Protein Network of HIV Budding. *Cell* **114**, 701-713, doi:10.1016/S0092-8674(03)00714-1 (2003).

13 Schmidt, M. H. H. SETA/CIN85/Ruk and its binding partner AIP1 associate with diverse cytoskeletal elements, including FAKs, and modulate cell adhesion. *Journal of Cell Science* **116**, 2845-2855, doi:10.1242/jcs.00522 (2003).

14 Wu, Y., Pan, S., Luo, W., Lin, S.-H. & Kuang, J. Hp95 promotes anoikis and inhibits tumorigenicity of HeLa cells. *Oncogene* **21**, 6801-6808, doi:10.1038/sj.onc.1205849 (2002).

15 Mahul-Mellier, A. L. Alix, Making a Link between Apoptosis-Linked Gene-2, the Endosomal Sorting Complexes Required for Transport, and Neuronal Death In Vivo. *Journal of Neuroscience* **26**, 542-549, doi:10.1523/JNEUROSCI.3069-05.2006 (2006).

16 Trioulier, Y. *et al.* Alix, a Protein Regulating Endosomal Trafficking, Is Involved in Neuronal Death. *Journal of Biological Chemistry* **279**, 2046-2052, doi:10.1074/jbc.M309243200 (2004).

17 Zhao, C. *et al.* The role of Alix in the proliferation of human glioma cells. *Human Pathology* **52**, 110-118, doi:10.1016/j.humpath.2015.09.046 (2016).

18 Chen, B., Borinstein, S. C., Gillis, J., Sykes, V. W. & Bogler, O. The Glioma-associated Protein SETA Interacts with AIP1/Alix and ALG-2 and Modulates Apoptosis in Astrocytes. *Journal of Biological Chemistry* **275**, 19275-19281, doi:10.1074/jbc.M908994199 (2000).

19 Hemming, F. J., Fraboulet, S., Blot, B. & Sadoul, R. Early increase of apoptosis-linked gene-2 interacting protein X in areas of kainate-induced neurodegeneration. *Neuroscience* **123**, 887-895, doi:10.1016/j.neuroscience.2003.10.036 (2004).

20 Martinez, A. *et al.* Quantitative proteomic analysis of Parkin substrates in Drosophila neurons. *Molecular Neurodegeneration* **12**, doi:10.1186/s13024-017-0170-3 (2017).

21 Laporte, M. H. *et al.* Alix is required during development for normal growth of the mouse brain. *Scientific Reports* **7**, 44767, doi:10.1038/srep44767 (2017).

22 Gervasi, C., Stewart, C.-B. & Szaro, B. G. Xenopus laevis peripherin (XIF3) is expressed in radial glia and proliferating neural epithelial cells as well as in neurons. *The Journal of Comparative Neurology* **423**, 512-531, doi:10.1002/1096-9861(20000731)423:3<512::AID-CNE13>3.0.CO;2-1 (2000).

23 Pfirrmann, T., Lokapally, A., Andréasson, C., Ljungdahl, P. & Hollemann, T. SOMA: A Single Oligonucleotide Mutagenesis and Cloning Approach. *PLoS ONE* **8**, e64870, doi:10.1371/journal.pone.0064870 (2013).

24 Tocchini, C. & Ciosk, R. TRIM-NHL proteins in development and disease. *Seminars in Cell & Developmental Biology* **47-48**, 52-59, doi:10.1016/j.semcdb.2015.10.017 (2015).
25 van Diepen, M. T. *et al.* The molluscan RING-finger protein L-TRIM is essential for neuronal outgrowth. *Molecular and Cellular Neuroscience* **29**, 74-81, doi:10.1016/j.mcn.2005.01.005 (2005).
26 Che, S. *et al.* Identification and Cloning of Xp95, a Putative Signal Transduction Protein in Xenopus Oocytes. *Journal of Biological Chemistry* **274**, 5522-5531, doi:10.1074/jbc.274.9.5522 (1999).
27 Missotten, M., Nichols, A., Rieger, K. & Sadoul, R. Alix, a novel mouse protein undergoing calcium-dependent interaction with the apoptosis-linked-gene 2 (ALG-2) protein. *Cell death and differentiation* **6**, 124-129 (1999).
28 Vito, P., Pellegrini, L., Guiet, C. & D'Adamio, L. Cloning of AIP1, a Novel Protein That Associates with the Apoptosis-linked Gene ALG-2 in a Ca ²⁺ -dependent Reaction. *Journal of Biological Chemistry* **274**, 1533-1540, doi:10.1074/jbc.274.3.1533 (1999).
29 Strack, B., Calistri, A., Craig, S., Popova, E. & Göttlinger, H. G. AIP1/ALIX Is a Binding Partner for HIV-1 p6 and EIAV p9 Functioning in Virus Budding. *Cell* **114**, 689-699, doi:10.1016/S0092-8674(03)00653-6 (2003).
30 Nieuwkoop, P. D. & Faber, J. *Normal table of Xenopus laevis (Daudin)*. (North Holland, Amsterdam., 1967).
31 Harland, R. M. in *Methods in Cell Biology* Vol. 36 685-695 (Elsevier, 1991).
32 Keilhauer, E. C., Hein, M. Y. & Mann, M. Accurate Protein Complex Retrieval by Affinity Enrichment Mass Spectrometry (AE-MS) Rather than Affinity Purification Mass Spectrometry (AP-MS). *Molecular & Cellular Proteomics* **14**, 120-135, doi:10.1074/mcp.M114.041012 (2015).

Acknowledgements: We thank Dr. Christian Ihling (MLU Halle-Wittenberg) for the mass spectroscopic analysis. *Xenopus* neurofilament light chain (*nefl*) plasmid was a gift from Prof. Ben G Szaro (University of Albany).

	Gene Name	**Gene Symbol**	**Accession Number**	**P value**	**Abundance**
1	phosphoribosylglycinamide formyltransferase, phosphoribosylglycinamide synthetase, phosphoribosylaminoimidazole synthetase	*gart*	NM_001099882	1.99E-09	99753557.71
2	phosphoglucomutase 3	*pgm3*	NM_001087415	2.27E-08	54689274.29
3	ATP synthase F1 subunit gamma	*atp5f1c*	NM_001091279	4.45E-08	103066222.90
4	serpin family A member 6	*serpina6*	NM_001085634	1.71E-07	6.16
5	programmed cell death 6-interacting protein	*pdcd6ip/ alix*	NM_001088401	9.27E-07	127818404.90
6	microsomal glutathione S-transferase 3	*mgst3*	NM_001092866	4.76E-06	131.32
7	ribosomal protein L27a	*rpl27a*	NM_001086720	6.90E-06	10.04
8	ATP synthase F1 subunit gamma	*atp5f1c*	NM_001087012	8.92E-06	647.69
9	voltage-dependent anion channel 3	*vdac3*	NM_001091887	1.07E-05	3.32
10	glyceraldehyde-3-phosphate dehydrogenase	*gapdh*	NM_001087098	1.39E-05	13.55
11	endoplasmic reticulum oxidoreductase alpha	*ero1a*	BC077754	1.69E-05	19.45
12	ribonucleotide reductase M1	*rrm1*	NM_001090843	1.93E-05	7.53
13	CNDP dipeptidase 2	*cndp2*	NM_001093621	2.24E-05	212.52
14	proteasome 26S subunit, non-ATPase 8	*psmd8*	NM_001091280	5.76E-05	31524095.71
15	heat shock protein family D (Hsp60) member 1	*hspd1*	NM_001086185	7.51E-05	10.39
16	glutathione S-transferase theta 1	*gstt1*	NM_001091734	1.05E-04	133086476.60
17	adenylosuccinate lyase	*adsl*	NM_001087124	1.20E-04	49220858.57
18	tripartite motif containing 2	*trim2*	XM_018236814	1.66E-04	998526258.90
19	acetyl-CoA acyltransferase 2	*acaa2*	NM_001087263	2.76E-04	21.10
20	tripartite motif containing 2	*trim2*	NM_001092023	3.28E-04	63.35
21	aspartyl-tRNA synthetase	*dars*	NM_001092021	3.60E-04	39632768.86
22	ribosomal protein L8	*rpl8*	NM_001086996	5.45E-04	110.75
23	bifunctional purine biosynthesis protein	*purh*	XM_018238947	6.60E-04	139875184.60
24	cytochrome c-1	*cyc1*	NM_001096171	6.63E-04	13.38
25	phosphorylase, glycogen; brain	*pygb*	XM_018259948	8.65E-04	43701513.71
26	proteasome 26S subunit, non-ATPase 13	*psmd13*	NM_001094267	1.02E-03	21.91
27	glutamyl-prolyl-tRNA synthetase	*eprs*	NM_001127874	1.09E-03	22483025.14
28	regulator of chromosome condensation 2	*rcc2*	NM_001095936	1.14E-03	96777897.14
29	ribosomal protein, large, P0	*rplp0*	NM_001086665	1.15E-03	7.93
30	eukaryotic translation initiation factor 5A	*eif5a*	NM_001087067	1.46E-03	5.92

Table 1. List of proteins identified in the interactome from LC-MS/MS analysis. Genes arranged according to decreasing P values. Alix (row 5) protein with one of the highest P values and abundance. Note, the identification of Trim2 in the interactome (row 18, 20).

Supporting Information

Interplay of TRIM2 E3 ubiquitin ligase and Alix/ESCRT complex: Control of developmental plasticity during early neurogenesis.

Ashwin Lokapally, Herbert Neuhaus, Juliane Herfurth and Thomas Hollemann

Institute for Physiological Chemistry, Martin-Luther University Halle-Wittenberg, Hollystrasse1, D-06114 Halle, Germany

Supplementary File

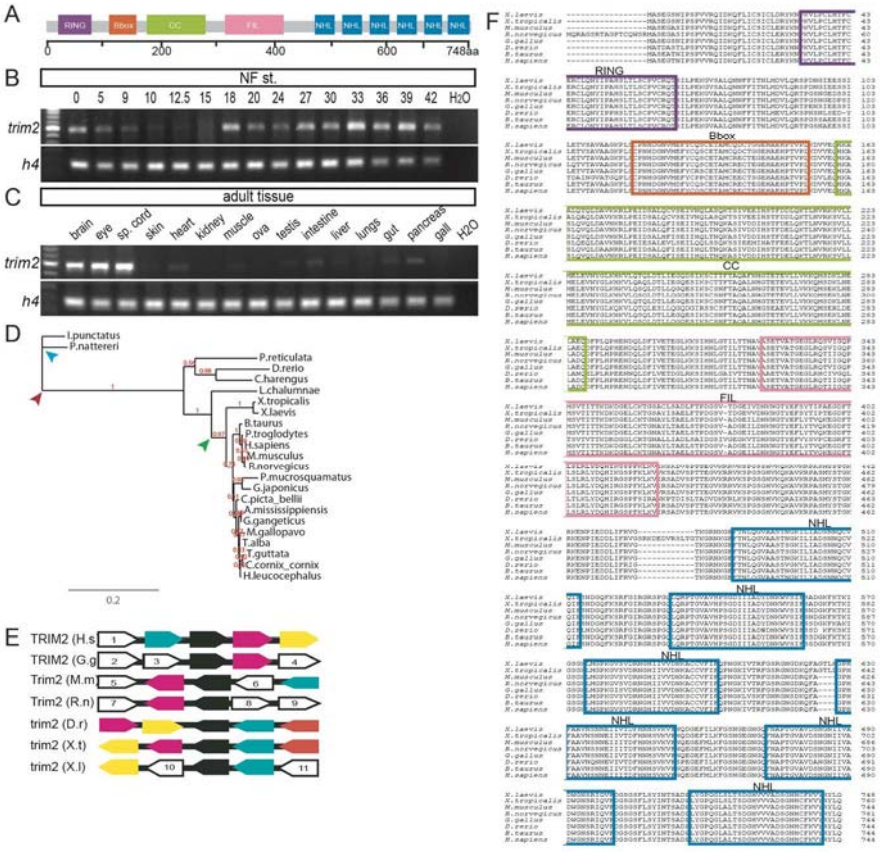

Supplementary figure 1. (A) *Xenopus* Trim2 protein consists of 748 amino acids and is organized in domains containing a single RING zinc finger, two B-box zinc fingers, a single coiled-coiled, Filamin/ABP 280 domain and six NHL repeats. (B) Semi-quantitative RT-PCR

analysis on ascending developmental stages. Maternal expression of *trim2* is observed followed by gradual decrease in expression by gastrulation (NF stage 10) and increasing again. Strong expression at neurulation (NF stage 18) until the latest stages analyzed (NF stage 42) in a gradually increasing manner. Expression of *histone H4* was monitored to control total RNA input. (C) Semi-quantitative RT-PCR analysis of *trim2* expression in adult tissues. Brain, eye, spinal cord showed strong expression, while skin, heart, kidney, muscle, testis, intestine and pancreas show weak expression of *trim2*. (D) Phylogenetic analysis: An evolutionary rooted tree is constructed based on maximum likelihood and bootstrap analysis. The branch length is proportional to the number of substitutions per site. The numbers in red next to nodes represents bootstrap support values. Red arrow indicates the root of the tree, the blue arrow the out-group and the green arrow indicates the common ancestral node between mammals and amphibians. The bar at the bottom of the phylogram indicates the evolutionary distance, to which the branch lengths are scaled based on the estimated divergence. There is a relatively very little divergence observed over time. (E) Synteny organization of *Trim2/trim2*: The chromosomal localization of the gene encoding *trim2* is conserved in mammals. On lower vertebrates the locus appeared reserved but grossly conserved. Each arrow stands for a single gene. The arrowhead indicates the direction of the ORF. Orthologues are marked with identical colors. *trim2* (black arrow) is present in all species analyzed. Upstream *trim2* is flanked by the same gene with minor exceptions. While downstream except for mammals *trim2* is flanked by the same gene. Arrow colors; black: *trim2*, red: *meiotic nuclear divisions 1/mnd1*, yellow: *transmembrane 131 like/tmem131l*, turquoise: *FH2 domain containing 1/fhdc1*, orange: *ADP ribosylation factor interacting protein 1 /arfip1*, white 1-10: yet uncharacterized proteins. (F) Comparison of amino acid sequences of TRIM2/Trim2. *H. sapiens* (GenBank Accession no. NP_001123539), *B. taurus* (GenBank Accession no. NP_001077204), *M. musculus* (GenBank Accession no. NP_109631), *R. norvegicus* (GenBank Accession no. NP_001102022), *G. gallus* (GenBank Accession no. NP_001244243), *D. rerio* (GenBank Accession no. NP_001014393), *X. tropicalis* (GenBank Accession no. NP_001005680), *X. laevis* (GenBank Accession no. NP_001085492). Conserved domains are indicated by colored boxes according to A.

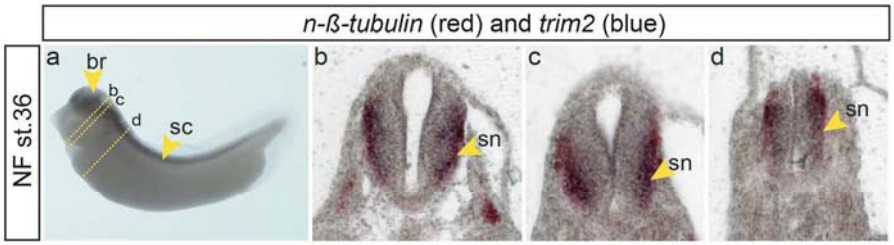

Supplementary figure 2. Whole mount double *in situ* expression of *trim2* and *n-ß-tubulin* at NF stage 35/36. (a) lateral view. (b-d) transverse section of midbrain, hindbrain, and the spinal cord region. *trim2* is mainly expressed in differentiated neurons (e.g. motor neurons) like *n-ß-tubulin*.

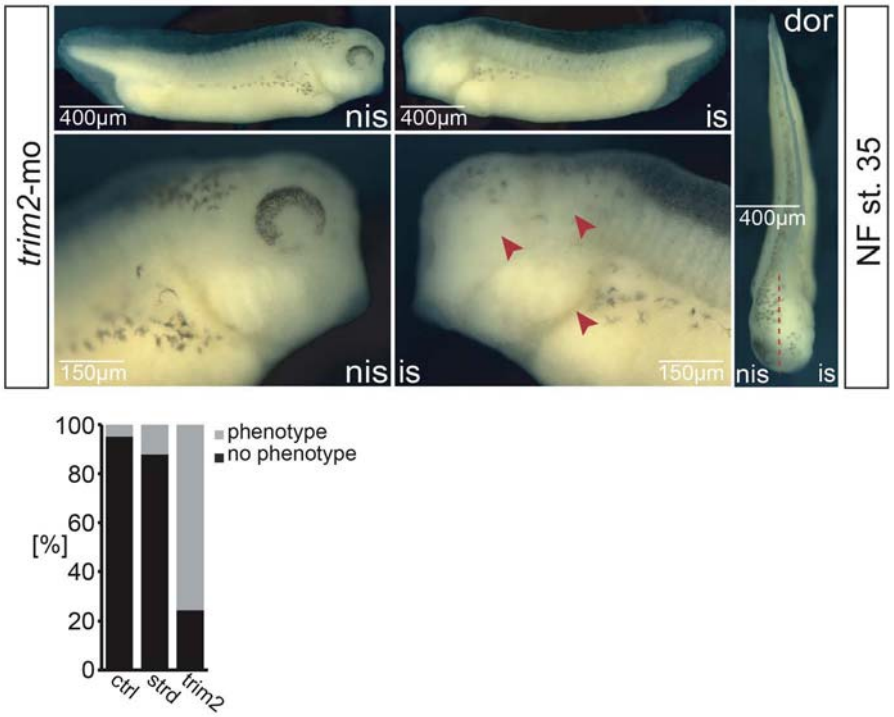

Supplementary figure 3. Phenotype of *trim2* morphants. Upper panel, whole embryo, lateral views, non-injected side (nis) and injected side (is). Bottom panel enlarged cranial lateral view. Red arrowhead indicates a suppression of proper head development (eye, otic vesicle and branchial arches) and pigmentation. The bar plot represents the survival percentage of *trim2*-

morphants compared to un-injected control and standard morpholino injected embryos. Survival rate was 24% for *trim2*-morphants. Total injected (ctrl N=186 embryos, *strd*-mo N=288 embryos, *trim2*-mo N=254). Survived (ctrl N=177 embryos, *strd*-mo N=253 embryos, *trim2*-mo N=62). Scales as indicated.

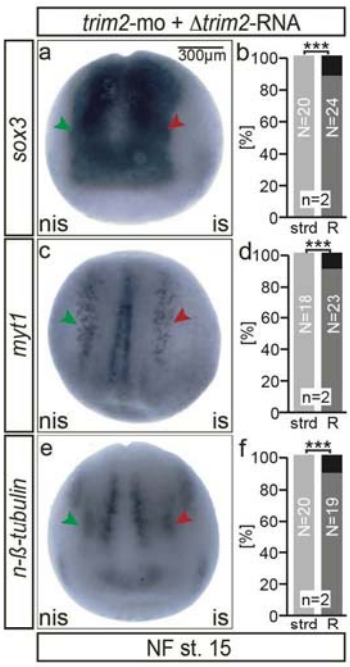

Supplementary figure 4. Phenotypic rescue of *trim2* morpholino injected embryos. Synthetic *Xenopus trim2* RNA (*Δtrim-2*), which did not contain a complementary sequence of the morpholino, was injected long with *trim2* morpholino into one cell of a two-cell stage embryo. (a) The expanded expression of *sox3*, (b, c) and the medial, intermediate and longitudinal stripes of *myt1* and *n-ß-tubulin* expressing cells were rescued on the injected side. Red arrows indicate the rescued side. (b, d, f) The percentage of embryos rescued (*sox3 strd*-mo N=20 embryos, *trim2*-mo N=24 embryos, p=*** 7.21E-09; *myt1* strd-mo N=18 embryos; *trim2*-mo N=23 embryos; p=6.46E-09; *n-ß-tub* strd-mo N=20 embryos; *trim2*-mo N=19 embryos; p=1.78E-08, unpaired χ^2 test). Scale as indicated.

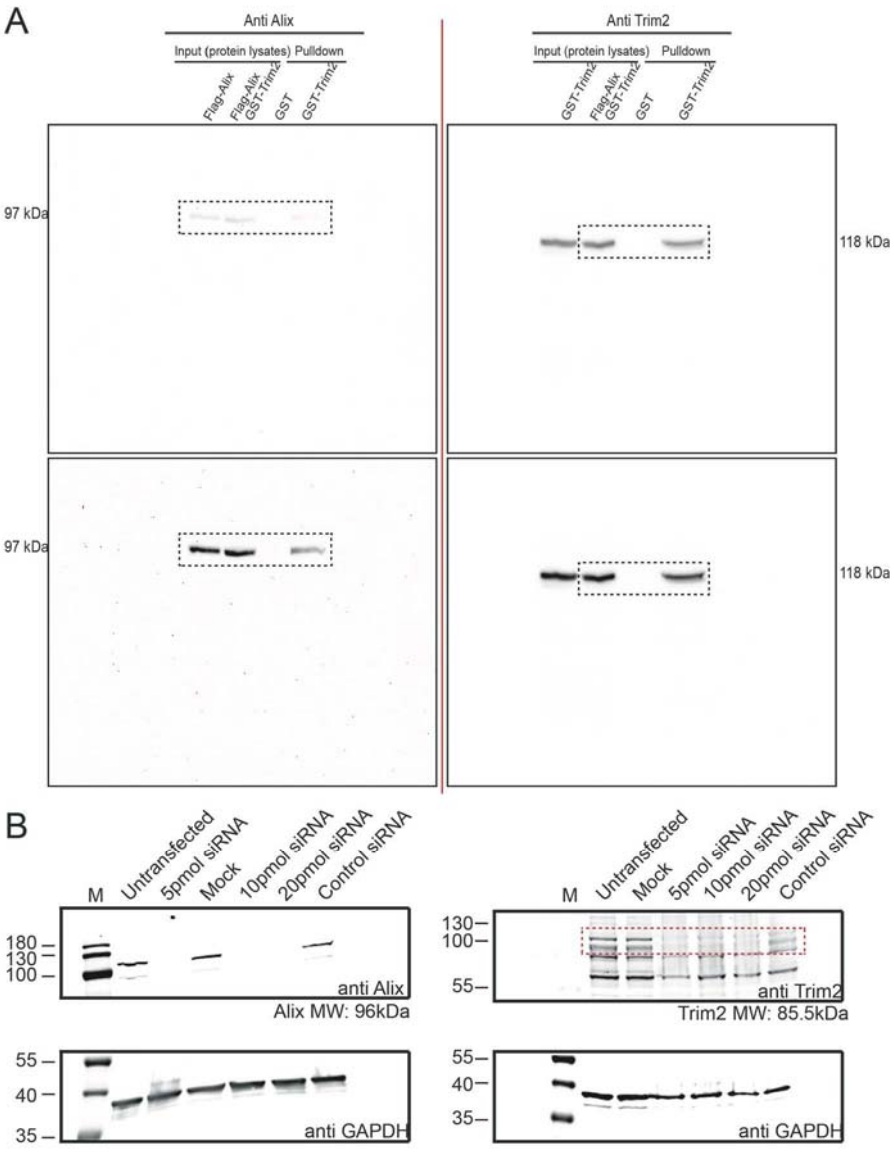

Supplementary figure 5. (A) Uncropped blots of the GST pull-down assay (Fig.6B) at different exposure times. Blot left of red line probed against anti-Alix and the right side against anti-Trim2. Dotted lines within the blot represent lanes. The rectangles with dashed lines indicate the presented detail in figures 5b. The GST-Trim2 lane was loaded as a positive control for the ab detection only. (B) Verification of antibody specificity by siRNA knockdown on of

Alix and *Trim2* in NIH-3T3 cells through WB. Left – upper blot using anti-Alix antibody. 3 different concentrations of siRNA were used. All 3 concentrations showed a clear knockdown of Alix against non-transfected, mock and control siRNA. Right – upper blot using anti-Trim2 antibody. Protein bands corresponding to Trim2 protein are boxed in red dotted line. A loss of protein expression in the siRNA knockdown cells was detected. Lower blots, loading control by monitoring GAPDH protein content using an anti-GAPDH antibody.

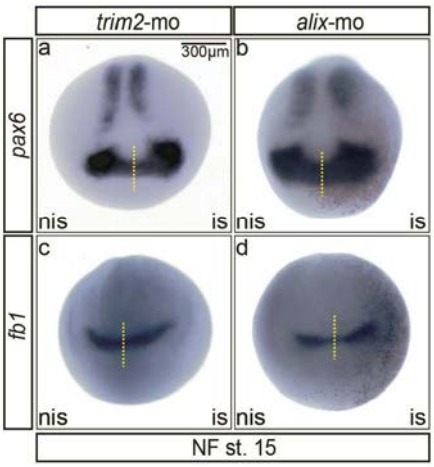

Supplementary figure 6. Comparison of whole-mount *in situ* expression pattern of early forebrain markers upon *trim2* and *alix* knock-down embryos at NF stage 15. Injection of both morpholinos resulted in almost identical alteration of marker gene expression. (a-b) Widened expression for *pax6* at the prospective forebrain and eye field region on the injected side in both *trim2* and *alix* morphants was observed. (c-d) forked head box G1 (bf1) also displayed a relatively expanded band in *trim2* and *alix* morphants. Yellow dotted line indicates the midline.

Movie legends

Movie 1. Sensory and motor function assessment in *trim2* knock-down embryos. *trim2*-morpholino injected into one blastomere at the two-cell stage. NF stage 36 embryos monitored for motility and sensory defects. Inset: control non-injected embryo. Control non-injected embryos N=100 embryos, *trim2-mo* N=298 embryos, p=*** (2.9E-79), unpaired χ^2 test.

Movie 2. Phenotypic rescue of *trim2* knock-down embryos. Synthetic *Xenopus trim2* RNA along with *trim2* morpholino was injected into one blastomere of a two-cell stage embryo. NF stage 36 embryos monitored for rescued motility. Inset: control non-injected embryo. Control non-injected embryos N=50 embryos, *trim2-mo* N=47 embryos, p=*** (4.64E-21), unpaired χ^2 test.

Movie 3. Complete loss of motor-sensory function in *trim2* knock-down embryos. *trim2* morpholino was injected either into a one-cell stage embryo or both blastomeres of a two-cell stage embryo. NF Stage 32 embryos monitored for motor-sensory function. Inset: control non-injected embryo. Control non-injected embryos N=20 embryos, *trim2-mo* N=12 embryos, p=*** (1.54E-08), unpaired χ^2 test.

Movie 4. Sensory and motor function assessment in *alix* knock-down embryos. *alix*-morpholino injected into one blastomere at the two-cell stage. NF stage 32 embryos monitored for motility and sensory function. Inset: control non-injected embryo. Control non-injected embryos N=30 embryos, *alix*-mo N=45 embryos, p=*** (2.9E-79), unpaired χ^2 test.

4.2 Manuscript 2: Hedgehog-dependent E3-ligase Midline1 regulates ubiquitin-mediated proteasomal degradation of Pax6 during visual system development

PNAS

Hedgehog-dependent E3-ligase Midline1 regulates ubiquitin-mediated proteasomal degradation of Pax6 during visual system development

Thorsten Pfirrmann[a,1], Enrico Jandt[a,1], Swantje Ranft[a,b], Ashwin Lokapally[a], Herbert Neuhaus[a], Muriel Perron[c], and Thomas Hollemann[a,2]

[a]Institute for Physiological Chemistry, University of Halle-Wittenberg, 06114 Halle, Germany; [b]Gynecological Hospital, University Medical Center Mannheim, 68167 Mannheim, Germany; and [c]Paris-Saclay Institute of Neuroscience, CNRS, Univ Paris Sud, Université Paris-Saclay, 91405 Orsay, France

Edited by Richard M. Harland, University of California, Berkeley, CA, and approved July 19, 2016 (received for review January 16, 2016)

Pax6 is a key transcription factor involved in eye, brain, and pancreas development. Although *pax6* is expressed in the whole prospective retinal field, subsequently its expression becomes restricted to the optic cup by reciprocal transcriptional repression of *pax6* and *pax2*. However, it remains unclear how Pax6 protein is removed from the eyestalk territory on time. Here, we report that Mid1, a member of the RBCC/TRIM E3 ligase family, which was first identified in patients with the X-chromosome–linked Opitz BBB/G (OS) syndrome, interacts with Pax6. We found that the forming eyestalk is a major domain of *mid1* expression, controlled by the morphogen Sonic hedgehog (Shh). Here, Mid1 regulates the ubiquitination and proteasomal degradation of Pax6 protein. Accordantly, when Mid1 levels are knocked down, Pax6 expression is expanded and eyes are enlarged. Our findings indicate that remaining or misaddressed Pax6 protein is cleared from the eyestalk region to properly set the border between the eyestalk territory and the retina via Mid1. Thus, we identified a posttranslational mechanism, regulated by Sonic hedgehog, which is important to suppress Pax6 activity and thus breaks *pax6* autoregulation at defined steps during the formation of the visual system.

Xenopus | mid1 | *pax6* | eye development | ubiquitin

Pax6 is an evolutionary highly conserved transcription factor, playing key roles as a potent cell fate determinant in the development of the eye, brain, and pancreas (1–4). Pax6 is a member of the PAX family of transcription factors (5, 6). Pax6 autoregulation was suggested based on mouse genetic experiments (7) and studies regarding the quail, as well as human, promoters (8, 9). Thus, to maintain *pax6* expression, Pax6 protein is required, which has been assumed already from studies of the *Small eye* (*SEY*) mutant mice (10, 11). In humans, heterozygous mutations in *PAX6* cause a wide variety of ocular defects, whereas the homozygous loss results in anophthalmia (12). Not only does the reduction of Pax6 protein levels cause severe developmental defects in the eye, but transgenic mice carrying multiple copies of the human *PAX6* gene also have similar ocular abnormalities as the small eye mice (13, 14). Moreover, in *Drosophila* and in vertebrates like *Xenopus*, overexpression of *pax6* is able to induce the formation of ectopic eyes (15, 16). As a whole, Pax6 is one of the most important regulators of eye development and its function is critically dependent on a temporarily and quantitatively defined expression level (4).

In *Xenopus*, *pax6* can be detected in all neuroblasts of the developing retina soon after gastrulation. In early tailbud stages, *pax6* is expressed homogenously in all parts of the optic vesicle. In tadpoles, *pax6* is limited to the lens epithelium and later to cells of the inner nuclear layer and the ganglion cell layer. However, *pax6* transcripts are barely detectable in the outer nuclear layer containing photoreceptor cells but clearly visible in the ciliary marginal zone (17, 18). On the one hand, the sharp boundary between the optic cup with *pax6* and the optic stalk region with *pax2* is established by reciprocal transcriptional repression of these two *pax* genes (19, 20). On the other hand, it remains unclear how Pax6 protein is removed from the eyestalk territory on time. Some authors report the regulation of Pax6 activity by posttranslational modifications (21–23), and most interestingly, Tuoc et al. showed that in cortical progenitor cells, Pax6 protein is degraded by the proteasome mediated by Trim11 (24). However, the existence of similar mechanisms leading to the development of the visual system is not known.

The data of our present study show that Midline1 (Mid1) serves as one of these links. *MID1*, a member of the RBCC/TRIM E3 ligase family, was first identified in patients with the X-chromosome–linked Opitz BBB/G (OS) syndrome. Patients suffer from multiple malformations of the ventral midline as a consequence of mutations in the *MID1* gene (25, 26). In previous studies, Mid1 has been described to regulate protein phosphatase 2A (PP2A) stability (27–30). PP2A/α4 is not the only known substrate, because recently it was shown that Mid1 interacts with the GLI regulator Fu, leading to a cytoplasmic retention of GLI3 in cancer cells (31). We show that Mid1 can physically interact with Pax6 leading to the ubiquitination and proteasomal degradation of Pax6 protein. We observe an overlapping expression of *mid1* and *pax6* in early stages of *Xenopus* development. In tadpole stages, *mid1* transcripts are concentrated in the optic stalk territory in contrast to *pax6*. Overexpression of *shh* strongly induces *mid1*, whose expression expands to the whole remaining eye vesicle. Accordingly, when Mid1 levels are knocked down, Pax6 expression is expanded, and eyes are enlarged. Taken together, we

Significance

The first morphological sign of vertebrate eye formation is the appearance of eye vesicles on both sides of the ventral diencephalon, which primarily originate from a uniform Pax6-positive eye field. A key regulator for this process, which coincides with the establishment of the proximo-distal axis of the eye with eyestalk and retina, is the morphogen Shh. Shh induces the expression of *pax2*, which represses *pax6* in the presumptive eyestalk region. Here, we report on the identification of the E3-ligase Mid1, which is induced by Shh and targets transcription factor Pax6 for proteasomal degradation. Our findings might provide insight into a mechanism, in which a morphogen initiates the degradation of a transcription factor to form sharp boundaries of gene expression.

Author contributions: M.P. and T.H. designed research; T.P., E.J., S.R., A.L., H.N., M.P., and T.H. performed research; T.P., E.J., and H.N. contributed new reagents/analytic tools; T.H. analyzed data; and T.H. wrote the paper.

The authors declare no conflict of interest.

This article is a PNAS Direct Submission.

[1]T.P. and E.J. contributed equally to this work.

[2]To whom correspondence should be addressed. Email: thomas.hollemann@medizin.uni-halle.de.

This article contains supporting information online at www.pnas.org/lookup/suppl/doi:10.1073/pnas.1600770113/-/DCSupplemental.

provide evidence that Pax6 is a substrate for Mid1 and insights into how remaining or misaddressed Pax6 protein is cleared from the eyestalk region to properly set the border between the eyestalk territory and the retina at the right time.

Results

Mid1 Expression in Cells of the Forming Optic Stalk Is Under the Control of Shh. We analyzed the expression of *mid1* during *Xenopus laevis* development by whole mount in situ hybridizations (Wmish) on embryos of Nieuwkoop and Faber (NF) stage 24–38 (Fig. 1*A*). While confirming the pattern described by Suzuki et al. (32), a closer look revealed that *mid1* is expressed early in the whole eye vesicle. From the NF stage 32 onward, high levels of *mid1* transcripts were detected in the ventral part of the forming eye and especially within the forming optic stalk (Fig. 1 *A*, *c4–c7* and *d1–d3*). Here, the expression of *mid1* appears similar, although not identical to those described for transcription factors *vax1* or *pax2*, known targets of the hedgehog (hh) pathway (Fig. S1*A*) (33). To analyze whether Hedgehog also regulates *mid1* expression, we injected synthetic *shh* RNA into a single cell of two-cell stage embryos and examined *mid1* expression at tadpole stage. Misexpression of *shh* resulted in an upregulation of the known target, the hh receptor *ptc1* (Fig. 1 *B*, *d–d′* and Fig. S1*B*, nptc1 = 20/27; nctrl = 6/60; P = 1.42E-11) in neural ectoderm. Moreover, *mid1* expression was strongly induced but restricted to the optic cup (Fig. 1 *B*, *a–a′*; nmid1 = 66/81; nctrl = 3/44; P = 1.08E-15) similar to *pax2* (Fig. 1 *B*, *b–b′*; npax2 = 74/83; nctrl = 3/42; P = 4.21E-18), whereas *pax6* was repressed on *shh* RNA injection (Fig. 1 *B*, *c–c′*; npax6 = 86/106; nctrl = 4/51; P = 3.47E-18) (33). Interestingly, Hh-dependent regulation of *mid1* is not mediated by *pax2* because suppression of *pax2* function did not impair *mid1* expression (Fig. 1 *B*, *e–e′*; 8/11 eyes analyzed in section) but resulted in an enlargement of the retina and ectopic *pax6* expression in the eye vesicle (Fig. 1*B*, *f–f′*; 13/16 eyes analyzed in section). Moreover, *pax2* is under the control of *pax6*, because suppression of *pax6* led to an expansion of *pax2* expression into the remaining eye vesicle (Fig. 1 *B*, *g–g″*; npax2 = 7/17; nctrl = 4/47; P = 1.45E-08) and *pax2* RNA injection impaired *pax6* expression as in mice (Fig. 1 *B*, *h–h″* and Fig. S1*C*; npax6 = 9/35; nctrl = 4/47; P = 1.5E-14) (20). Because Mid1 is an E3 ubiquitin ligase, we assume that Mid1 regulates Pax6 expression on a posttranslational level rather than on a transcriptional level like Pax2.

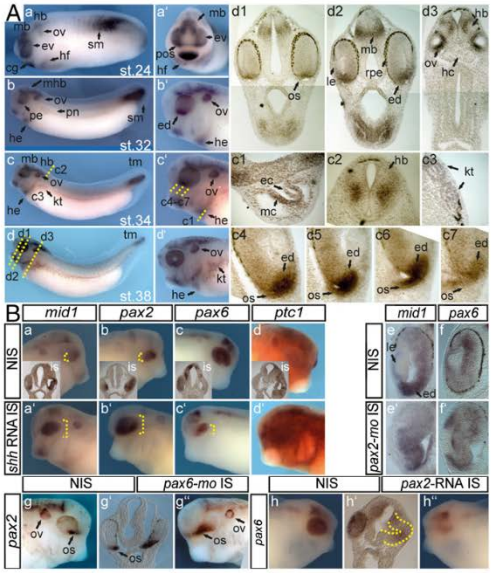

Fig. 1. Mid1 is expressed in cells of the forming optic stalk and induced on *shh* RNA injection. (*A*) *mid1* mRNA expression was assessed by Wmish on *Xenopus laevis* embryos at different NF stages. (*a–d*) Lateral view, (*a′*) cranial view, and (*b′–d′*) lateral view. Twenty-micrometer gelatin/albumin sections at the level of the tadpole's head (*d1–d3*), heart (*c1*), neural tube (*c2*), and pronephric anlage (*c3*). cg, cement gland; ec, endocardium; ed, eye disk; ev, eye vesicle; hd, hindbrain; he, heart; hf, heart field; kt, kidney tubules; mb, midbrain; mc, myocardium; op, olfactory placode; os, optic stalk; ov, otic veside; pnt, pronephric tubule; pos, presumptive os; sm, somites. (*c4–c7*) *mid1* expression in eye stalk region in serial sections. (*B*) Injections were done into one cell of two-cell stage embryos. (*a–d′*) Synthetic *shh*-RNA (500 pg) was injected and Wmish against *mid1*, *pax2*, *pax6*, and *ptc1* was performed as indicated. (*e–f*) *pax2*-mo (2.5 pmol) was injected, and expression of *mid1* and *pax6* was monitored. Shown are transversal sections of the eye at the level of the lens. (*g–g″*) *pax6*-mo (2.5 pmol) was injected, and *pax2* was monitored. Shown are lateral views of the head region and a transversal section of the head region at the level of the optic vesicles (*g′*). (*h–h″*) *pax2* RNA (100 pg) was injected and expression of *pax6* was analyzed.

Mid1 Interacts with Pax6. To investigate whether Mid1 and Pax6 interact physically, we expressed *pax6* alone or together with *mid1* in cell lines. We observed Pax6 within the nucleus and Mid1 predominantly in the cytoplasm (Fig. 2*A*). A physical interaction requires at least a temporary localization in the same cellular compartment. Thus, we generated cytoplasmic and nuclear fractions from transfected HEK293 cells. Western blot revealed that major fractions of Pax6 reside in the nucleus and of Mid1 in the cytoplasm. However, a minor amount of Mid1 protein was detected in the nucleus (Fig. 2*B*). This result suggests that Mid1 and Pax6 are able to interact in vivo in the nucleus. To demonstrate a direct interaction, we performed coimmunoprecipitation experiments. Cotransfection of HEK293 with myc-*mid1* and *pax6*-flag revealed that Pax6 precipitates Mid1 (Fig. 2*C*). Similarly, Mid1 was able to precipitate Pax6 (Fig. S2*A*). To further confirm that Mid1 binds to Pax6, we performed a GST pull-down assay using purified GST-fused Pax6 and lysates of myc-*mid1*–transfected HEK293 cells. As shown in Fig. 2*D*, Mid1 physically interacts with GST-Pax6. To show that Mid1 primes Pax6 for degradation, we cotransfected HEK293 cells with *pax6*-flag and myc-*mid1*. Lysates of these cells show a clear reduction of the Pax6 protein level when Mid1 was present (Fig. 2*E*, lanes 1 and 2). To determine whether the lower Pax6 content is due to proteasomal degradation, we compared Pax6 expression levels in HEK293 cells in the presence or absence of two inhibitors of the proteasomal pathway. Both treatments restored Pax6 in the presence of Mid1, whereas the apoptotic inhibitor Z-VAD-FMK did not, as a control for Mid1 activity in the presence of an arbitrary inhibitor (Fig. 2*E*, lanes 3–5). In addition, overexpression of Mid1 in αTN4-1 cells or in neuralized animal cap explants, which both express Pax6 endogenously, led to a reduction of Pax6 protein level, in particular when Mid1 was forced to enter the nucleus by the fusion of a nuclear localization signal (*mid1nls*; Fig. S2*B*). These results strongly suggest that Mid1 mediates proteasomal degradation of Pax6.

Mid1 Modulates Abundance of Pax6 Protein and Induces Ubiquitination. To further support our finding that Mid1 controls Pax6 degradation, we analyzed the abundance of Pax6 protein in HEK293 cells transfected with *pax6*-flag and either myc-*mid1* or empty vector (EV), using a cycloheximide-chase approach (Fig. 3*A*). Quantification of Pax6 protein relative to β-tubulin contents indicates that the level of Pax6 protein is considerably reduced in cells overexpressing Mid1 (Fig. 3*A*, diagram). Next, we tested whether Pax6 could serve as a substrate for the ubiquitin ligase activity of Mid1.

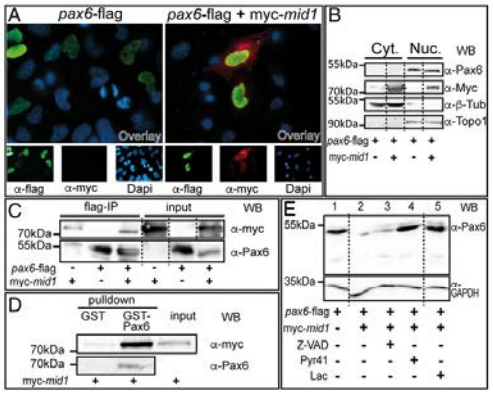

Fig. 2. Mid1 physically interacts with Pax6. (*A*) HeLa cells were transfected with *pax6*-flag alone or combined with myc-*mid1* and analyzed by immunohistochemistry. Nuclei were stained with DAPI. Pictures are shown in false colors: green for Pax6, red for Mid1, blue for nuclei (*Bottom*). (*B*) HEK293 cells were transfected as in *A*. Cytosolic proteins were extracted with hypotonic buffer. Soluble nuclear proteins were extracted from the remaining fraction with high salt buffer. Blot shows Mid1 and Pax6 in the cytosolic (Cyt.) and nuclear (Nuc.) fractions, as well as the reprobes with anti-β-tubulin or anti-topoisomerase 1 antibody to control purity. (*C*) Interaction of Mid1 with Pax6 was assessed by coimmunoprecipitation performed in HEK293. (*Left*) Eluted myc-tagged proteins after immunoprecipitation (upper blot) and precipitated Pax6 (lower blot, reprobed with anti-Pax6 antibody). (*Right*) Blots for the input proteins. (*D*) Interaction of Mid1 and Pax6 was verified by GST using purified GST-Pax6 or purified GST as a control and lysates of HEK293 cells transfected with myc-*mid1*. (*Left*) Eluted myc-tagged proteins after GST pull down (upper blot) and precipitated Pax6 (lower blot, reprobed with anti-Pax6 antibody). (*Right*) Input protein of the lysate. (*E*) *Pax6*-flag was expressed alone or together with myc-Mid1 in HEK293 cells in the presence or absence of the proteasome inhibitor lactacystin (Lac), the E1 activating enzyme inhibitor Pyr41, or the caspase inhibitor Z-VAD-FMK (Z-VAD) as indicated. For loading control, blots were reprobed with an anti-GAPDH antibody.

We looked for ubiquitinated Pax6 in HEK293 cells, overexpressing *pax6*-flag alone or in combination with ubiquitin (his-*ubi*) and myc-*mid1* in the presence of the proteasome inhibitor, MG132. Pax6 was immunoprecipitated from RIPA cell lysates and was analyzed for Ubi-conjugated forms (Fig. 3*B*). Considerable amounts of ubiquitinated protein were detected only with immunoprecipitates from cells transfected with all three components, suggesting that Mid1 mediates ubiquitination of Pax6.

Knockdown of *mid1* Leads to Enlarged Eyes and Overexpression of Pax6 in Vivo. Because Mid1 interacts with Pax6 and controls Pax6 levels in cell culture, we wanted to know if this holds true in *Xenopus* embryos. To suppress *mid1* function, we injected a *mid1* antisense morpholino (*mid1*-mo1) into one cell at the two-cell stage. At NF stage 38, the eyes on the injected sides (IS) appeared larger than on the noninjected side (NIS) and often showed aberrant retinal folds, accompanied by a loss of sharp boundaries of retinal layers ($n = 54/59$; Fig. 4*A* and Fig. S3*A*). In transversal sections of the affected eyes, the outer and inner layers of the retina are morphologically not clearly defined and still express *pax6*. (Fig. 4 *B*, *a*–*a*′). We conclude that Mid1 is necessary for proper eye development, confining the area of Pax6 expression. Additionally we investigated the effect of Mid1 suppression on retinal cell fate specification and therefore analyzed marker gene expression of all retinal layers. We found that injection of *mid1*-mo1 interferes with the ordered expression of all retinal marker genes analyzed. The expression pattern of the ganglion cell marker (*bm3.0*), bipolar (*vsx1*), and horizontal (*prox1*) genes were irregular, whereas the expression of *rhodopsin* expression was reduced slightly (Fig. 4 *B*, *b*–*e*′). Repeating the experiment using a second morpholino (*mid1*-mo2) that targets only *mid1*, allowed to exclude the possibility that the observed increase in eye size is due to knockdown of *mid2*, a close homolog of *mid1*, which is potentially affected by the morpholino used thus far (32). Again, all of the *mid1*-mo2 injected embryos ($n = 212$) displayed a larger eye on the injected side (Fig. 4*C*). These eyes had an ~30% larger volume compared with those on the noninjected side ($n = 25$; $P = 0.001$; Fig. 4 *C*, *c*). To test whether the increased eye size on suppression of *mid1* function was the result of a higher rate of proliferative cells, we compared the number of phospho-histone H3 (pH3)-positive cells in the injected eye area of sections to those of the noninjected side. Remarkably, we counted almost twice as much pH3-positive cells in eyes of *mid1*-mo2 injected embryos compared with the control side (ctrl-mo: $n = 6$; mean 14.4 pH3+ cells per section; *mid1*-mo2: $n = 8$; mean 27.2 pH3+ cells per section; $P = 0.0006$; Fig. 4 *C*, *d*). To rule-out off target effects of the second morpholino, we tested the specificity by coinjecting synthetic *mid1*-RNA (1–2 ng), which cannot be targeted by the morpholino, along with *mid1*-mo2. As a result, *mid1*-mo2 injected embryos were rescued with equal volumes of the eyes on both sides (Fig. S3*B*). To take a closer look on the effect of the *mid1* knockdown on Pax6 protein in retinal cells, we performed immunohistology of cryosections from morphant embryos at NF stage 38. Using an anti-Pax6 antibody, Pax6 was found in the inner part of the inner nuclear layer (INL) and in the ganglion cells of the control side (NIS). However, in *mid1* morphant eyes, Pax6 expression was strongly expanded within the neural retina (Fig. 4*D*). The number of Pax6-expressing cells increased from an average of 67 cells per section on the noninjected side to 130 cells per section on the injected side ($n = 3$; $^*P = 0.03$; Fig. 4 *D*, *c*). Because the retina was enlarged on the injected side, we normalized the number of Pax6-positive cells to the retinal area, and a higher ratio compared with the noninjected side was still measured (Fig. 4 *D*, *d*). These results indicate that an enhanced expression of Pax6 protein in the enlarged eyes is accompanied by a higher rate of cell proliferation in the retinal region on suppression of *mid1* function.

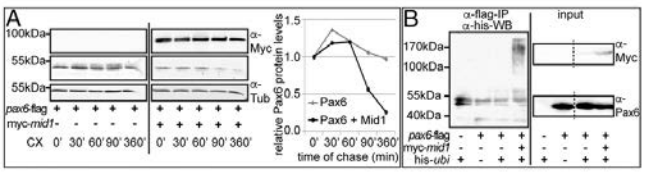

Fig. 3. Mid1 induces ubiquitination and reduces the abundance of Pax6 protein. (*A*) Blots show levels of Pax6, Mid1, and β-tubulin in HEK293 cells after cotransfection on *pax6*-flag expression plasmid and either EV or myc-*mid1* at different time points (min) on cydoheximide block of protein synthesis. Diagram shows the quantified values of Pax6 protein relative to β-tubulin levels in Western blot. Amounts of Pax6 protein before the cydoheximide treatment are designated as 1 (100%). (*B*) In vivo ubiquitination of Pax6 was analyzed by transfection of HEK293 cells with plasmids coding for *pax6*-flag, myc-*mid1*, and his-*ubiquitin* as indicated and anti-his Western blot of proteins eluted after an anti-flag-IP (*Left*). Input of the proteins was verified by Western blot of the corresponding lysates with anti-Myc and anti-Pax6 antibodies, respectively (*Right*).

DEVELOPMENTAL BIOLOGY

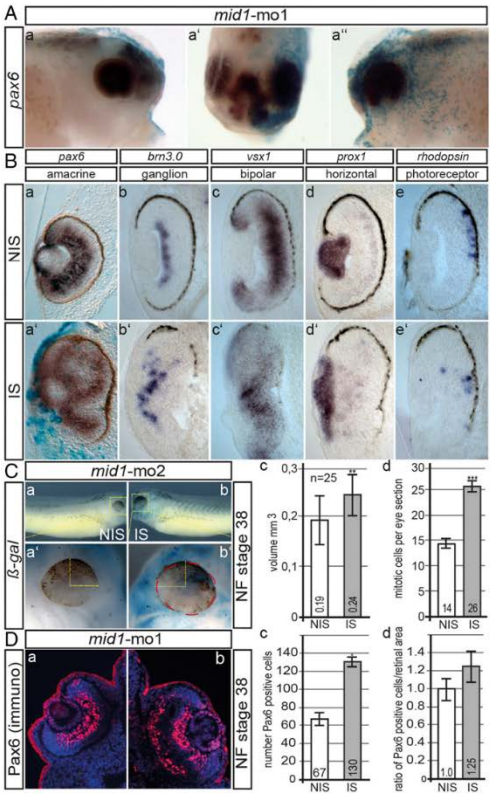

Fig. 4. Mid1 loss of function interferes with eye development. (*A* and *B*) 2.5 pmol of *mid1*-mo1 was injected into one cell at the two-cell stage and analyzed by Wmish at NF stage 38. (*Upper*) Lateral views of head region of noninjected (*a*; NIS) or injected side (*a'*; IS), dorsal view (*a'*). (*B*) Analysis of retinal stratification on *mid1* suppression in transversal sections at the level of the lens using probes against *pax6, brn3.0, vsx1, prox1*, and *rhodopsin*. For better comparison, all images are oriented with the lens to the left. (*C*) Lateral view (*a* and *b*) of NF stage 38 embryos injected with *mid1*-mo2 into one cell at the two-cell stage and 10× enlarged view of the eye region of *a'* and *b'* (*Lower*). All *mid1*-mo2–injected embryos showed an increase in eye size ($n = 212$ *mid1*-mo2 and $n = 126$ ctrl-mo–injected embryos). The graph shows the mean values for 25 embryos (*c*; $^{**}P = 0.001$). Analysis of cell proliferation of *mid1*-mo2–injected embryos. The number of phospho-histone H3 (pH3) positive cells were counted and compared. (*d*; ctrl-mo: six embryos, mean 14.4 pH3+ cells per section; *mid1*-mo2: eight embryos, mean 27.2 pH3+ cells per section; $^{***}P = 0.0006$). (*D*) Pax6 immunoreactivity in cryosections on *mid1*-mo1 injection. The number of Pax6-positive cells per sections within the retinal region was counted for both sides of two embryos, and the area of the total retina was estimated. The numbers of Pax6-positive cells from sections of three *mid1*-mo1–injected embryos were counted (*c*; $^{*}P = 0.03$); the numbers of Pax6-positive cells relative to the area of the retina is shown in the right diagram (*d*). The value for the noninjected side was set to 1.

Targeted Overexpression of *mid1* in Retinal Precursor Cells Shifts the Ratio of Bipolar and Photoreceptor Cells. Because Pax6 has been shown to be required for retinal cell-fate determination (4), we investigated direct cell autonomous effects of Mid1 in a clonal analysis of the progeny of human or *Xenopus tropicalis mid1* transfected cells following in vivo lipofection experiments. Compared with control embryos, which were lipofected with GFP alone, *mid1*-lipofected embryos showed a significant increase in the proportion of photoreceptor cells (human *mid1*, $P < 0.1$; *X. tropicalis mid1*, $P < 0.01$). In the same time, the proportion of bipolar cells was decreased by almost 30% ($P < 0.01$), whereas the proportion of ganglion, amacrine, horizontal, and Müller cells was not significantly changed (Fig. 5*B* and Fig. S4). Moreover, colipofection of *pax6* and *mid1* rescued the *mid1* induced change in the proportion of retinal cell types (Fig. 5*B*). These data suggest that the increased proportion of photoreceptors observed upon Mid1 lipofection is due to a decrease in Pax6 expression.

Discussion

In this study, we examined whether the E3-Ligase Mid1 can lower Pax6 protein levels. We provide evidence supported by gain- and loss-of-function experiments that Mid1 mediates polyubiquitination of Pax6. We also demonstrate that *mid1* expression during eye development is in part mediated by the morphogen Shh, implicating a further level of control conducted by Shh on the development of the visual system.

Recent studies reveal new insights into mechanisms that posttranscriptionally regulate spatiotemporal Pax6 protein levels beyond the well-characterized genetic regulatory circuits (6, 22, 34). Tuoc et al. (24) reported that in the developing cortex Pax6 protein is specifically degraded by the proteasome after ubiquitination by Trim11 and Pax6 regulates *trim11* transcription, a RING finger E3 ligase, which is not present in the *Xenopus* genome. This dual mechanism ensures the adjustment of a physiological level of Pax6 protein within tight limits, which is likewise important for eye development. Initially, Pax6 is required for the specification of the eye prospective retinal field, including the lens placode (8, 10). Later, Pax6 needs to be removed from various territories of the forming visual system, e.g., for a proper formation of the eyestalk and the differentiation of retinal precursor cells. Moreover, Pax6 can act autonomously in the lens surface ectoderm and in the optic vesicle (10, 35). Thus, concerning timing and level of expression, Pax6 is a tightly controlled transcription factor for the early and late stages of retina

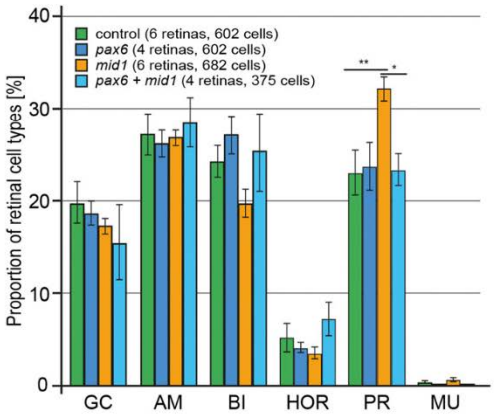

Fig. 5. Targeted overexpression of *mid1* affects fate of retinal precursor cells, which can be reversed by *pax6* coexpression. Cell fate analysis at stage 41 following overexpression of the indicated constructs by in vivo lipofection at the neurula stage. GFP was used as a tracer to visualize transfected cells. The error bars represent SEM. AM, amacrine cells; BI, bipolar cells; GC, ganglion cells; HOR, horizontal cells; MU, Müller cells; PR, photoreceptor cells.

and lens development (4, 35–37). Our present findings provide insights into how Pax6 protein can be removed specifically from the eyestalk territory. Several lines of evidence point to Mid1 (Trim18), which mediates the proteasomal degradation of Pax6 in time and space. We were able to show that Pax6 protein levels are reduced in those cells, which concordantly express Mid1. The degradation of Pax6, mediated by Mid1, can be suppressed by treatment of the cells with proteasome inhibitors. In the cell, the majority of either Mid1 or Pax6 protein is present in different cellular compartments. Mid1 is mainly located at microtubules in the cytoplasm and Pax6 reside in the nucleus (38). We show that a minor fraction of Mid1 protein is in the nucleus allowing Mid1 and Pax6 to interact physically as indicated by coimmunoprecipitation and GST-pull-down experiments.

In 1997, *MID1* was identified as the causative gene for X-linked Opitz G/BBB syndrome (OS) (26). Mutations in *MID1* led to defects in the development of midline derived structures with a wide range of anomalies. The major activity of MID1 was related to ubiquitination and proteasome dependent degradation of PP2A and/or α4 protein (27). Recent studies revealed that additional proteins interact with Mid1 in vitro, which are involved in mRNA transport and translation or microtubule dynamics and might be part of the syndrome, affecting patients with OS (28, 29, 32). Our studies present evidence that part of Mid1 function in vertebrates is the control of Pax6 protein levels during visual system development. We could show that in *Xenopus*, early *mid1* expression overlaps with early *pax6* expression (optic vesicle). Shortly after, expression of *pax6* and of *mid1* appears to be almost exclusive with *mid1* in the forming eyestalk and *pax6* in the retina. In mouse embryos, *mid1* is expressed in the outer nuclear layer (39), whereas *pax6* expression becomes mainly restricted to the inner nuclear layer of the eyecup. When we suppressed *mid1* function by injecting anti-*mid1* morpholinos into embryos, we observed a significant increase in the size of the embryonic eyes due to a higher rate of cell proliferation. The enlargement of the optic vesicles led to folds of nonregular stratified retina with ectopic *pax6* expression. In line with these results, the inhibition of *pax2* led to a similar, *mid1*-like eye phenotype, whereas suppression of *pax6* led to smaller eyes but enlarged *pax2* domains of expression. Of note, Mid1 and Pax6 were retrieved together in a group of genes associated with diseases leading to abnormal corpus callosum (40). Thus, suppression of *mid1* function allows to maintain *pax6* expression in a region where normally Mid1 restricts Pax6.

Little is known about the regulation of the MID1 gene. An apparent regulator of ventral *mid1* expression during development is the secreted factor Sonic hedgehog. It was shown that Shh induces the expression of *pax2* and *vax1* and thus indirectly allows *pax6* expression only in the developing retina of *Xenopus* and zebrafish embryos (19, 33). Mid1 expression was therefore examined in Hedgehog-injected embryos. Ectopic Shh expands *mid1* expression into the entire optic vesicle but also in the prospective forebrain. Therefore, the ventralization of these territories by Shh may partially depend on the rapid degradation of distal (eye) or dorsal (brain) determinants. Interestingly, Shh was also described to repress *mid1* expression and *mid1* can act upstream of SHH, most likely due to the induction of *bmp4* expression in Hensen's node of the chicken (31, 41). Recently it has been reported that human Fu, a Ser/Thr kinase important for Hh signaling in *Drosophila*, permits nuclear localization of GLI3. In a cancer cell line, MID1 marks Fu by ubiquitination for subsequent cleavage leading to the cytosolic retention of GLI3 (31) and thus blocks Hh signaling. In the eye, *gli3* was shown to interact with other transcription factors to define retinal stem cells and *gli3* may cooperate with *pax6* during eye morphogenesis (42, 43). Thus, a feedback loop may exist, which regulates a balance between *mid1* expression with medium levels of Shh that induce *mid1* and lower levels that suppress *mid1* expression. We show that in prospective brain areas close to the Shh source *mid1* was not expressed, whereas the highest levels of *mid1* transcripts were found in the eyestalk region but faded away in the dorsal retina (Fig. 1 *A*, *d2* and *c5*). Even after misexpression of *shh*, *mid1* was not found in central parts of the prospective brain, but distally in the remaining eye vesicle (Fig. 1*B*). Moreover, we show that *pax2* and *mid1* expression is up-regulated on misexpression of *shh* in the forming eye and that Pax2 protein is not necessary for *mid1* expression. These results suggest that *pax2* and *mid1* expression are regulated by the Hh pathway independently and act in concert to restrict Pax6 activity.

Pax6 is expressed in all cells of the forming optic cup in mice initially. When differentiation proceeds, higher *Pax6* expression is maintained in the peripheral optic cup, where cells differentiate later, and in centrally located retinal progenitors cells (RPCs) with lower levels of *Pax6* (44). Pax6 is required in RPCs for both proliferation and cell-fate acquisition (4). However, different activities of Pax6 have been reported in RPCs according to their location along the central-to-peripheral axis (36, 45). Interestingly, in the chick and *Xenopus* retina, decreasing Pax6 activity increases cone cell genesis (46, 46), whereas nonphotoreceptor neurons increase on Pax6 overexpression (48). It has thus been proposed that Pax6 inhibits the differentiation of photoreceptor cells. Consistent with this, in mouse peripheral retina, Pax6 was shown to play a role in suppressing the expression of Crx, a transcription factor essential for photoreceptor cell differentiation (4). We observed a bias toward a photoreceptor fate following Mid1 overexpression in the retina and a reduction of rhodopsin on Mid1 knockdown. We thus propose that such abnormal cell type distribution in clones generated from Mid1-lipofected RPCs may be due to Mid1-dependent Pax6 degradation.

We conclude that in addition to transcriptional and post-transcriptional mechanisms (37, 44, 49, 50), the specific and fast regulation of Pax6 protein levels by protein degradation is essential for the normal formation of the visual system. Our results reveal an important aspect of E3-ligases, which are often considered as general negative regulators of protein abundance. The tight control of *mid1* expression by Shh, which then further targets Pax6 for degradation, might serve as an important example of how a morphogen is able to accelerate the switch from one cell fate to another above the pure genetic regulation of transcription factors when time becomes limited during development.

Materials and Methods

***Xenopus* Embryos.** Production and rearing, whole mount in situ hybridization, and morpholino and RNA microinjections were done as previously described (51). All procedures were performed according to guidelines set by the German animal use and care laws (Tierschutzgesetz) and approved by the German state administration Saxony-Anhalt (Projekt/AZ: 42502–3-600 MLU). Details are presented in *SI Materials and Methods*.

Lipofection. The retinoblasts-targeted lipofection was performed with NF stage 17/18 *Xenopus* embryos according to the protocol from Ohnuma et al. with minor modifications (52). Details are presented in *SI Materials and Methods*.

Plasmids, Morpholinos, Antibodies, and Chemicals. Description of morpholinos (Table S1), plasmids (Table S2), antibodies (Table S3) can be found in *SI Materials and Methods*. Morpholino specificity has been addressed (Fig. S2). If not otherwise stated, drugs and chemicals were purchased from the Carl Roth GmbH.

Cell Cultures and Transfections. HeLa, αTN4-1, and HEK29 cells were maintained in DMEM supplemented with 10% (vol/vol) FCS. Details are presented in *SI Materials and Methods*.

Immunohistochemistry. HeLa cells were seeded on glass coverslips 24 h prior to transfection and fixed in paraformaldehyde 48 h after transfection. To detect Pax6 in *Xenopus* embryos, cryostat sections were taken. Fluorescence images were documented with a microscope Nikon Eclipse E600. Details are presented in *SI Materials and Methods*.

Coimmunoprecipitation and GST pull down. GST pull down and coimmunoprecipitation assays were done according to standard procedures. The details of these assays are provided in *SI Materials and Methods*.

Protein Expression, in Vivo Ubiquitination Assay, and Pax6 Protein Levels over Time. HEK293 cells were cotransfected with *pax6*-flag with either myc-*mid1* or EV. Inhibitors were applied after 24 h for 24 h (MG132, 20 μM; lactacystin; Sigma; 1 μM) or 32 h after transfection for an additional 16 h (Pyr 41; Boston Biochem; 20 μM; Z-VAD-FMK; Sigma; 20 μM) before harvesting. Lysates were separated by SDS/PAGE and probed for Pax6 protein. Details of these assays are provided in *SI Materials and Methods*.

Nuclear and Cytoplasmic Fractionation. To separate cytosol, soluble nuclear proteins, and the insoluble membrane/DNA fraction, transfected HEK293 cells were collected in PBS. The pellets and nuclei were sedimented by centrifugation following standard procedures. Details are presented in *SI Materials and Methods*.

Statistical Analysis. Results are presented as means ± SD. Statistical differences were evaluated using Student *t* test or χ^2 test. Cell culture, pull down, Western blot, and PCR experiments were repeated at least three times, and a representative experiment is shown. Quantification of Western blots was done using ImageJ software (NIH).

ACKNOWLEDGMENTS. We thank J. Herfurth for excellent technical help; Z. Kozmik for aTN4-1 cells; and D. Gradl, A. Brändli, and S. C. Ekker for plasmids. S.R. received a travel grant from the Deutsche Akademische Austauschdienst. This work was supported by the University of Halle and by the Deutsche Forschungsgemeinschaft (HO 1879/3-3). M.P.'s laboratory is supported by grants from L'Agence nationale de la recherche, Retina France, Association Valentin Haüy, and Fondation pour la recherché médicale.

1. Walther C, Gruss P (1991) Pax-6, a murine paired box gene, is expressed in the developing CNS. *Development* 113(4):1435–1449.
2. Glaser T, Walton DS, Maas RL (1992) Genomic structure, evolutionary conservation and aniridia mutations in the human PAX6 gene. *Nat Genet* 2(3):232–239.
3. Gosmain Y, Cheyssac C, Heddad Masson M, Dibner C, Philippe J (2011) Glucagon gene expression in the endocrine pancreas: The role of the transcription factor Pax6 in α-cell differentiation, glucagon biosynthesis and secretion. *Diabetes Obes Metab* 13 (Suppl 1):31–38.
4. Shaham O, Menuchin Y, Farhy C, Ashery-Padan R (2012) Pax6: A multi-level regulator of ocular development. *Prog Retin Eye Res* 31(5):351–376.
5. Cvekl A, Piatigorsky J (1996) Lens development and crystallin gene expression: Many roles for Pax-6. *BioEssays* 18(8):621–630.
6. Davis N, et al. (2009) Pax6 dosage requirements in iris and ciliary body differentiation. *Dev Biol* 333(1):132–142.
7. Grindley JC, Davidson DR, Hill RE (1995) The role of Pax-6 in eye and nasal development. *Development* 121(5):1433–1442.
8. Plaza S, Dozier C, Turque N, Saule S (1995) Quail Pax-6 (Pax-QNR) mRNAs are expressed from two promoters used differentially during retina development and neuronal differentiation. *Mol Cell Biol* 15(6):3344–3353.
9. Kleinjan DA, Seawright A, Childs AJ, van Heyningen V (2004) Conserved elements in Pax6 intron 7 involved in (auto)regulation and alternative transcription. *Dev Biol* 265(2):462–477.
10. Ashery-Padan R, Marquardt T, Zhou X, Gruss P (2000) Pax6 activity in the lens primordium is required for lens formation and for correct placement of a single retina in the eye. *Genes Dev* 14(21):2701–2711.
11. Grindley JC, Hargett LK, Hill RE, Ross A, Hogan BL (1997) Disruption of PAX6 function in mice homozygous for the Pax6Sey-1Neu mutation produces abnormalities in the early development and regionalization of the diencephalon. *Mech Dev* 64(1-2): 111–126.
12. Glaser T, et al. (1994) PAX6 gene dosage effect in a family with congenital cataracts, aniridia, anophthalmia and central nervous system defects. *Nat Genet* 7(4):463–471.
13. Schedl A, et al. (1996) Influence of PAX6 gene dosage on development: Overexpression causes severe eye abnormalities. *Cell* 86(1):71–82.
14. Manuel M, Pratt T, Liu M, Jeffery G, Price DJ (2008) Overexpression of Pax6 results in microphthalmia, retinal dysplasia and defective retinal ganglion cell axon guidance. *BMC Dev Biol* 8:59.
15. Halder G, Callaerts P, Gehring WJ (1995) Induction of ectopic eyes by targeted expression of the eyeless gene in Drosophila. *Science* 267(5205):1788–1792.
16. Chow RL, Altmann CR, Lang RA, Hemmati-Brivanlou A (1999) Pax6 induces ectopic eyes in a vertebrate. *Development* 126(19):4213–4222.
17. Perron M, Kanekar S, Vetter ML, Harris WA (1998) The genetic sequence of retinal development in the ciliary margin of the Xenopus eye. *Dev Biol* 199(2):185–200.
18. Hirsch N, Harris WA (1997) Xenopus Pax-6 and retinal development. *J Neurobiol* 32(1): 45–61.
19. Macdonald R, et al. (1995) Midline signalling is required for Pax gene regulation and patterning of the eyes. *Development* 121(10):3267–3278.
20. Schwarz M, et al. (2000) Spatial specification of mammalian eye territories by reciprocal transcriptional repression of Pax2 and Pax6. *Development* 127(20):4325–4334.
21. Mikkola I, Bruun JA, Bjorkoy G, Holm T, Johansen T (1999) Phosphorylation of the transactivation domain of Pax6 by extracellular signal-regulated kinase and p38 mitogen-activated protein kinase. *J Biol Chem* 274(21):15115–15126.
22. Kim EA, et al. (2006) Phosphorylation and transactivation of Pax6 by homeodomain-interacting protein kinase 2. *J Biol Chem* 281(11):7489–7497.
23. Yan Q, et al. (2010) Sumoylation activates the transcriptional activity of Pax-6, an important transcription factor for eye and brain development. *Proc Natl Acad Sci USA* 107(49):21034–21039.
24. Tuoc TC, Stoykova A (2008) Trim11 modulates the function of neurogenic transcription factor Pax6 through ubiquitin-proteosome system. *Genes Dev* 22(14):1972–1986.
25. Opitz JM (1987) G syndrome (hyperlerorism with esophageal abnormality and hypospadias, or hypospadias-dysphagia, or "Opitz-Frias" or "Opitz-G" syndrome)–perspective in 1987 and bibliography. *Am J Med Genet Suppl* 2(2):275–285.
26. Quaderi NA, et al. (1997) Opitz G/BBB syndrome, a defect of midline development, is due to mutations in a new RING finger gene on Xp22. *Nat Genet* 17(3):285–291.
27. Trockenbacher A, et al. (2001) MID1, mutated in Opitz syndrome, encodes an ubiquitin ligase that targets phosphatase 2A for degradation. *Nat Genet* 29(3):287–294.
28. Berti C, Fontanella B, Ferrentino R, Meroni G (2004) Mig12, a novel Opitz syndrome gene product partner, is expressed in the embryonic ventral midline and co-operates with Mid1 to bundle and stabilize microtubules. *BMC Cell Biol* 5:9.
29. Aranda-Orgillés B, et al. (2008) The Opitz syndrome gene product MID1 assembles a microtubule-associated ribonucleoprotein complex. *Hum Genet* 123(2):163–176.
30. Du H, et al. (2014) MID1 catalyzes the ubiquitination of protein phosphatase 2A and mutations within its Bbox1 domain disrupt polyubiquitination of alpha4 but not of PP2Ac. *PLoS One* 9(9):e107428.
31. Schweiger S, et al. (2014) The E3 ubiquitin ligase MID1 catalyzes ubiquitination and cleavage of Fu. *J Biol Chem* 289(46):31805–31817.
32. Suzuki M, Hara Y, Takagi C, Yamamoto TS, Ueno N (2010) MID1 and MID2 are required for Xenopus neural tube closure through the regulation of microtubule organization. *Development* 137(14):2329–2339.
33. Hallonet M, Hollemann T, Pieler T, Gruss P (1999) Vax1, a novel homeobox-containing gene, directs development of the basal forebrain and visual system. *Genes Dev* 13(23): 3106–3114.
34. de Chevigny A, et al. (2012) miR-7a regulation of Pax6 controls spatial origin of forebrain dopaminergic neurons. *Nat Neurosci* 15(8):1120–1126.
35. Klimova L, Kozmik Z (2014) Stage-dependent requirement of neuroretinal Pax6 for lens and retina development. *Development* 141(6):1292–1302.
36. Oron-Karni V, et al. (2008) Dual requirement for Pax6 in retinal progenitor cells. *Development* 135(24):4037–4047.
37. Farhy C, et al. (2013) Pax6 is required for normal cell-cycle exit and the differentiation kinetics of retinal progenitor cells. *PLoS One* 8(9):e76489.
38. Schweiger S, et al. (1999) The Opitz syndrome gene product, MID1, associates with microtubules. *Proc Natl Acad Sci USA* 96(6):2794–2799.
39. Pinson L, et al. (2004) Embryonic expression of the human MID1 gene and its mutations in Opitz syndrome. *J Med Genet* 41(5):381–386.
40. Poot M, Badea A, Williams RW, Kas MJ (2011) Identifying human disease genes through cross-species gene mapping of evolutionary conserved processes. *PLoS One* 6(5):e18612.
41. Granata A, Quaderi NA (2003) The Opitz syndrome gene MID1 is essential for establishing asymmetric gene expression in Hensen's node. *Dev Biol* 258(2):397–405.
42. Zaki P, et al. (2006) Penetrance of eye defects in mice heterozygous for mutation of Gli3 is enhanced by heterozygous mutation of Pax6. *BMC Dev Biol* 6:46.
43. Reinhardt R, et al. (2015) Sox2, Tlx, Gli3, and Her9 converge on Rx2 to define retinal stem cells in vivo. *EMBO J* 34(11):1572–1588.
44. Davis-Silberman N, et al. (2005) Genetic dissection of Pax6 dosage requirements in the developing mouse eye. *Hum Mol Genet* 14(15):2265–2276.
45. Marquardt T, et al. (2001) Pax6 is required for the multipotent state of retinal progenitor cells. *Cell* 105(1):43–55.
46. Zaghloul NA, Moody SA (2007) Changes in Rx1 and Pax6 activity at eye field stages differentially alter the production of amacrine neurotransmitter subtypes in Xenopus. *Mol Vis* 13:86–95.
47. Hsieh YW, Yang XJ (2009) Dynamic Pax6 expression during the neurogenic cell cycle influences proliferation and cell fate choices of retinal progenitors. *Neural Dev* 4:32.
48. Toy J, Norton JS, Jibodh SR, Adler R (2002) Effects of homeobox genes on the differentiation of photoreceptor and nonphotoreceptor neurons. *Invest Ophthalmol Vis Sci* 43(11):3522–3529.
49. Ashery-Padan R, Gruss P (2001) Pax6 lights-up the way for eye development. *Curr Opin Cell Biol* 13(6):706–714.
50. Xu S, et al. (2007) The proliferation and expansion of retinal stem cells require functional Pax6. *Dev Biol* 304(2):713–721.
51. Metikala S, Neuhaus H, Hollemann T (2016) Suppression of vascular network formation by chronic hypoxia and prolyl-hydroxylase 2 (phd2) deficiency during vertebrate development. *Angiogenesis* 19(2):119–131.
52. Ohnuma S, Mann F, Boy S, Perron M, Harris WA (2002) Lipofection strategy for the study of Xenopus retinal development. *Methods* 28(4):411–419.
53. Koenig SF, et al. (2010) En2, Pax2/5 and Tcf-4 transcription factors cooperate in patterning the Xenopus brain. *Dev Biol* 340(2):318–328.
54. Thélie A, et al. (2015) Prdm12 specifies V1 interneurons through cross-repressive interactions with Dbx1 and Nkx6 genes in Xenopus. *Development* 142(19):3416–3428.

Supporting Information

Pfirrmann et al. 10.1073/pnas.1600770113

SI Materials and Methods

Animals, Microinjections, and Animal Cap Explants. Pigmented and albino *Xenopus laevis* were obtained from Nasco. Production, rearing, and staging of embryos was as previously described (33). In case of loss of function experiments, antisense-morpholino-oligonucleotides (mo) were designed and ordered from GeneTools. For control injections, the standard control morpholino from GeneTools are listed in Table S1. Sequences are listed in the supplement. All morpholinos were dissolved in DEPC-H_2O and stored in aliquots at −20 °C. For all experiments, 2.5 pmol morpholinos or synthetic RNA (500 pg *shh;* 100 pg *pax2*; 100 pg *noggin*; 1 or 2 ng *mid1*) RNA was injected unilaterally into one blastomere at the two-cell stage (6). Synthetic *β-gal* (100 pg) RNA was coinjected as a lineage tracer in all experiments. Capped human *mid1* and *Xenopus tropicalis mid1, Xenopus laevis pax2*, and *noggin* mRNA was generated using the mMESSAGE mMACHINE kit (Ambion). NotI linearized pCS2+ containing the gene was used as a template for SP6 transcription, and 5 nl capped mRNA was injected along with the morpholino into one blastomere of a two-cell stage embryo. The noninjected side served as internal control. Animal caps were excised with the help of a gastromaster (XENOTEK) at stage 8.5 in 0.5× Modified Barth's saline (MBS), and sets of 30–40 caps were cultured for 24 h at 18–22 °C in 0.5× MBS supplemented with penicillin/streptomycin.

Lipofection. The retinoblasts-targeted lipofection was performed with NF stage 17/18 *Xenopus* embryos according to the protocol from Ohnuma et al. (52). Plasmids were mixed with 3 μL *N*-(2,3-dioleoyloxy-1-propyl)trimethylammonium methyl sulfate (DOTAP) (Roche)/μg DNA directly before loading the mixture into a glass needle (same as microinjection). A plasmid coding for GFP was either mixed with Mid1 coding plasmids as lineage marker to identify lipofected cells or alone as negative control. Embryos were arranged with the anterior side upward, the opened tip of the needle was introduced into the embryo's retinal area just underneath the epidermis, and 4–10 nL lipofection mixture was injected using several pulses. After injection, embryos were kept in a 0.1× MBS solution until NF stage 41–42, fixed with 4 g/100 ml (4%) paraformaldehyde, and embedded for cryostat sections (Microm HM500 OM).

Whole Mount in Situ Hybridization. To analyze the spatiotemporal expression of the respective marker genes, *Xenopus* embryos were fixed at different developmental stages with paraformaldehyde, and whole-mount in situ hybridization was carried out as previously described (32). For a more detailed analysis of gene expression, we performed gelatin/albumin sections of stained embryos with a thickness of 25 μm using a vibratome (Leica). Digoxigenin (DIG) labeled antisense probes of *mid1*, *pax2*, *pax6*, *ptc1*, *brn3.0*, *vsx1*, *prox1*, and *rhodopsin* were made from plasmids *brn3.0*/pBlueScript (BamH1/T7), *vsx1*/pGEM-T (Not1/T7), *prox1*/pCR2.1 (BamH1/T7), *rhodopsin*/pGEM-T (Not1/T7), *mid1*/pCS2+ (ClaI/T3), *ptc1*/pGEM-T (Not1/T7), *pax6*/pCS2+ (HindIII/T7), and *pax2*/pCS2+ (HindIII/T7), respectively. X-gal staining was carried out before whole mount in situ hybridization.

Plasmids, Antibodies, and Chemicals. Description of plasmids (Table S2) and antibodies (Table S3) can be found in the supplemental material. If not otherwise stated, drugs and chemicals were purchased from the Carl Roth GmbH.

Cell Cultures and Transfections. HeLa, αTN4-1, and HEK29 cells were maintained in DMEM supplemented with 10 ml/100 ml (10%) FCS. All media and sera were purchased from PAA Laboratories. Transfections were performed using Lipofectamin 2000 (Invitrogen) according to the manufacturer's protocol, except for HEK293 cells, which were transfected using polyethylenimin (25 kDa, branched; Sigma-Aldrich) with 2.5 μL 10 mM Poly(ethyleneimine) (PEI)/μg DNA in PBS. Empty vector pCS2+ was used to obtain equal amounts of transfected DNA and as a negative (EV) control. If not otherwise stated, cells were harvested 48 h after transfection. To detect Pax6 in lysates of animal caps, ∼30 explants were used per lane.

Immunohistochemistry. HeLa cells were seeded on glass coverslips 24 h prior to transfection, fixed in paraformaldehyde 48 h after transfection, permeabilized with 0.2% Triton X-100, and blocked with 2 g/100 ml (2%) BSA. Following the incubation with the primary antibodies (anti-flag, mouse, 1:800 + anti-myc, rabbit, 1:400), cells were blocked again and incubated with the secondary antibodies (anti-mouse-Alexa 488, anti–rabbit-Alexa 594, 1:400). Cells were washed three times with PBS after each step except blocking and were finally desalted in H_2O, dehydrated with 100% ethanol, and mounted on superfrost glass slides with Mowiol containing DAPI (1:1,000). To detect Pax6-positive cells in the eye region of *Xenopus* embryos, cryostat sections were rehydrated in PBS, permeabilized, and blocked with permeabilization solution. Thereafter, the first antibody (anti-Pax6, rabbit; Covance) diluted in antibody buffer (1:50) was applied. Afterward, the sections were intensively washed three times with PBS, and the secondary antibody (anti–rabbit-Alexa594) was applied with a dilution of 1:1,000 in PBS. Sections were washed again and mounted with Mowiol containing DAPI (1:1,000). Fluorescence images were documented with a microscope Nikon Eclipse E600 installed with a camera Vosskühler CCD-1300QLN. Sixteen-bit grayscale images with a size of 1,388 × 1,040 pixels were acquired using the AxioVision software under automated exposure settings for all channels. Images were exported as JPG and TIF files either separately for each channel or with combined channels.

Coimmunoprecipitation and GST-Pulldown. HEK293 cells were transfected with myc-tagged *mid1* and harvested in PBS, and proteins were extracted with IP lysis buffer containing protease inhibitors. Fifty micrograms of bacterial expressed and purified GST or GST-Pax6 was added to 1 mL (1 mg protein) lysate and after 1 h at 4 °C under continuous rotation, 50 μL GSH-Sepharose beads were added to the mixture. After 60 min of incubation, the beads were washed three times with IP lysis buffer and once with 0.1 mM Tris, pH 7.4. Proteins were eluted with 2× Laemmli buffer, separated by SDS/PAGE, and analyzed by Western blotting. For coimmunoprecipitation experiments, HEK293 cells were transfected with *pax6*-flag and myc-*mid1* or *pax6*-flag and myc-*mid1* alone, respectively. Cells were harvested in PBS and lysed in IP lysis buffer (with protease inhibitors + 20 μM MG132), and proteins were immunoprecipitated with 2 μg anti-flag antibody and 30 μL Protein A Sepharose per sample. After 2 h at 4 °C under continuous rotation, the beads were washed three times with IP lysis buffer and once with 0.1 mM Tris, pH 7.4. Proteins were eluted with 2× Laemmli buffer. For Western blot analyses, input and eluted proteins were separated by SDS/PAGE and probed with the corresponding antibodies.

Protein Expression, in Vivo Ubiquitination Assay, and Pax6 Protein Levels over Time. To examine protein expression, αTN4-1 (expresses Pax6 endogenously) or HEK293 cells were transfected with *pax6*-flag with either myc-*mid1* or EV as indicated. Inhibitors were applied 24 h after transfection for an additional 12 or 24 h (MG132, 20 μM; lactacystin; Sigma; 1 μM) or 32 h after transfection for an additional 16 h (Pyr 41; Boston Biochem; 20 μM, Z-VAD-FMK; Sigma; 20 μM) before harvesting. Lysates of harvested cells were separated by SDS/PAGE and probed for Pax6 protein by Western blotting using an anti-Pax6 antibody. As a control for equal loading, blots were subsequently reprobed with anti–β-tubulin antibody. For analysis of Pax6 ubiquitination, HEK293 cells were transfected with plasmids for his-*ubi*, myc-*mid1*, and *pax6*-flag as indicated. Twenty-four hours after transfection, MG132 (20 μM) was added, and cells were incubated for an additional 8 h, harvested in PBS, and lysed in RIPA buffer [with protease inhibitors, 20 μM MG132, 10 mM *N*-ethylmaleimide (NEM); Sigma-Aldrich], and proteins were immunoprecipitated with 3 μg anti-flag antibody and 50 μL protein A Sepharose per sample. After 2 h at 4 °C under continuous rotation, the beads were washed three times with RIPA buffer and once with 0.1 mM Tris, pH 7.4. Proteins were eluted with 2× Laemmli buffer and were separated by SDS/PAGE and probed with the corresponding antibodies for Western blot analysis. To determine Pax6 protein abundance over time, cycloheximide (40 μg/mL; Sigma-Aldrich) was added to HEK293 cells 24 h after transfection with the indicated combination of plasmids. At different time points, cells were collected in PBS and lysed in RIPA buffer (with protease inhibitor). Five to 20 μg total protein per sample was separated by SDS/PAGE probed with the corresponding antibodies in Western blot analyses. The relative amount of Pax6 protein compared with β-tubulin as loading control was quantified densitometrically using ImageJ software (NIH).

Nuclear and Cytoplasmic Fractionation. To separate cytosol, soluble nuclear proteins, and the insoluble membrane/DNA fraction, transfected HEK293 cells were collected in PBS. The pellet was resuspended in 5× the volume hypotonic buffer (10 mM Hepes, pH 7.9, 1.5 mM $MgCl_2$, 10 mM KCl, 0.5% Nonidet P-40) and incubated for 5 min on ice. Nuclei were sedimented by centrifugation, and the supernatant containing the cytoplasmic fraction was removed. The nuclei were washed two times with PBS and incubated with high salt buffer [20 mM Hepes, pH 7.9, 25 ml/100 ml (25%) glycerol, 1.5 mM $MgCl_2$, 420 mM NaCl, 0.2 mM EDTA], using 5× the volume of the pellet, for 30 min under continuous rotation at 4 °C to extract the soluble nuclear proteins, which were in the supernatant after centrifugation. The final pellet contained the insoluble membrane/DNA fraction with proteins still bound.

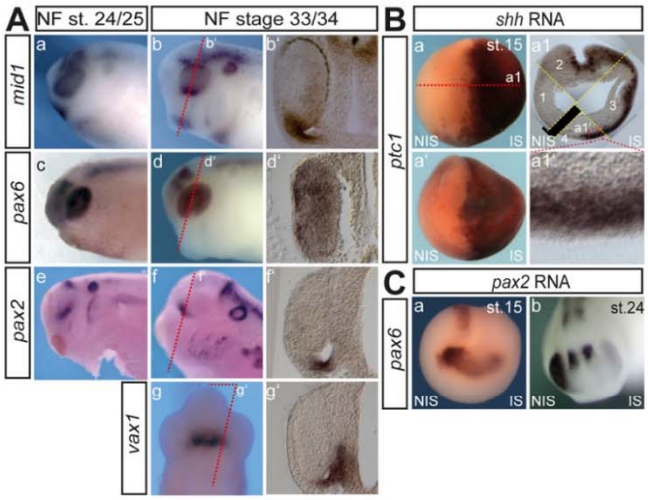

Fig. S1. (*A*) *a*–*f*, Lateral view of the head region; *g*, ventral view of the head region; *b*′–*g*′, sections at the level of the forming eye stalk as indicated by the red dashed lines. Though *pax2*, *vax1*, and *mid1* are clearly expressed within the forming eye stalk, their pattern of expression in this part is not identical and appears to follow a proximodistal axis with *mid1* more distally, *pax2* centrally, and *vax1* proximally located. (*B*) a, dorsal view; *a*′, anterior view; *a1*, transversal section as indicated in *a*. The misexpression of *shh* upon the microinjection of synthetic 500 pg *shh* RNA induced the expression of *ptc1* strongly at the open neural tube stage (NF stage 15) within the sensorial layer of the ectoderm (*a1*′) and this induction of *ptc1* is maintained though less intense at tadpole stage (see also Fig. 1 *B*, *d*–*d*′). (*C*) *a* and *b*, anterior view. Misexpression of *pax2* upon the microinjection of synthetic 100 pg *pax2* RNA repressed the expression of *pax6* already at the open neural tube stage (NF stage 15) and this suppression of *pax6* is maintained at tadpole stage (see also Fig. 1 *B*, *h*–*h*′).

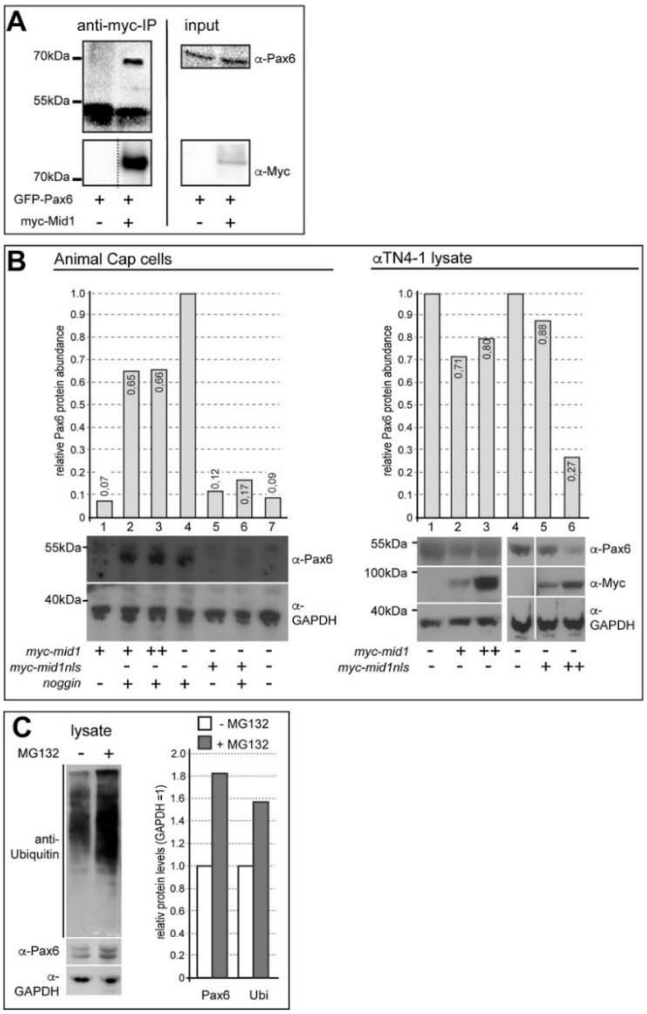

Fig. S2. Mid1 reduces endogenous Pax6 protein. (*A*) Mid1 physically interacted with Pax6. HEK293 cells were transfected with *GFP-pax6* + *myc-mid1* or *myc-mid1* alone. The left panels show eluted Pax6 protein after immunoprecipitation with an anti-Myc antibody (upper blot) and precipitated myc-Mid1 (lower blot, reprobe with anti-Myc antibody). The right panels show blots with the respective lysates for the input proteins. (*B*) *Xenopus* animal cap explants expressed Pax6 upon neuralization by microinjection of 400 μg synthetic RNA of the BMP4 inhibitor *noggin*. Approximately 30 animal cap explants were separated in each lane. Coinjection of *Xenopus mid1* RNA (1 ng) led to a reduction of Pax6 protein abundance. The reduction of Pax6 protein levels was considerably stronger, when Mid1 protein was forced to enter the nucleus by the fusion of a nuclear localization signal (*mid1nls*). The mouse lens epithelial cell line αTN4-1 expresses pax6 endogenously. Transfection of *mid1* and of *mid1nls* led to a reduction of endogenous Pax6 protein. Corresponding Western blots were quantified with the help of ImageJ and normalized against GAPDH. (*C*) Pax6 levels increased upon proteasome inhibition. αTN4-1 cells were grown in DMEM medium (10% FCS) and were treated with DMSO (–) or with MG132 (5 μM) (+). Pax6 levels increased upon MG132 treatment (+), as well as polyubiquitinated proteins. Anti-GAPDH was used as a loading control. Densitometry was performed using ImageJ (right graph).

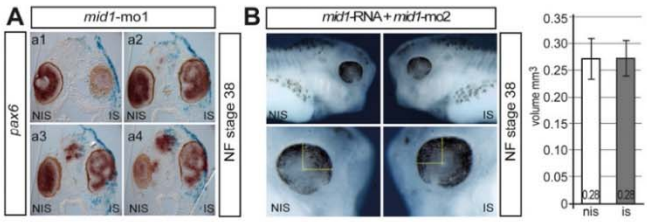

Fig. S3. (*A*) *a1–a4* show a series of transversal sections at the level of the eye of the *mid1* injected tadpole (NF stage 38) shown in Fig. 1 *A*, *a*. (*B*) Rescue of the *mid1* knockdown eye phenotype. Lateral view of NF stage 38 embryos injected with *mid1*-mo2 (1.25 pmol) along with synthetic human *mid1* RNA (1–2 ng) into one cell of a 2-cell stage embryo. The lower panel shows a 10× enlarged view of the respective eye region. Considering the eye to be an oblate spheroid, the mean radius was estimated by measuring the drawn distances and total volume was calculated. The graph shows the mean values for 20 embryos. The specificity of the *pax2* and *pax6* morpholino had been tested already by rescue experiments in refs. 53 and 54, respectively.

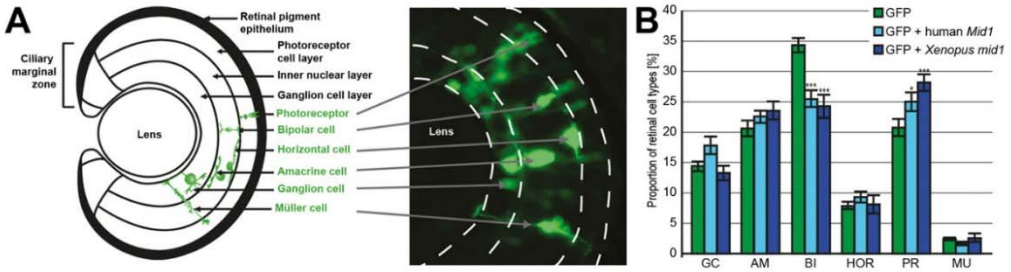

Fig. S4. Human and *Xenopus mid1*/*Mid1* affects fate of retinal precursor cells similarly. (*A*) Schematic of the retina showing the different cellular layers and retinal cell types. The picture on the right illustrates a clone of GFP-positive cells following lipofection. Cell types are identified according to their position in the layers and their morphology. (*B*) Human or *Xenopus mid1* expression plasmids together with GFP or GFP plasmid alone were lipofected into the area of the eye prospective retinal field at NF stage 17. At NF stage 41, cryosections were done, and the fluorescent cells in the central retina were counted. The different cell types were identified according to their morphology. The diagram shows the percentages of the different cell types for GFP-lipofected embryos (green, $n = 40$), human Mid1 (light blue, $n = 24$), and *Xenopus* mid1 (dark blue, $n = 17$); error bars represent SEM. AM, amacrine cells; BI, bipolar cells; GC, ganglion cells; HOR, horizontal cells; MU, Müller cells; PR, photoreceptor cells.

Table S1. Morpholinos were obtained from Gene Tools

Morpholino	Sequence	Source
ctrl-mo	5′-CCTCTTACCTCAGTTACAATTTATA-3′	GeneTools
mid1-mo1	5′-TCAGTTCAGACTCCAGTGTTTCCAT-3′	(32)
mid1-mo2	5′-TTCCATCTTCAGGCAAAGCTTTCCT-3′	This work
pax2-mo	5′-TGCAGTGCATATCCATGGGGAGGCA-3′	(53)
pax6-mo	5′-CCAACATCTGCTGATCAACGCCTAG-3′	(54)

Table S2. Plasmids for transfection, lipofection, mRNA, and WMISH probe preparation

Plasmid	Source
mid1 in pCMV-Sport6	RZPD, CF239162
mid1nls in pCS2+	Cloned PCR fragment
Human *Mid1* in pCMV-Sport6	ImaGenes, BC053626
*mid1*mo2bs-gfp-reporter in pCS2+	Cloned PCR fragment
*mid1*mo2mut-gfp-reporter in pCS2+	Cloned PCR fragment
mid1 in pBsk(−)	ImaGenes, BJ087663
Gfp in pCS2+	Gift from David Turner, Fred Hutchinson Cancer Research Center, Seattle
rhodopsin in pGEM-T	Cloned PCR fragment
brn3.0 in pBlueScript	Gift from Rob Grainger, University of Virginia, Charlottesville, VA
vsx1 in pGEM-T	Cloned PCR fragment
prox1 in pGEM-T	Cloned PCR fragment
pax2 in pGEM-T	Cloned PCR fragment
pax2 in pCS2+-MT	Gift from Dietmar Gradl, Karlsruhe Institute of Technology, Karlsruhe, Germany
pax2mo1bs-gfp-reporter in pCS2+	Cloned PCR fragment
pax2mo1mut-gfp-reporter in pCS2+	Cloned PCR fragment
pax6 in pCS2+	Gift from Nicolas Hirsch, University of Virginia, Charlottesville, VA
pax6mo1bs-gfp-reporter in pCS2+	Cloned PCR fragment
pax6mo1mut-gfp-reporter in pCS2+	Cloned PCR fragment
Mouse *Pax6*-flag in pCS2+	Gift from Anastassia Stoykova, Max Planck Institute for Biophysical Chemistry, Göttingen, Germany
ptc1 in pCS2+	Cloned PCR fragment
his-*Ubiquitin* in pDNA3.1	Gift from Dirk Bohmann, University of Rochester Medical Center, Rochester, NY
myc-human *Mid1* in pCS2+	Cloning of hs*Mid1* PCR product into pCS2+ MT
Gfp-pax6 in peGFP-N	Cloning of *pax6* PCR product into peGFPN
GST-pax6 in pGex-4-T1	Cloning of *pax6* PCR product into pGex-4-T1

Table S3. Antibodies

Antibody	Purpose	Source
anti-Pax6, rabbit	IHC	Covance
anti-Pax6, mouse	IHC, WB	Merck Millipore
anti-Pax6, rabbit	WB	ThermoFisher
anti-GAPDH, mouse	WB	Sigma-Aldrich
anti-Ubiquitin, rabbit	WB	Santa-Cruz BT
anti-Rhodopsin, rabbit	IHC	Merck Millipore
anti-myc, rabbit	IP, IHC	Sigma-Aldrich
anti-myc, mouse	WB	Sigma-Aldrich
anti-his-HRP coupled	WB	Merck Millipore
anti-his, mouse	WB	Sigma-Aldrich
anti-flag, rabbit	IP	Sigma-Aldrich
anti-flag, mouse	IHC, WB	Sigma-Aldrich
anti-b-tubulin, mouse	WB	Merck Millipore
anti-Topoisomerase 1, rabbit	WB	Merck Millipore
Peroxidase-conj. goat anti-rabbit IgG	WB	Sigma-Aldrich
Alexa 488 goat anti-mouse	IHC	Invitrogen, Life Technologies
Alexa 594 goat anti-rabbit	IHC	Invitrogen, Life Technologies

4.3 Manuscript 3: *Xenopus laevis* neuronal cell adhesion molecule (*nrcam*): plasticity of a CAM in the developing nervous system

Dev Genes Evol (2017) 227:61–67
DOI 10.1007/s00427-016-0569-9

SEQUENCE CORNER

Xenopus laevis neuronal cell adhesion molecule (*nrcam*): plasticity of a CAM in the developing nervous system

Ashwin Lokapally[1] · **Sanjeeva Metikala**[1,2] · **Thomas Hollemann**[1]

Received: 3 August 2016 / Accepted: 24 November 2016 / Published online: 10 December 2016

Abstract Neuron-glial-related cell adhesion molecule (NRCAM) is a neuronal cell adhesion molecule of the L1 immunoglobulin superfamily, which plays diverse roles during nervous system development including axon growth and guidance, synapse formation, and formation of the myelinated nerve. Perturbations in NRCAM function cause a wide variety of disorders, which can affect wiring and targeting of neurons, or cause psychiatric disorders as well as cancers through abnormal modulation of signaling events. In the present study, we characterize the *Xenopus laevis* homolog of *nrcam*. Expression of *Xenopus nrcam* is most abundant along the dorsal midline throughout the developing brain and in the outer nuclear layer of the retina.

Keywords Neuronal cell adhesion molecule (nrcam) · Cell adhesion molecules (CAMs) · Glial cells · Nervous system development

Introduction

In the neural system, cell adhesion molecules (CAMs) form cell-cell interactions at various stages of development governing neural projections of both the peripheral and central nervous system (Brümmendorf and Rathjen 1996). One such CAM of the nervous system is the neuron-glial-related cell adhesion molecule (NRCAM)—a member of the L1 family of CAMs (Hortsch 2000). In the early 1990s, NRCAM was isolated based on its high homology to L1 CAM (Grumet et al. 1991). Further NRCAM was identified as the Bravo antigen during the characterization of antibodies against chick brain glycoproteins (Kayyem et al. 1992). Since its identification, several studies revealed homophilic as well as heterophilic interactions with other CAMs belonging to the immunoglobulin superfamily (Mauro et al. 1992). For example, interactions with neurofascin and contactin1 are involved in neurite outgrowth (Volkmer et al. 1996) and with axonin1 (Lustig et al. 1999) and semaphorins for axon guidance (Julien et al. 2005).

Moreover, Nrcam serves as a co-receptor of Neurophilin2 specific for Sema3B and Sema3F (Julien et al. 2005) and together with Plexin A1 as a receptor for Sema6D (Kuwajima et al. 2012). The *Caenorhabditis elegans* ortholog lad-2 interacts with Sema2, serving as a receptor in axon pathfinding (Wang et al. 2008). Though NRCAM induces neurite outgrowth in vitro (Volkmer et al. 1996), it has been proposed that NRCAM-mediated interactions are more relevant to axon guidance than axon growth in vivo (Fitzli et al. 2000). Apart from these functions, NRCAM is also involved in several cellular processes of the nervous system, including myelination, fasciculation of nerve fibers, and cell migration (Hortsch 2000).

In vivo, NRCAM is present in both, neurons and glial cells of the developing and adult nervous system of chick and mouse (Krushel et al. 1993; Lustig et al. 2001a). In chicken, NRCAM first expresses at the onset of neurogenesis in the floor plate and in the motor neurons of the spinal cord. This expression disappears during the later stages from the floor plate but is retained in the spinal cord (Krushel et al. 1993). In chick dorsal root ganglion (DRG) cell cultures, neuritic axonin-1 and glial-NRCAM interaction is involved in the

Communicated by Caroline Brennan

✉ Thomas Hollemann
thomas.hollemann@medizin.uni-halle.de

[1] Institute for Physiological Chemistry, Martin-Luther-University Halle-Wittenberg, Halle (Saale), Germany

[2] National Xenopus Resource Centre, Marine Biological Laboratory, Woods Hole, MA, USA

formation of myelinated nerve sheaths (Suter et al. 1995). Chick NRCAM is also expressed in growing retinal ganglion cells, where the lack of NRCAM results in RGC axons that misroute at the optic fissure. Instead of diving into the optic nerve head, these axons cross onto the opposite side of the retina (Zelina et al. 2005). In mouse CNS, *Nrcam* is exclusively expressed in the glial cells of the ventral midline throughout the nervous system and as well as in the olfactory system (Williams et al. 2006). In *Nrcam*-null mice, projections of olfactory nerves are altered (Heyden et al. 2008). *Nrcam* is also expressed in the hippocampus and cerebellum; here, it is required for the formation and function of synapses. Further, studies in humans showed that mutations in *NRCAM* result in neuropsychiatric disorders such as autism (Bonora et al. 2005; Hutcheson et al. 2004) and addiction-related behaviors (Ishiguro et al. 2006, 2012).

Despite numerous studies regarding the function and expression of *nrcam* in other species so far, *nrcam* has not been described in *Xenopus*. Therefore, we analyzed the spatiotemporal expression of *nrcam* in the developing *Xenopus* nervous system. A comparison of the *nrcam* expression pattern between *Xenopus*, mice (Lustig et al. 2001a; Williams et al. 2006), and chick (Krushel et al. 1993) revealed a very similar generic expression pattern. However, we also observed subtle differences in the expression of *nrcam* in the *Xenopus* visual system as well as in the spinal cord.

Results and discussion

Sequence analysis and evolutionary relationship

A full-length clone of *X. laevis nrcam* was obtained from the I.M.A.G.E. consortium, Source Biosciences (NM_001092018.1) and used in this study. The 4494-bp full-length *nrcam* sequence contains an open-reading frame of 3534 bases, encoding a putative protein of 1177 amino acids. Like other CAMs of the L1 family of cell adhesion molecules, *Xenopus* Nrcam consists of six Ig-like domains and four fibronectin-type III repeats in the extracellular part, a single transmembrane domain, and an intracellular domain. However, in contrast to other vertebrates, *X. laevis* Nrcam lacks the fifth fibronectin-type III repeat (Fig. 1a) and expresses exclusively in the nervous system. Studies have shown that human *NRCAM*, which undergoes splicing events producing several isoforms, including one lacking the fifth FNIII repeat, exclusively expresses in the nervous system (Lane et al. 1996; Wang et al. 1998), while other splice forms are reportedly expressed in the pancreas, adrenal glands, and placenta. The fatty acid modification site (Cys residue) at the end of the transmembrane domain (Grumet et al. 1991), the spiral ganglion neuron modulator, and ankyrinG binding "FIGQY" sequence in the intracellular (Bravo) domain, as well as glycosylation sites, are conserved. Overall, excluding the fifth FNIII domain, a highly conserved domain structure is seen and a sequence similarity of >85% is observed between mammalian and *X. laevis nrcam*.

Based on the above sequence similarity analysis, we further looked at the ancestral lineage of the protein. Evolutionary analysis of the vertebrate (fish, amphibians, reptiles, aves, and mammals) and arthropod Nrcam, identified here as out-group (blue arrowhead), show a conserved phylogenic evolution, although one observes a high estimated divergence (Fig. 1b). Nevertheless, the presence of common ancestral node (green arrowhead) and comparatively smaller branch lengths between amphibians and mammals during vertebrate evolution highlights evolutionary conservation, which is further strengthened by the presence of sequence signatures (insertions and deletions were not shown) and the stronger bootstrap support values. To further confirm the orthology of *Xenopus nrcam*, we looked at the positioning of the gene at the chromosomal level. The genomic region corresponding to *nrcam* in *X. laevis* was compared to that of vertebrate model organisms (Fig. 1c). Nrcam shows a conserved synteny among species. Similarly, the gene loci directly up and downstream of nrcam are generally conserved. In mice and rats, downstream genes (3, 6) are still uncharacterized and inversed, whereas in humans, contactin1 is exchanged by laminin beta4. Interestingly, it has been shown that interaction of nrcam with contactin1 is involved in neurite outgrowth (Volkmer et al. 1996) which co-localize at the chromosomal level in *Xenopus*.

Expression of *X. laevis nrcam* during early neurogenesis

At first, we examined the temporal expression of *Xenopus* neuronal cell adhesion molecule by semiquantitative RT-PCR analysis (Fig. 2A). Intron-spanning primer pairs were used to avoid amplification of genomic DNA. Low levels of maternal expression of *nrcam* are detectable in stages before mid-blastula transition (MBT). Then, transcript levels of *nrcam* gradually increased until the latest stages were analyzed (NF st. 42). In particular, zygotic expression of *nrcam* is upregulated at early neurulation (NF st. 15) suggesting a role in the formation of structures of the nervous system.

To analyze the spatial expression of *nrcam* during early development, we performed whole mount in situ hybridization. The blastulae of *Xenopus* show low levels of *nrcam* transcripts in the animal hemisphere as well as in the ectoderm of gastrula embryos (Fig. 2B). At early and late neurula stages, expression is in the anterior neural

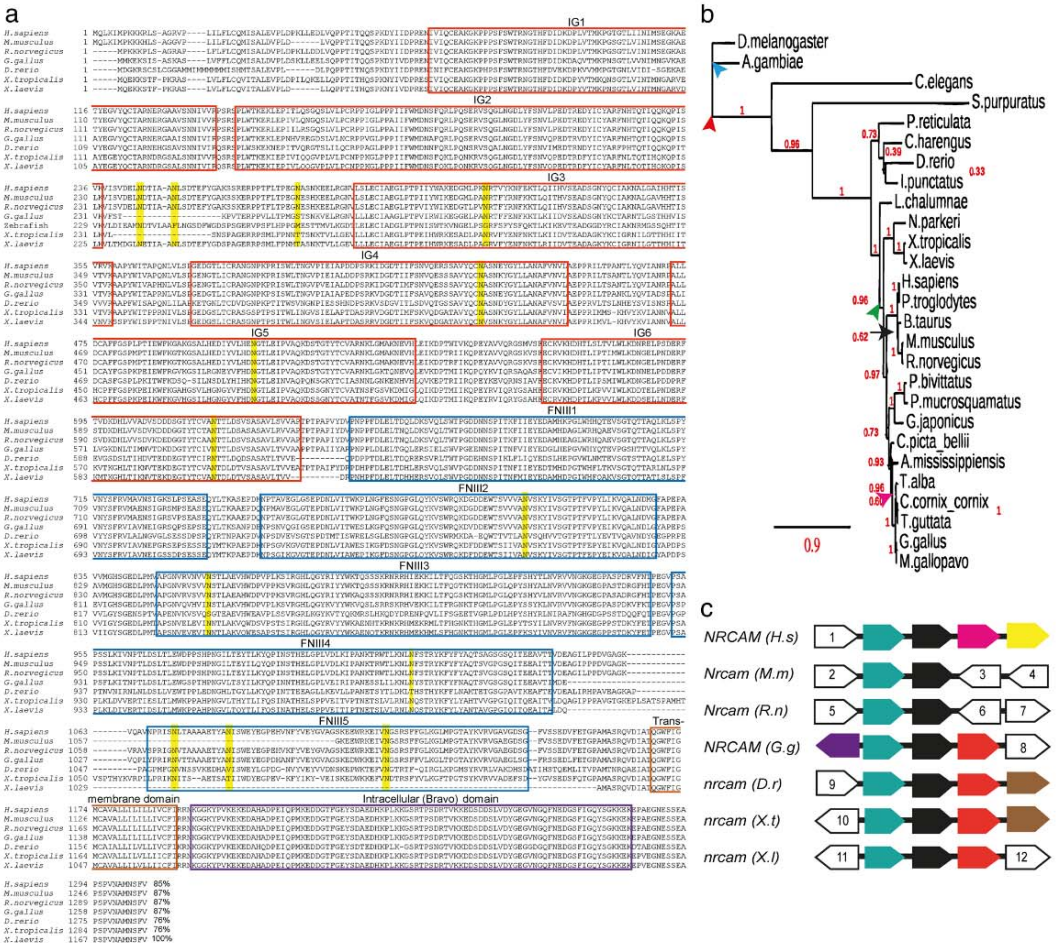

Fig. 1 Alignment of vertebrate NRCAM protein sequences. **a** Comparison of amino acid sequences of NRCAM. *Homo sapiens* (GenBank Accession No. NP_001032209), *Mus musculus* (GenBank Accession No. NP_795904), *Rattus norvegicus* (GenBank Accession No. NP_037282), *Gallus gallus* (GenBank Accession No. NP_990597), *Danio rerio* (GenBank Accession No. NP_001038270), *Xenopus tropicalis* (GenBank Accession No. NP_001135654), *X. laevis (*GenBank Accession No. NP_001085487). The six immunoglobulin domains are boxed in *red*. The five fibronectin-type III domains are boxed in *blue*. Note the lack of the fifth FNIII domain in mouse and *X. laevis*. The transmembrane domain is boxed in *orange* while the intracellular Bravo domain is in *purple*. The glycosylation sites are highlighted in *yellow*. Sequence identities compared against *X. laevis* protein are indicated at the end of the alignment. **b** Phylogenetic analysis: an evolutionary rooted tree is constructed based on maximum likelihood and bootstrap analysis. The branch length is proportional to the number of substitutions per site. The numbers in *red* next to nodes represent bootstrap support values. *Red arrowhead* indicates the root of the tree, the *blue arrowhead* the outgroup, and the *green arrowhead* the common ancestral node between mammals and amphibians. The *bar* at the bottom of the phylogram indicates the evolutionary distance, to which the branch lengths are scaled based on the estimated divergence. There is a relative divergence observed over time. **c** Synteny analysis of *nrcam*: the location and orientation of *nrcam* in the respective genomes are conserved. Each *arrow* stands for a single gene while the *arrowhead* indicates the direction of the ORF. Orthologs are marked with *identical colors*. *nrcam* (*black arrow*) is present in all the species analyzed. Upstream *nrcam* is flanked by the same gene across species, while downstream nrcam is flanked by the same genes with the exception of mammals. Arrow colors: *black*: *nrcam*; *turquoise*: patatin-like phospholipase domain containing 8/pnpla8; *purple*: coiled-coil domain containing 8/ccdc8; *pink*: laminin, beta 4/lamb4; *yellow*: laminin beta 1/lamb1; *red*: contactin1 b/cntn1b; *brown*: PDZ domain containing ring finger 4/pdzrn4; and *white 1–12*: yet uncharacterized proteins

plate and the eye field. At early tailbud stage, *nrcam* is detectable in the prospective forebrain, the caudal part of the midbrain and the hindbrain region (Fig. 2B (f–f)). Furthermore, at late tailbud stages, *nrcam* transcripts were

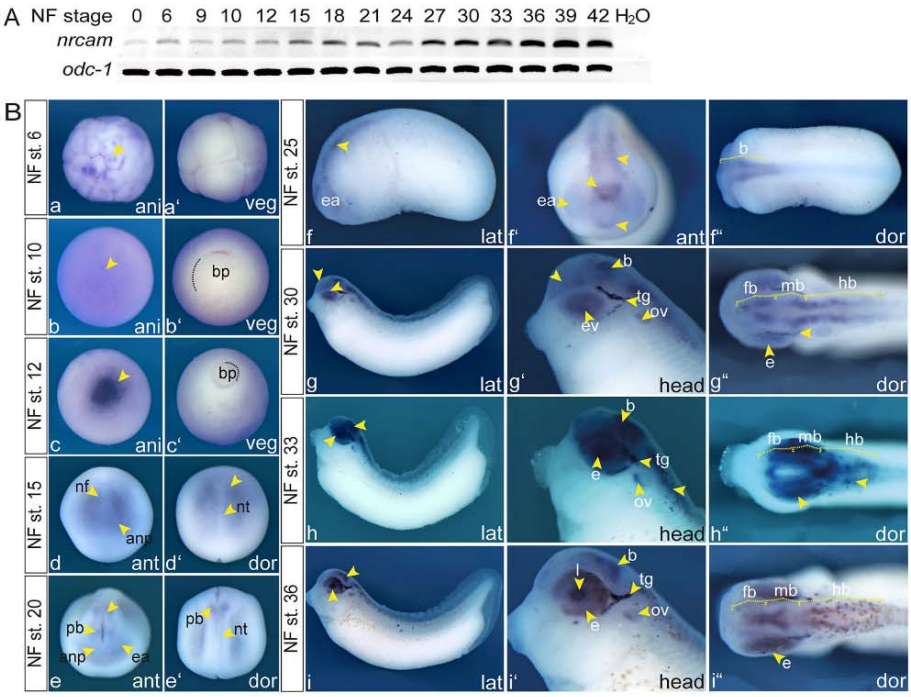

Fig. 2 Temporal and spatial expression. **A** Semiquantitative RT-PCR revealed maternal presence of nrcam RNA. Expression was detectable in all developmental stages in a gradually increasing manner. Expression of the housekeeping gene ODC1 was used as a control for equal RNA input. **B** Spatial expression of *nrcam*. Whole-mount in situ hybridization of wild-type albino embryos at developmental stages 6–36. *a–c'* indicate animal and vegetal views of stage 6–12 embryos. *nrcam* transcripts express weakly in the animal hemisphere of the embryo. *d–e'* indicate anterior and dorsal views of stages 15 and 20. *f–f''* indicate lateral, anterior, and dorsal view of an embryo at stage 24. *nrcam* transcripts are detectable in the optic bulb (*arrowhead*) and fore-, mid-, and hindbrain (*arrowhead*). *g–i''* indicate lateral and dorsal views of embryos at stages 30, 33, and 36. *nrcam* expression is observed in the fore-, mid-, and hindbrain regions; the eye; the trigeminal ganglion; and the otic vesicle. *e* eye, *ea* eye anlage, *ev* eye vesicle, *fb* forebrain, *hb* hindbrain, *l* lens, *mb* midbrain, *ov* otic vesicle, *tg* trigeminal ganglion

also expressed in the optic vesicle, the lens, the trigeminal ganglion nerve, and the otic vesicle (Fig. 2B (g–i)).

Expression in the forebrain

To analyze *nrcam* expression in more detail, transverse histological sections of late tailbud stage embryos were generated. Although *nrcam* messenger RNA (mRNA) was distributed throughout the forebrain (Fig. 3A), we observed a strong expression in the mitotically active ventricular region (vz). Crossing fibers of the floor plate (fp), roof plate (rp), and the cells of the medial ganglionic eminence (mge) and lateral ganglionic eminence (lge) show strong expression. The cortex (c) of the telencephalon also showed a strong expression in the stages analyzed, which is specific to *Xenopus* and not observed in either mouse or chicken. At the level of diencephalon, similar to the forming optic chiasm in mice and chicken (Krushel et al. 1993; Lustig et al. 2001a), *nrcam* expression in *Xenopus* is also observed in the ventral midline region where radial glial cells are present (Fig. 3B (a). Migrating axons of the forming optic stalk (os) crossing the midline, the retinal axons of the optic vesicle (ov), and the cells of dorsal midline (dm) also show *nrcam* expression. The dorsal commissure and cells of the rp, which are essential for dorsal interneuron specification, also show strong expression. Later, at stage 36 (Fig. 3B (c)), when primary and secondary neurogenesis is almost completed and myelination is in progress, the radial glia at the optic chiasm (oc), the retinal ganglion cells in the optic vesicle, the commissural axons, the pineal body (pb), and the dorsal midline show strong *nrcam* expression.

Expression in midbrain and the midbrain-hindbrain boundary

In the midbrain (Fig. 4A, st. 30) *nrcam* is expressed in the dorsal midline. This expression is observed during the entire development of CNS, which is in contrast to the earlier reported expression in mouse (Lustig et al. 2001b). Here, NRCAM transiently expresses in the radial glial fibers at E13 and disappears at later

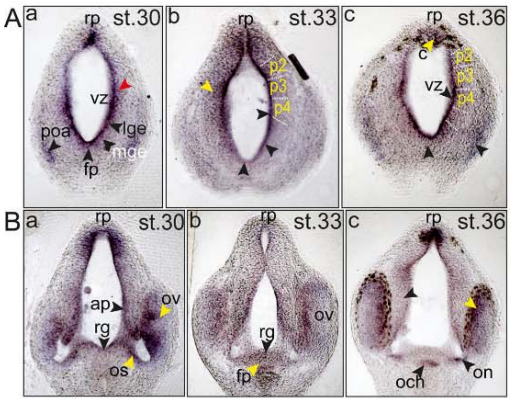

Fig. 3 *nrcam* in the forebrain. Transverse sections of the forebrain at stage 30, 33, and 36 embryos. **A** The telencephalon of the forebrain. *nrcam* is expressed in the roof plate (*rp*), floor plate (*fp*), lateral (*lge*) and medial ganglionic eminence (*mge*), the preoptic area (*poa*), the prosomeres (*p2–p4*), and the ventricular zone (*vz*). **B** The diencephalic region of the forebrain. Strong expression is observed in the ventral diencephalon. Apical progenitors (*ap*), floor plate (*fp*), optic chiasm (*och*), optic nerve (*on*), optic stalk (*os*), optic vesicle (*ov*), radial glia (*rg*), and the roof plate (*rp*)

stages. Only at P0, the axons of the corpus callosum again express NRCAM. In *Xenopus*, the retinal axons of the optic vesicle, the hypothalamus (hyp), and the zona limitans intrathalamica (zli) show *nrcam* expression. At stage 33, expression was most abundant in the lens pit and the trigeminal nerve (tgn) fiber. The level of *nrcam* expression in these structures increased until stage 36, while staining of the radial glia in the ventricular zone (vz), the rp, and the fp is comparatively weaker. In the developing eye, *Xenopus nrcam* is highly enriched in the outer nuclear layer and might be involved in the differentiation of photoreceptor and Müller glial cells, which are formed late during retinogenesis. This is in contrast to the expression of *Nrcam* in mouse retina, which was observed in the retinal ganglion cells (Williams et al. 2006). At the midbrain-hindbrain boundary (Fig. 4B), the tgn fiber and the dorsal interneurons (din), which arise from the asymmetric division of radial glia, show strong expression, whereas in the ventral midline, the expression is relatively weak.

Expression in the hindbrain and the spinal cord

In the hindbrain, *nrcam* expression is detected in the dorsal midline, in the intermediate zone, where prospective interneurons (din) are found, and in the floor plate (Fig. 5A). Further, *nrcam* transcripts are also expressed in the inner otic vesicle (iov). Studies have shown that murine NRCAM is involved in the modulation of the spiral ganglion neurite outgrowth towards their target in the cochlea (Brand et al. 2014). In the spinal cord at stage 30, *nrcam* was expressed all along the midline, in the mitotically active ventricular and subventricular zone and the floor plate cells. By stage 36, this expression pattern disappears completely and *nrcam* is visible only in the dorsal midline, in the interneuron region, and in the dorsolateral sensory neuron fibers. Weak expression was also detectable in the motor neuron region. In contrast, in chick and mouse at early stages, NRCAM was exclusively detected in the commissural cells and the floor plate cells. While at later stages, the ventral commissure, the floor plate, and the dorsal root ganglion (DREZ) are stained (Krushel et al. 1993; Lustig et al. 2001b).

Taken together, we show that *Xenopus nrcam* is conserved compared to other vertebrates. Protein domains show a >95% identity in respect to their amino acid sequence, while the overall similarity was at >85%. The evolutionary tree supported by bootstrap values confirmed the phylogenic conservation of *nrcam*. This observation is further supported by syntenic blocks, which strengthen the shared evolutionary origin of *nrcam*. In *Xenopus*, *nrcam* is expressed along the entire axis of the developing

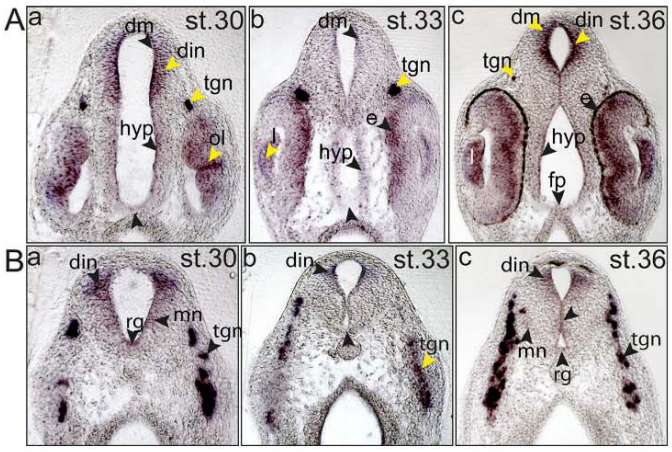

Fig. 4 *nrcam* in midbrain and midbrain-hindbrain boundary. **A** Midbrain. *nrcam* is expressed in the dorsal median (*dm*), dorsal intermediate neurons (*din*), eye (*e*), hypothalamus (*hyp*), lens (*l*), floor plate (*fp*), and the trigeminal nerve (*tgn*). **B** Midbrain-hindbrain boundary. *nrcam* is seen in the motor neurons (*mn*), radial glial cells (*rg*), and the trigeminal ganglion nerve (*tgn*)

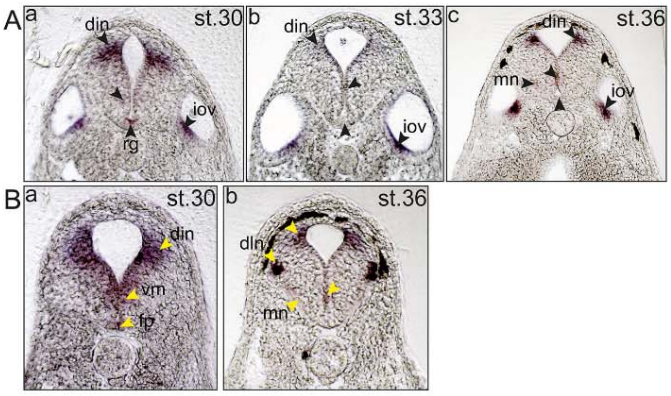

Fig. 5 *nrcam* in the hindbrain and the spinal cord. **A** Hindbrain. Apart from the dorsal inter neurons and the radial glia (*rg*), the inner otic vesicle (*iov*) is also strongly stained for *nrcam*. **B** Spinal cord. At stage 30, *nrcam* expression is observed in the radial glia of the ventricular region, floor plate (fp), dorsal interneurons (din), and at stage 36, in the dorsolateral sensory neuron (dln) as well as motor neurons (mn).

CNS, from the forebrain extending into the spinal cord region. Expression of *nrcam* is mostly restricted to structures along the dorsal as well as the ventral midline. In earlier stages, expression is mainly observed in radial glia, which later differentiate into various cell types upon interaction with the environment. Earlier studies using NRCAM antibody in chick and mice (Krushel et al. 1993; Lustig et al. 2001b) during CNS development revealed a similar expression pattern. However, we also observed that *Xenopus nrcam* is highly enriched in the outer nuclear layer of the retina where progenitor cells differentiate into various cell types depending on the cues, as opposed to *Nrcam* expression in mouse retina. Similarly, the ventricular region of the spinal cord in the early tailbud stage and the dorsal interneuron region in the later stages of development showed *nrcam* expression specific to *Xenopus*. A contrast in such expression pattern suggests roles other than that of axon growth and guidance in lower vertebrates. An intriguing question is whether, in lower vertebrates as opposed to higher vertebrates, the enrichment of *nrcam* in mitotically active zones may also contribute towards proliferation and differentiation of neurons or simply illustrate a higher grade of plasticity during amphibian development. Overall, we show the expression of a lesser-known member of the immunoglobulin superfamily *nrcam* in the nervous system.

Materials and methods

Experimental model

Albino *X. laevis* frogs were purchased from Nasco (Ft. Atkinson, WI). Production and rearing of embryos were performed as described earlier (Hollemann and Pieler 1999) and staged according to Nieuwkoop and Faber 1967.

Whole-mount in situ hybridization

Whole-mount in situ hybridization was performed as described (Hollemann et al. 1998). Anti-sense *nrcam* RNA probe was transcribed in the presence of digoxigenin-labeled UTP (Roche) from plasmid *nrcam*/pCMV-Sport6 (*SacII*/*T7*). Chromogenic reactions were carried out using NBT/BCIP (Roche). Embryos were photographed after the chromogenic reaction. Thirty-micrometer sections were cut from embryos embedded in gelatin/albumin using a microtome (Leica, Germany) and mounted on glass slides.

Total RNA extraction, cDNA preparation, and semiquantitative RT-PCR

Total RNA was extracted from snap frozen embryos. Embryos were homogenized in TRIZOL and phase-separated using chloroform. The mixture was centrifuged and re-extracted using chloroform. Total RNA was precipitated using isopropanol and re-suspended in RNase free water. Five hundred nanograms of total RNA was used for complementary DNA (cDNA) synthesis using *Protoscript II RT ase* (NEB) and random primers following manufacturer's protocol. Semiquantitative RT-PCR was performed using intron-spanning primer pairs, *nrcam*: 5′-CCAA CTCTGGAACCCTGGTG-3′ and 5′-CACG GGTATCTTCTGGTTGC-3′. Annealing temperature was 59 °C for 29 cycles, respectively. *odc-1* was used to control the input mRNA (56 °C, 26 cycles) and water as negative control.

Alignment, phylogeny, and synteny

Full-length fasta sequences for the protein families analyzed were obtained by Blast tool (http://blast.ncbi.nlm.nih.gov) and were aligned using T-Coffee (http://tcoffee.vital-it.ch/apps/tcoffee/index.html). A phylogenetic tree of the proteins was generated through maximum-likelihood and bootstrap analysis using an "A la Carte" mode (http://www.phylogeny.fi). The synteny analysis is based on the individual gene sequences and gene loci from respective genomes of the organisms depicted and the data derived with the help of metazome v3.0 (http://www.metazome.com).

References

Bonora E, Lamb JA, Barnby G, Sykes N, Moberly T, Beyer KS, Klauck SM, Poustka F, Bacchelli E, Blasi F et al (2005) Mutation screening and association analysis of six candidate genes for autism on chromosome 7q. Eur J Hum Genet 13:198–207

Brand Y, Sung M, Pak K, Chavez E, Wei E, Radojevic V, Bodmer D, Ryan AF (2014) Neural cell adhesion molecule NrCAM is expressed in the mammalian inner ear and modulates spiral ganglion neurite outgrowth in an in vitro alternate choice assay. J Mol Neurosci 55:836–844

Brümmendorf T, Rathjen FG (1996) Structure/function relationships of axon-associated adhesion receptors of the immunoglobin superfamily. Curr Opin Neurobiol 6:584–593

Fitzli D, Stoeckli ET, Kunz S, Siribour K, Rader C, Kunz B, Kozlov SV, Buchstaller A, Lane RP, Suter DM et al (2000) A direct interaction of axonin-1 with NgCAM-related cell adhesion molecule (NrCAM) results in guidance, but not growth of commissural axons. J Cell Biol 149:951–968

Grumet M, Mauro V, Burgoon MP, Edelman GM, Cunningham BA (1991) Structure of a new nervous system glycoprotein, Nr-CAM, and its relationship to subgroups of neural cell adhesion molecules. J Cell Biol 113:1399–1412

Heyden A, Angenstein F, Sallaz M, Seidenbecher C, Montag D (2008) Abnormal axonal guidance and brain anatomy in mouse mutants for the cell recognition molecules close homolog of L1 and NgCAM-related cell adhesion molecule. Neuroscience 155:221–233

Hollemann T, Chen Y, Grunz H, Pieler T (1998) Regionalized metabolic activity establishes boundaries of retinoic acid signalling. EMBO J. 17(24):7361–72

Hollemann T, Pieler T (1999) Xpitx-1: a homeobox gene expressed during pituitary and cement gland formation of Xenopus embryos. Mech Dev. 88(2):249–52

Hortsch M (2000) Structural and functional evolution of the L1 family: are four adhesion molecules better than one? Mol Cell Neurosci 15:1–10

Hutcheson HB, Olson LM, Bradford Y, Folstein SE, Santangelo SL, Sutcliffe JS, Haines JL (2004) Examination of NRCAM, LRRN3, KIAA0716, and LAMB1 as autism candidate genes. BMC Med Genet 5:12

Ishiguro H, Liu Q-R, Gong J-P, Hall FS, Ujike H, Morales M, Sakurai T, Grumet M, Uhl GR (2006) NrCAM in addiction vulnerability: positional cloning, drug-regulation, haplotype-specific expression, and altered drug reward in knockout mice. Neuropsychopharmacology 31:572–584

Ishiguro H, Hall FS, Horiuchi Y, Sakurai T, Hishimoto A, Grumet M, Uhl GR, Onaivi ES, Arinami T (2012) NrCAM-regulating neural systems and addiction-related behaviors: NrCAM and addiction. Addict Biol 19:343–353

Julien F, Bechara A, Fiore R, Nawabi H, Zhou H, Hoyo-Becerra C, Bozon M, Rougon G, Grumet M, Püschel AW et al (2005) Dual functional activity of semaphorin 3B is required for positioning the anterior commissure. Neuron 48:63–75

Kayyem JF, Roman JM, de la Rosa EJ, Schwarz U, Dreyer WJ (1992) Bravo/Nr-CAM is closely related to the cell adhesion molecules L1 and Ng-CAM and has a similar heterodimer structure. J Cell Biol 118:1259–1270

Krushel LA, Prieto BA, Cunningham BA, Edelman GM (1993) Expression patterns of the cell adhesion molecule Nr-CAM during histogenesis of the chick nervous system. Neuroscience 53:797–812

Kuwajima T, Yoshida Y, Takegahara N, Petros TJ, Kumanogoh A, Jessell TM, Sakurai T, Mason C (2012) Optic chiasm presentation of Semaphorin6D in the context of Plexin-A1 and Nr-CAM promotes retinal axon midline crossing. Neuron 74:676–690

Lane RP, Chen X-N, Yamakawa K, Vielmetter J, Korenberg JR, Dreyer WJ (1996) Characterization of a highly conserved human homolog to the chicken neural cell surface protein Bravo/Nr-CAM that maps to chromosome band 7q31. Genomics 35:456–465

Lustig M, Sakurai T, Grumet M (1999) Nr-CAM promotes neurite outgrowth from peripheral ganglia by a mechanism involving axonin-1 as a neural receptor. Dev Biol 209:340–351

Lustig M, Erskine L, Mason CA, Grumet M, Sakurai T (2001a) Nr-CAM expression in the developing mouse nervous system: ventral midline structures, specific fiber tracts, and neuropilar regions. J Comp Neurol 434:13–28

Lustig M, Zanazzi G, Sakurai T, Blanco C, Levinson SR, Lambert S, Grumet M, Salzer JL (2001b) Nr-CAM and neurofascin interactions regulate ankyrin G and sodium channel clustering at the node of Ranvier. Curr Biol 11:1864–1869

Mauro VP, Krushel LA, Cunningham BA, Edelman GM (1992) Homophilic and heterophilic binding activities of Nr-CAM, a nervous system cell adhesion molecule. J Cell Biol 119:191–202

Nieuwkoop PD, Faber J (1967) Normal table of xenopus laevis (Daudin). North Holland, Amsterdam

Suter DM, Pollerberg GE, Buchstaller A, Giger RJ, Dreyer WJ, Sonderegger P (1995) Binding between the neural cell adhesion molecules axonin-1 and Nr-CAM/Bravo is involved in neuron-glia interaction. J Cell Biol 131:1067–1081

Volkmer H, Leuschner R, Zacharias U, Rathjen FG (1996) Neurofascin induces neurites by heterophilic interactions with axonal NrCAM while NrCAM requires F11 on the axonal surface to extend neurites. J Cell Biol 135:1059–1069

Wang B, Williams H, Du J-S, Jonathan T, Kenwrick S (1998) Alternative splicing of human nrcam in neural and nonneural tissues. Mol Cell Neurosci 10:287–295

Wang X, Zhang W, Cheever T, Schwarz V, Opperman K, Hutter H, Koepp D, Chen L (2008) The C. elegans L1CAM homologue LAD-2 functions as a coreceptor in MAB-20/Sema2 mediated axon guidance. J. Cell Biol 180:233–246

Williams SE, Grumet M, Colman DR, Henkemeyer M, Mason CA, Sakurai T (2006) A role for Nr-CAM in the patterning of binocular visual pathways. Neuron 50:535–547

Zelina P, Avci HX, Thelen K, Pollerberg GE (2005) The cell adhesion molecule NrCAM is crucial for growth cone behaviour and pathfinding of retinal ganglion cell axons. Development 132:3609–3618

4.4 Manuscript 4: Expressional characterization of mRNA (guanine-7) methyltransferase (*rnmt*) during early development of *Xenopus laevis*

Int. J. Dev. Biol. 60: 65-69 (2016)
doi: 10.1387/ijdb.150409th

THE INTERNATIONAL JOURNAL OF DEVELOPMENTAL BIOLOGY
www.intjdevbiol.com

Expressional characterization of mRNA (guanine-7) methyltransferase *(rnmt)* during early development of *Xenopus laevis*

ASHWIN LOKAPALLY, SANJEEVA METIKALA and THOMAS HOLLEMANN*

Martin-Luther-University Halle-Wittenberg, Institute for Physiological Chemistry, Halle (Saale), Germany

ABSTRACT Methylation of the guanosine cap structure at the 5' end of mRNA is essential for efficient translation of all eukaryotic cellular mRNAs, gene expression and cell viability and promotes transcription, splicing, polyadenylation and nuclear export of mRNA. In the current study, we present the spatial expression pattern of the *Xenopus laevis rnmt* homologue. A high percentage of protein sequence similarity, especially within the methyltransferase domain, as well as an increased expression in the cells of the transcriptionally active stages, suggests a conserved RNA cap methylation function. Spatial expression analysis identified expression domains in the brain, the retina, the lens, the otic vesicles and the branchial arches.

KEY WORDS: *rnmt, methylation, 5' cap structure*

Methylation is one of the most common RNA modification, which is carried out by members of the AdoMet-dependent (adenosylmethionine) methyltransferase superfamily. A member of this superfamily is the 5'mRNA (guanine-7-) methyltransferase (RNMT) (Wang and Shuman, 1997), which catalyses the addition of a 5' cap structure to the 5'-triphosphate ends of nascent nuclear pre-mRNAs shortly after transcription initiation by RNA polymerase II (RNSPII) (Shatkin, 1985). The formation of a methylated 5'-terminal cap structure m7G(5')ppp(5')N, directs the processing and transport pathways of pre-mRNA in the cell nucleus and regulates both mRNA turnover and the initiation of translation in the cytoplasm and has been studied intensively (Rottman *et al.*, 1974; Shatkin, 1976).

The mRNA cap methyltransferase (RNMT) is highly conserved in eukaryotes and the highest similarity is maintained in the S-adenosylmethionine (SAM)-binding site necessary for catalytic activity (Saha *et al.*, 1999; Wang and Shuman, 1997). Interestingly, the C-terminus of human RNMT could be substituted by the C-terminus of *S. cerevisiae* Abd1, the first characterized methyltransferase (Saha *et al.*, 1999). However, mammalian RNMT has an additional non-catalytic N-terminal domain, required for efficient recruitment of RNAPII, which is absent in yeast. The N-terminus contains 2 nuclear localization signal motifs (Aregger and Cowling, 2013) and it has been shown that nuclear localization of RNMT is essential for cell viability (Shafer *et al.*, 2005). Yeast Abd1 and human RNMT are also required for cell growth and cell survival (Chu and Shatkin, 2008). Abd1 mutants are lethal, since inhibition of Abd1 function results in an almost complete loss of protein synthesis (Mao *et al.*, 1996). In *Xenopus* oocytes, injection of synthetic RNA containing a m7G cap structure leads to increased stability and more efficient translation of the RNA (Gillian-Daniel *et al.*, 1998).

It is now clear that methylation of the cap structure is necessary for the splicing of pre-mRNA, mRNA export, polyadenylation and translation initiation (Cowling, 2010). The cap methylation activity of RNMT is regulated by various factors, e.g. expression of the myelocytomatosis viral oncogene (Myc) protein leads to up-regulated mRNA cap methylation on specific target mRNAs (Cole and Cowling, 2009). Myc binds directly to a subunit of TFIIH (transcription factor IIH) and increases RNAPII phosphorylation of Ser5 in the C-terminal domain (CTD), which is the binding site of RNMT during transcription initiation (Cowling and Cole, 2007). E2F1 – a transcription factor, promoting cell proliferation, was also demonstrated to up-regulate mRNA cap methylation (Cole and Cowling, 2009). SAHH (S-adenosylhomocysteine hydrolase) hydrolyses SAH (S-adenosyl homocysteine) a by-product of cellular methylation that inhibits RNMT, thus relieving suppression of RNMT activity. In line with this finding, mRNA cap methylation is up-regulated by Sahh (SAH hydrolase) during gastrulation in

Abbreviations used in this paper: RNMT, 5' mRNA (guanine-7-) methyltransferase;

***Address correspondence to:** Thomas Hollemann. Martin-Luther-University Halle-Wittenberg, Institute for Physiological Chemistry, Halle (Saale), Germany. e-mail: thomas.hollemann@medizin.uni-halle.de

Supplementary Material (one figure) for this paper is available at: http://dx.doi.org/10.1387/ijdb.150409th

Accepted: 4 February 2016.

ISSN: Online 1696-3547, Print 0214-6282

Xenopus and Sahh was immunoprecipitated with Rnmt (Radomski *et al.*, 2002).

Numerous cellular studies contributed to a better understanding of the mechanisms underlying the regulation of 5' mRNA cap methylation. Especially, extensive studies in yeast, mammalian cell cultures and in *Xenopus laevis* oocytes have identified many essential regulators that govern 5' capping and cap methylation. However, not much attention is paid to the developmental aspects of capping enzymes. We report on the spatio-temporal expression of *Xenopus laevis* mRNA (guanine-7-) methyltransferase (*rnmt*) during early development.

Results and Discussion

Sequence analysis and evolutionary relationship

We identified an expressed sequence tag (EST) containing the full-length *Xenopus laevis* RNA (guanine-7-) methyltransferase (*rnmt*) sequence using the BLAST programme. A full-length clone was obtained from the I.M.A.G.E. consortium, Source Biosciences (NM_001088535.1) and used in this study. The 1959 bp full-length

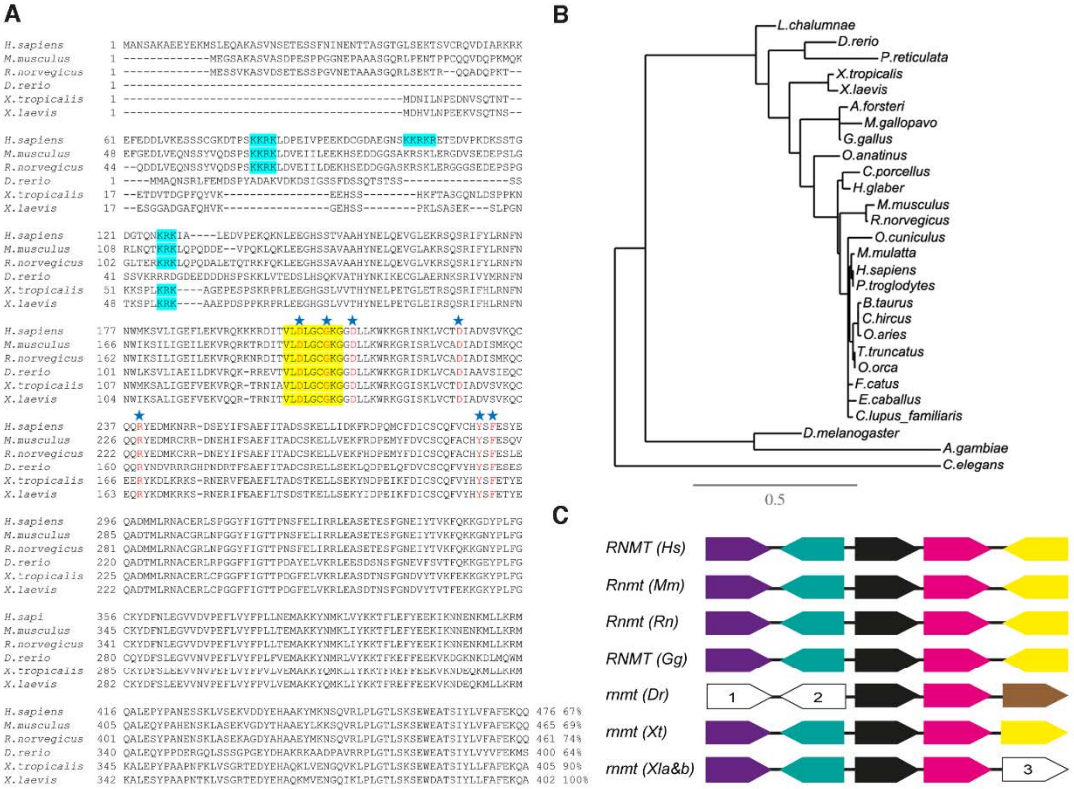

Fig. 1. Alignment of vertebrate Rnmt protein sequences. (A) *Comparison of amino acid sequences of vertebrate Rnmt.* H. sapiens *(GenBank Accession no. NP_003790),* M. musculus *(GenBank Accession no. NP_080716),* R. norvegicus *(GenBank Accession no. NP_001008300),* D. rerio *(GenBank Accession no. NP_001038465),* X. tropicalis *(GenBank Accession no. NP_001017053),* X. laevis *(GenBank Accession no. NP_001082004). The nuclear localization signal motifs are highlighted in blue, while the SAM (S-adenosylmethionine) binding domain is highlighted in yellow. The stars above the sequence indicate the amino acids necessary for the methyl transferase activity of RNMT. Sequence identities compared to the* X. laevis *protein in percent are indicated at the end of the alignment.* **(B)** *Phylogenetic analysis: The common ancestral node indicates orthology among species. The bar at the bottom of the phylogram indicates the evolutionary distance, to which the branch lengths are scaled based on the estimated divergence. There is a 50% relative divergence observed over time.* **(C)** *Synteny analysis of* rnmt. *The location and orientation of* rnmt *in the respective genomes is conserved. Each arrow stands for a single gene while the arrowhead indicates the direction of the ORF. Orthologues are marked with identical colours.* rnmt *(black arrow) is present in all the species analysed. The genes flanking* rnmt *downstream are identical in all species except for* D. rerio *where the identity of the flanking genes (1 & 2) is still unknown. Similarly, the genes flanking* rnmt *upstream are identical in all species other than* D. rerio *(brown arrow) and* X. laevis *(3) with unknown identity. Arrow colours; black:* rnmt, *turquoise: family with sequence similarity 210 member A/*fam*210a, violet: low-density lipoprotein receptor class A domain containing 4/*ldlrad*4, pink: melanocortin 5 receptor/*mc5r, *yellow: melanocortin 2 receptor/*mc2r, *brown: collagen triple helix repeat containing 1a/*cthrc*1a, white 1,2 & 3: unknown identity.*

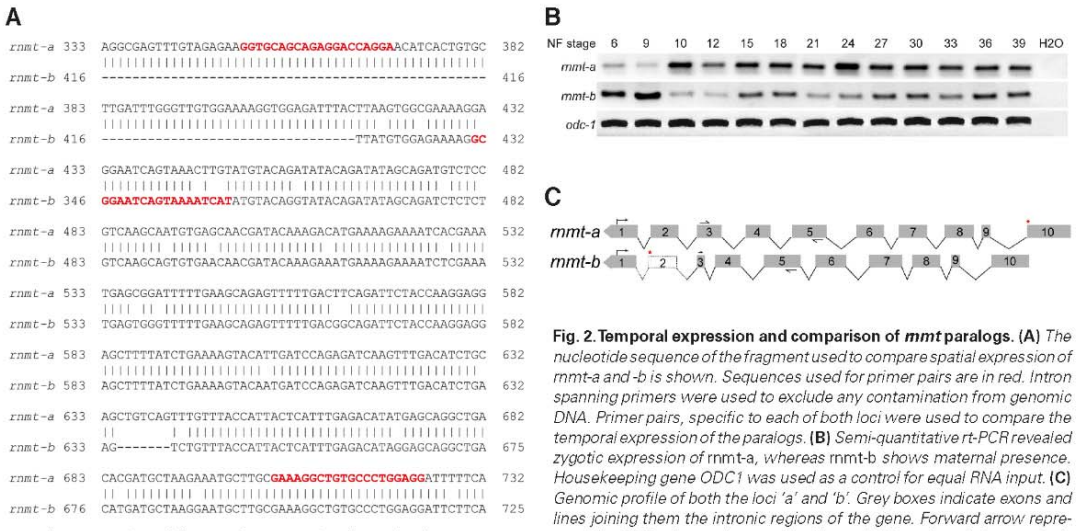

Fig. 2. Temporal expression and comparison of *rnmt* paralogs. (A) *The nucleotide sequence of the fragment used to compare spatial expression of* rnmt-a *and* -b *is shown. Sequences used for primer pairs are in red. Intron spanning primers were used to exclude any contamination from genomic DNA. Primer pairs, specific to each of both loci were used to compare the temporal expression of the paralogs.* **(B)** *Semi-quantitative rt-PCR revealed zygotic expression of* rnmt-a, *whereas* rnmt-b *shows maternal presence. Housekeeping gene ODC1 was used as a control for equal RNA input.* **(C)** *Genomic profile of both the loci 'a' and 'b'. Grey boxes indicate exons and lines joining them the intronic regions of the gene. Forward arrow represent the start codon while star the stop codon. Arrowheads over exons represent the PCR primer pairs used in this study. Note the missing genomic sequence is shown in dotted lines between exon 1 and exon 3 and including the whole exon.*

rnmt cDNA sequence contains an ORF of 1209 bases, encoding a putative protein of 402 amino acids. The alignment of the predicted amino acid sequences of known homologues reveals high similarity in the region essential for RNA (guanine-7-) methyltransferase activity (100 %). The similarity over the whole length of the protein is >65% among vertebrates (Fig. 1A). It is important to note that the length and sequence of different N-terminal regions differs substantially (Fig. 1A). In human RNMT, the N-terminal residues 1 to 120 are dispensable for enzymatic activity but they are necessary for the recruitment of RNMT to the transcription initiation site (Aregger and Cowling, 2013) and for nuclear localization of the methyltransferase (Fig. 1A) (Shafer *et al.*, 2005). However, *Xenopus* Rnmt, has a shorter N-terminus, lacking the two nuclear localization signal (NLS) motifs present in the human protein. It has been shown that a third NLS motif at K126 of the human protein sequence is sufficient for alternative nuclear localization (Shafer *et al.*, 2005). This NLS motif is also present in the *Xenopus laevis* protein at position K53. Similarly, the *SAM* (S-adenosylmethionine) binding site as well as the sites necessary for methyltransferase activity are well conserved between mammals and amphibians (Fig. 1A) (Bujnicki *et al.*, 2001; Saha *et al.*, 1999). Further, we identified the sequence of a paralogue (*rnmt-b*) within the *Xenopus laevis* genome. Sequence comparison of the paralogues revealed a large un-sequenced region, which lies between the first and the third exon including exon 2 (Fig. 2C). A search for *Xenopus laevis* EST clones lead to the identification of a cDNA sequence, encoding a truncated protein (Supplementary Fig. S1) thus making it difficult for any further analysis.

A phylogenetic tree was constructed for the identified proteins from vertebrates based on maximum likelihood using phylogeny.fr. The branches originate from a phylogenetically common ancestral lineage (Fig. 1B). Varying lengths of protein sequences contribute to the length of branches over the course of evolution. The phylogenetic groups correlate well with the presence of the sequence signatures that can be regarded as synapomorphies (shared features derived from a common ancestor). To further confirm orthology of *Xenopus rnmt*, we looked at the synteny. *Xenopus laevis rnmt* shows a shared synteny among the species analysed (Fig. 1C). However, the orientation of the second gene (brown and yellow arrows and 3) upstream to *rnmt* in lower vertebrates differs from that of higher vertebrates, due to a possible shift in orientation of the respective genes.

Temporal expression of Xenopus laevis *(guanine-7) methyltransferase* (rnmt) *during early development*

To analyse the temporal expression of both paralogues of *Xenopus rnmt* during early embryogenesis, we designed two primer pairs, each pair specific for only one of the two loci (a and b). Using semi-quantitative RT-PCR we could detect relatively low maternal expression of *rnmt*-a at the earliest developmental stage analysed (NF stage 6). At gastrulation (NF stage 10), expression of *rnmt-a* is slightly upregulated, due to the initiation of zygotic expression (Fig. 2B). The expression level remains constant throughout further stages. In contrast, much stronger maternal expression of *rnmt-b* is detectable, but during gastrulation expression decreases and remains relatively low during later development. This temporal expression pattern is in contrast to the earlier reported expression (Yokoska *et al.*, 2000, Liu *et al.*, 2014), wherein the expression is shown only up to stage 20, with expression levels of *rnmt* gradually decreasing after gastrulation. Interestingly, later studies reported an upregulation of mRNA cap methylation during oocyte maturation (Gillian-Daniel *et al.*, 1998), probably an indirect effect of *sahh*. *sahh* hydrolyses *sah*; an inhibitor of *rnmt*, thus relieving the repression of the methyltransferase. During early gastrulation *sahh* translocates from the cytoplasm to the nucleus, coinciding with the increase in zygotic mRNA synthesis and thereby the expres-

sion of *rnmt* (Radomski *et al.*, 1999, 2002). We observed a similar regulation of *rnmt-a* but not of *rnmt-b* at gastrulation suggesting differential expression of both isoforms. Although, the 5'UTR is similar in both isoforms, the 3'UTR differs hugely. Also reported earlier, the human isoforms of RNMT, hCMT1a, -b and -c, hCMT1a and hCMT1c encode for the same protein but the 5' and 3' UTR regions of hCMT1a differs from hCMT1c, while hCMT1b shares the same N-terminus as hCMT1c but differs thereafter. Recombinant hCMT1a/c are active in an *in vitro* RNA methyltransferase assay, whereas hCMT1b is not (Tsukamoto *et al.*, 1998). This leads to the hypothesis that, a similar differential regulation of Rnmt among the active and non-active isoform exists here for *Xenopus laevis rnmt-a* and *rnmt-b*. Radomski *et al.*, (1999) proposed earlier that efficient cap methylation of mRNA requires the expression of *rnmt* in transcriptionally active cells. We also see a similar increased expression of the transcript from gastrulation onwards.

Spatial expression of Xenopus laevis *mRNA (guanine-7) methyltransferase* (rnmt) *during early development*

Since the spatial expression of *rnmt* during early *Xenopus* development is not analysed yet, we examined the spatial expression of RNA (guanine-7-) methyltransferase in frog embryos using whole mount *in situ* hybridization. Due to lack of complete *rnmt-b* sequence and its high similarity towards locus-a, it was not possible to generate an *in situ* probe for the -b locus. Transcripts of *rnmt* are weakly detected early in the animal hemisphere of blastulae (data not shown). At gastrulation (Fig. 3 A-D), *rnmt* transcripts were detected in the ectoderm of the animal hemisphere. At early and late neurula stages expression of *rnmt* was restricted to the anterior neural plate, the neural folds (Fig. 3 E-H) and the eye anlage.

From early to late tailbud stages (Fig. 3 I-N) *rnmt* transcripts were detected in prospective brain areas, i.e. proscencephalon, mesencephalon and rhombencephalon, the retinal layers of eye vesicles and the branchial arches. Furthermore, at late tailbud stages, *rnmt* transcripts are also expressed in the otic vesicle (Fig. 3 O-V), in the lens, head mesenchyme (hm) (Fig. 3 Q,R), ventral aorta (va) (Fig. 3 U) and the ventral interneuron (vi) region of the hindbrain (Fig. 3 R,V). The functional role of this gene in transcriptional hierarchy of RNA cap methylation during develop-

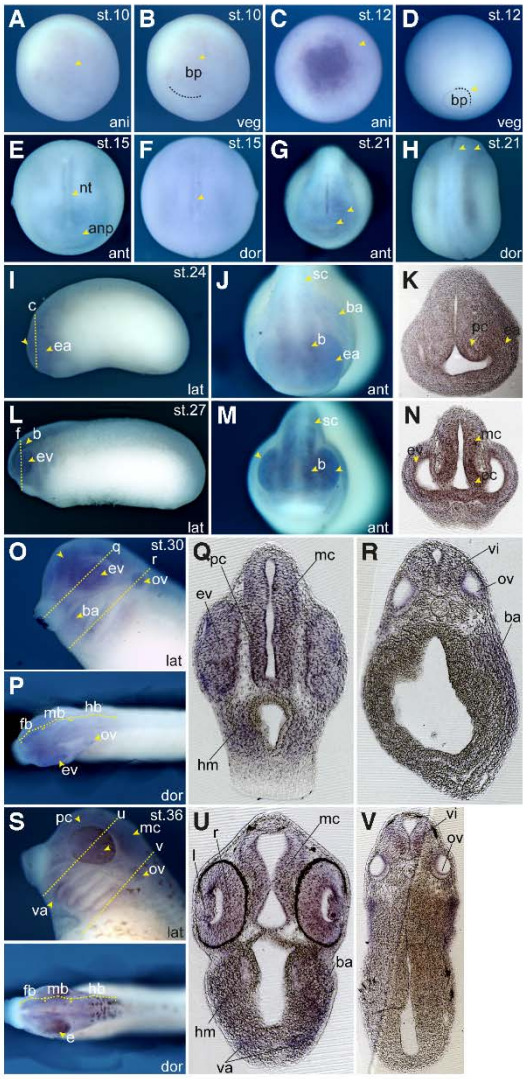

Fig. 3. Spatial expression of *rnmt*. *Whole-mount* in situ *hybridization of wild type albino embryos at developmental NF stages 10 to 21. At gastrulation; stage 10 and 12, transcripts of* rnmt *are visible in the animal hemisphere but not in the vegetal (blastopore) (yellow arrowheads; A-D). During early and late neurulation transcripts are detectable in the anterior neural plate (anp), and the neural tube (nt) (E-H). At stage 21 transcripts were detected in the prospective eye anlage (G,H).* **(I-L)** rnmt *expression during embryonic development.* **(I,J)** *Lateral and anterior view of an embryo at stage 24.* rnmt *transcript were detectable in the eye anlage (ea) and brain (b) The expression in the branchial arches (ba) and the spinal cord (sc) is relatively weak.* **(L,M)** *Lateral and anterior view of an embryo at stage 27. Similar to stage 24* rnmt *is detectable in the brain (b) eye vesicle (ev), the spinal cord (sc) and the branchial arches (ba).* **(K,N)** *Transverse sections of stage 24 and stage 27 embryos show expression in the eye vesicle (ev), procencephalon (pc) and mesencephalon (mc).* **(O-T)** *Expression of* rnmt *during late tail bud stages.* **(O)** *Lateral view of the head of a stage 30 embryo.* rnmt *is expressed in the eye vesicle (ev), otic vesicle (ov) and the branchial arches (ba). Yellow dotted lines indicate the level of sections shown in e & f.* **(P).** *Dorsal view of stage 30 embryo. Expression in forebrain (fb) and midbrain (mb) is visible, while a weak expression is seen in hind brain (hb).* **(S).** *Lateral view of the head of a stage 36 embryo.* rnmt *mRNA is localized in the neural system, ventral branchial arches and ventral aorta. Yellow dotted lines indicate the level of sections shown in G & H.* **(T).** *Dorsal view of stage 36 embryo.* rnmt *mRNA transcript is visible in eyes and the brain region.* **(Q,R,U,V).** *Transverse sections through* Xenopus *embryos at indicated stages.* **(Q)** rnmt *is expressed in the eye vesicle (ev), prosencephalon (pc), mesencephalon (mc) and head mesenchyme (hm).* **(R)** rnmt *expression can be viewed in inter neuronal region of the hind brain (hb), otic vesicle (ov) and branchial arches (ba).* **(U).** rnmt *is expressed in mid brain (mc), retina (r), lens (l), head mesenchyme (hm), branchial arches (ba) and ventral aorta (va).* **(V)** rnmt *expression is seen in ventral inter neurons (vi) of the hind brain and the otic vesicle (ov).*

ment needs to be further established. It is of note that Xp54nrb, another RNA processing enzyme involved in splicing was reported to be expressed in neural structures recently (Neant *et al.*, 2001).

Concluding, this paper describes the expression of a vertebrate RNA cap methylation enzyme expressed in early development of *Xenopus laevis*. Our data shows that *rnmt* is expressed in a restricted pattern, specifically in the developing brain, the retina, the lens, the otic vesicles and the branchial arches.

Materials and Methods

Experimental model

Albino *Xenopus laevis* frogs were purchased from Nasco (Ft. Atkinson, WI). Production and rearing of embryos was performed as described earlier (Hollemann and Pieler, 1999) and staged according to Nieuwkoop and Faber, 1994.

Whole mount in situ *hybridization*

Whole mount *in situ* hybridization was performed as described (Hollemann *et al.*, 1998). Anti-sense *xl-rnmt* RNA probe was transcribed in the presence of digoxigenin-labelled UTP (Roche) from plasmid *xl-rnmt*/pCMV-Sport6.ccdb (*SacI*/*T7*). Chromogenic reactions were carried out using NBT/BCIP (Roche). Embryos were photographed after the chromogenic reaction. 30 μm sections were cut from embryos embedded in gelatin/albumin using a microtome (Leica, Germany) and mounted on glass slides.

Total RNA extraction, cDNA preparation and semi-quantitative RT-PCR

Total RNA was extracted from snap frozen embryos. Embryos were homogenized in TRIZOL, and phase separated using chloroform. The mixture was centrifuged and re-extracted using chloroform. Total RNA was precipitated using isopropanol and re-suspended in RNase free water. 500 ng total RNA was used for cDNA synthesis using *Protoscript II RTase* (NEB) and random primers following manufacturer's protocol. Semi-quantitative RT-PCR was performed using following intron spanning primer pairs, *rnmt-a*: 5'-GGTGCAGCAGAGGACCAGGA and CCTCCAGGGCACAGCCTTTC, *rnmt-b*: 5'- GGCGGAATCAGTAAAATCAT and reverse same as above. Annealing temperatures were 62 °C and 56 °C, 28 and 32 cycles respectively. *xl-odc-1* was used to control the input mRNA (56 °C, 26 cycles).

Alignment, phylogeny, synteny

The fasta sequences for the protein families analysed were obtained by Blast tool (http://blast.ncbi.nlm.nih.gov) and aligned using T-Coffee and Box shade tool (http://tcoffee.vital-it.ch/apps/tcoffee/index.html). A phylogenetic tree of the proteins was generated through maximum-likelihood using one-click mode (http://www.phylogeny.fr). The synteny analysis is based on data derived with the help of metazome v3.0 (http://www.metazome.com). The individual gene sequences and the corresponding information regarding *Xenopus laevis* gene loci were obtained from Xenbase (http://gbrowse.xenbase.org) and depicted accordingly.

References

AREGGER M, COWLING V H (2013). Human cap methyltransferase (RNMT) N-terminal non-catalytic domain mediates recruitment to transcription initiation sites. *Biochem J* 455: 67–73.

BUJNICKI J M, FEDER M, RADLINSKA M and RYCHLEWSKI L (2001). mRNA: guanine-N7 cap methyltransferases: identification of novel members of the family, evolutionary analysis, homology modeling, and analysis of sequence-structure-function relationships. *BMC Bioinformatics* 2: 2.

CHU C, SHATKIN A J (2008). Apoptosis and Autophagy Induction in Mammalian Cells by Small Interfering RNA Knockdown of mRNA Capping Enzymes. *Mol Cell Biol* 28: 5829–5836.

COLE M D, COWLING V H (2009). Specific regulation of mRNA cap methylation by the c-Myc and E2F1 transcription factors. *Oncogene* 28: 1169–1175.

COWLING V H (2010). Regulation of mRNA cap methylation. *Biochem J* 425: 295–302.

COWLING V H, COLE M D (2007). The Myc Transactivation Domain Promotes Global Phosphorylation of the RNA Polymerase II Carboxy-Terminal Domain Independently of Direct DNA Binding. *Mol Cell Biol* 27: 2059–2073.

GILLIAN-DANIEL D L, GRAY N K, ÅASTRÖM J, BARKOFF A and WICKEN M (1998). Modifications of the 5′ Cap of mRNAs during *Xenopus* Oocyte Maturation: Independence from Changes in Poly (A) Length and Impact on Translation. *Mol Cell Biol* 18: 6152–6163.

HOLLEMANN T, PIELER T (1999). Xpitx-1: a homeobox gene expressed during pituitary and cement gland formation of *Xenopus* embryos. *Mech Dev* 88: 249–252.

HOLLEMANN T, CHEN Y, GRUNZ H and PIELER T (1998). Regionalized metabolic activity establishes boundaries of retinoic acid signalling. *EMBO J* 17: 7361–7372.

LIU M M, DAVEY J W, JACKSON D J, BLAXTER M L and DAVISON A (2014). A conserved set of maternal genes? Insights from a molluscan transcriptome. *Int J Dev Biol* 58: 501-511

MAO X, SCHWER B and SHUMAN S (1996). Mutational analysis of the Saccharomyces cerevisiae ABD1 gene: cap methyltransferase activity is essential for cell growth. *Mol Cell Biol* 16: 475–480.

NEANT I, DEISIG N, SCERBO P, LECLERC C and MOREAU M (2011). The RNA-binding protein Xp54nrb isolated from a Ca2+-dependent screen is expressed in neural structures during *Xenopus laevis* development. *Int J Dev Biol*, 55: 923-931

RADOMSKI N, KAUFMANN C and DREYER C (1999). Nuclear Accumulation of S-Adenosylhomocysteine Hydrolase in Transcriptionally Active Cells during Development of *Xenopus laevis*. *Mol Biol Cell* 10: 4283–4298.

RADOMSKI N, BARRETO G, KAUFMANN C, YOKOSKA J, MIZUMOTO K and DREYER C (2002). Interaction of S-adenosylhomocysteine hydrolase of *Xenopus laevis* with mRNA (guanine-7-) methyltransferase: implication on its nuclear compartmentalisation and on cap methylation of hnRNA. *Biochim Biophys Acta* 1590: 93–102.

ROTTMAN F, SHATKIN A J and PERRY R P (1974). Sequences Containing Methylated Nucleotides at the 5′ Termini of Messenger RNAs: Possible Implications for Processing. *Cell* 3: 197–199.

SAHA N, SCHWER B and SHUMAN S (1999). Characterization of human, Schizosaccharomyces pombe, and Candida albicans mRNA cap methyltransferases and complete replacement of the yeast capping apparatus by mammalian enzymes. *J Biol Chem* 274: 16553–16562.

SHAFER B, CHU C and SHATKIN A J (2005). Human mRNA Cap Methyltransferase: Alternative Nuclear Localization Signal Motifs Ensure Nuclear Localization Required for Viability. *Mol Cell Biol* 25: 2644–2649.

SHATKIN A J (1976). Capping of Eukaryotic mRNAs. *Cell* 9: 645–653.

SHATKIN A J (1985). mRNA cap binding proteins: essential factors for initiating translation. *Cell* 40: 223–224.

TSUKAMOTO T, SHIBAGAKI Y, NIIKURA Y and MIZUMOTO K (1998). Cloning and Characterization of Three Human cDNAs Encoding mRNA (Guanine-7-)-methyltransferase, an mRNA Cap Methylase. *Biochem Biophys Res Commun* 251: 27–34.

WANG S P, and SHUMAN S (1997). Structure-function analysis of the mRNA cap methyltransferase of Saccharomyces cerevisiae. *J Biol Chem* 272: 14683–14689.

YOKOSKA J, TSUKAMOTO T, MIURA K, SHIOKAWA K and MIZUMOTO K (2000). Cloning and Characterization of mRNA Capping Enzyme and mRNA (Guanine-7-)-methyltransferase cDNAs from *Xenopus laevis*. *Biochem Biophys Res Commun* 268: 617–624.

THE INTERNATIONAL JOURNAL OF DEVELOPMENTAL BIOLOGY
www.intjdevbiol.com

doi: 10.1387/ijdb.150409th

SUPPLEMENTARY MATERIAL

corresponding to:

Expressional characterization of mRNA (guanine-7) methyltransferase *(rnmt)* during early development of *Xenopus laevis*

ASHWIN LOKAPALLY, SANJEEVA METIKALA and THOMAS HOLLEMANN*

***Address correspondence to**: Thomas Hollemann. Martin-Luther-University Halle-Wittenberg, Institute for Physiological Chemistry, Halle (Saale), Germany. e-mail: thomas.hollemann@medizin.uni-halle.de

Full text for this paper is available at: http://dx.doi.org/10.1387/ijdb.150409th

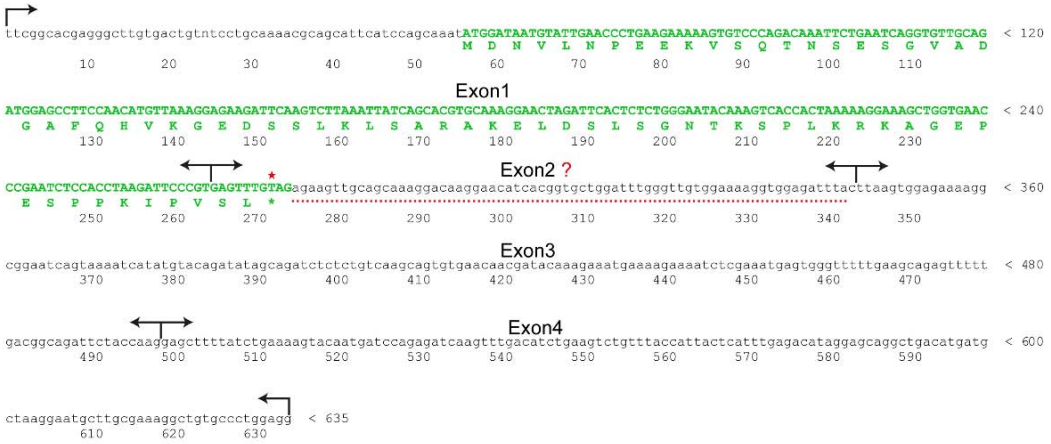

Supplementary Fig. S1. *Xenopus laevis* cDNA: EST clone BJ062466. *cDNA sequence from an EST clone in* X. laevis *genome. The sequence in green represents the ORF, red star the premature stop codon at the beginning of exon 2 while the arrows in both directions i.e. forward and reverse represent the splicing regions in the 5′ and 3′ direction.*

4.5 Manuscript 5: SOMA: A Single Oligonucleotide Mutagenesis and Cloning Approach

OPEN ACCESS Freely available online

PLOS ONE

SOMA: A Single Oligonucleotide Mutagenesis and Cloning Approach

Thorsten Pfirrmann[1]*, Ashwin Lokapally[1], Claes Andréasson[2], Per Ljungdahl[2], Thomas Hollemann[1]

1 Department of Molecular Medicine, Institute for Physiological Chemistry, Martin-Luther University Halle-Wittenberg, Halle, Germany, 2 Department of Molecular Biosciences, The Wenner-Gren Institute, Stockholm University, Stockholm, Sweden

Abstract

Modern biology research requires simple techniques for efficient and restriction site-independent modification of genetic material. Classical cloning and mutagenesis strategies are limited by their dependency on restriction sites and the use of complementary primer pairs. Here, we describe the Single Oligonucleotide Mutagenesis and Cloning Approach (SOMA) that is independent of restriction sites and only requires a single mutagenic oligonucleotide to modify a plasmid. We demonstrate the broad application spectrum of SOMA with three examples. First, we present a novel plasmid that in a standardized and rapid fashion can be used as a template for SOMA to generate GFP-reporters. We successfully use such a reporter to assess the *in vivo* knock-down quality of morpholinos in *Xenopus laevis* embryos. In a second example, we show how to use a SOMA-based protocol for restriction-site independent cloning to generate chimeric proteins by domain swapping between the two human hRMD5a and hRMD5b isoforms. Last, we show that SOMA simplifies the generation of randomized single-site mutagenized gene libraries. As an example we random-mutagenize a single codon affecting the catalytic activity of the yeast Ssy5 endoprotease and identify a spectrum of tolerated and non-tolerated substitutions. Thus, SOMA represents a highly efficient alternative to classical cloning and mutagenesis strategies.

Citation: Pfirrmann T, Lokapally A, Andréasson C, Ljungdahl P, Hollemann T (2013) SOMA: A Single Oligonucleotide Mutagenesis and Cloning Approach. PLoS ONE 8(6): e64870. doi:10.1371/journal.pone.0064870

Editor: Hector Candela, Universidad Miguel Hernández de Elche, Spain

Received January 25, 2013; **Accepted** April 13, 2013; **Published** June 4, 2013

Funding: This research was supported by funding from the Swedish Research Council and the Fonds der Chemischen Industrie, Frankfurt. The funders had no role in study design, data collection and analysis, decision to publish, or preparation of the manuscript.

Competing Interests: The authors have declared that no competing interests exist.

* E-mail: thorsten.pfirrmann@medizin.uni-halle.de

Introduction

The study of modern molecular biology requires techniques that facilitate the flexible and targeted manipulation of genetic material. Novel methods for DNA domain shuffling and site-directed or random mutagenesis of genes are critical for advancement in fields of molecular biology like synthetic biology, developmental biology and protein engineering [1]. Site-directed mutagenesis is a commonly used method for the engineering of proteins with wide applications in contemporary biological studies [2,3]. Advanced methods to manipulate DNA are used to create internal deletions and insertions, to carry out site-directed and random mutagenesis, and to precisely shuffle defined genetic elements. Literature documents a variety of methodological approaches [4]. However, most methods apply PCR with oligonucleotide primer pairs to introduce respective mutations, e.g. Stratagene's QuikChange™ protocol [5]. This has several drawbacks, e.g. primer pairs carrying desired mutations anneal stronger to each other than to the target sequences. Often this limits the efficiency of the reaction. Moreover, the use of primer pairs may cause the introduction of non-homologous base pairs within the mutagenized codon when generating semi-random mutagenized gene libraries. To circumvent this problem, several alternative methods have been published [6,7,8], often with modified primer designs and time consuming additional working steps. An interesting method commercially available as QuikChange Multi™ (Stratagene) involves Pfu-DNA polymerase extension and ligation of plasmids. However, the required composition of the reagents is not published [9] and the method does not employ state-of-the-art reagents such as high-speed proofreading polymerases based on Sso7d fusions [10] commercialized as Phusion High-Fidelity DNA Polymerase (Finnzymes, Thermo Scientific).

Here, we describe the Single-Oligonucleotide Mutagenesis and Cloning Approach (SOMA) that is based on high-speed proofreading Phusion High-Fidelity DNA polymerase extension of a single phosphorylated and mutagenic primer annealed to a plasmid template. The extended DNA is concomitantly ligated by thermostable Taq DNA ligase and the reaction containing single stranded DNA can directly be used to transform *Escherichia coli* after removal of the template plasmid by DpnI digestion. We present three SOMA applications that exemplify the enormous potential of this method.

Results and Discussion

SOMA is a technique for the site-directed mutagenesis of plasmids including substitutions, deletions and insertions. Additionally, the insertion feature can be employed to clone and shuffle DNA fragments. We routinely use SOMA to introduce mutations at single and multiple positions with success rates up to 90% depending on the primer design as assessed by diagnostic restriction digestion analysis of individual clones after primary transformation. The basic methodology is outlined in Fig. 1 and a specific application is schematically depicted in Fig. 2B. Briefly, a mutagenic primer complementary to the target sequence is

designed to carry the desired mutation. It can either be directly synthesized with a 5′ phosphate group or it can be phosphorylated as described in the Methods section. In a thermocycler the mutagenic primer is annealed to the plasmid template, extended with Phusion High-Fidelity DNA polymerase and the fully extended product is made circular by ligation using Taq DNA ligase. Following 30 cycles of amplification, the template is removed by DpnI digestion and the circular, single stranded mutagenized plasmid is used for *E.coli* transformation. After appropriate selection the plasmids are isolated and subjected to diagnostic restriction digestion or DNA sequencing. Standard thermocycler conditions are presented in Fig. 1. SOMA is based on Phusion High-Fidelity DNA polymerase that is a proofreading polymerase with extremely high extension rates, thus making the method suitable also for very large plasmids. To this end we have successfully mutagenized pBR322-derived plasmids as large as 14.3 kb. Out of 4 clones analyzed, 1 contained the desired substitution mutation as scored by diagnostic restriction analysis facilitated by the introduction of an HaeII restriction site together with the substitution mutation. To demonstrate the versatility of SOMA we present several applications.

Cloning of *in vivo* GFP Reporter Plasmids using SOMA

Morpholino oligonucleotides (Morpholinos) are anti-sense gene knock-down tools applied in many model organisms most prominently in embryos of *Xenopus* and *Teleostei* for developmental studies [11,12]. Morpholinos are either applied to block splicing or translation [13,14]. To inhibit translation, morpholinos are designed to bind around the start codon and block ribosome assembly. The level of impaired translation is best assessed using specific antibodies [11], however, their availability is often restricted and the quality too low to detect endogenous proteins. For this reason we have developed a basic plasmid (pTP218; Table 1) that easily can be modified by an insertion mutagenesis based on SOMA to produce specific GFP-reporters designed to assess morpholino capacity to block translation *in vivo*. The method outline and the standardized primer design are presented in Fig. 2.

Plasmid pTP218 contains a GFP encoding gene without a start codon downstream of the SP6-promotor (Fig. 2A). A unique EcoRI site is removed during the insertion of the morpholino target sequence in front of GFP by SOMA thereby facilitating the identification of correct clones by diagnostic restrictions (EcoRI). Additionally, the plasmid contains *Saccharomyces cerevisiae* plasmid replication sequences (*CEN/ARS* sequence) and a selection marker (*URA3*) to allow yeast homologous recombination cloning [15].

The standard primer employed to introduce the morpholino target sequences contains homologous regions up- and downstream of the GFP start codon (black/green). An insertion (red) contains a start codon and 25 bp of the morpholino target sequence in frame with GFP.

As an example we have inserted the morpholino target sequence for *Xenopus laevis* 'Tripartite Motif-containing Protein 2' (TRIM2) in the GFP open reading frame using SOMA. For functional testing, we employed the SP6 promoter for *in vitro* amplification of synthetic GFP-reporter sense RNA. To assess the knock-down quality of our TRIM2 morpholino, 2.5 ng of RNA was injected into *Xenopus laevis* 1-cell embryos immediately after fertilization to ensure an even distribution of the reporter. At the two-cell stage the embryos were additionally injected with 2.5 pmol of standard morpholino (Figure 2C; upper panel) or TRIM2 morpholino

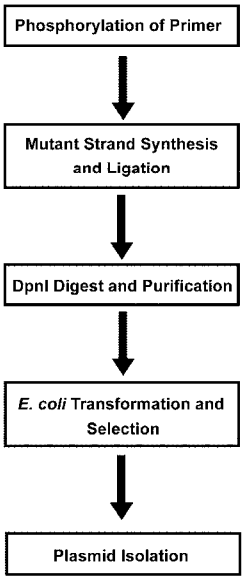

Step	Temp	Time	Cycles
Denature	95 °C	1 min	1
Denature	95 °C	1 min	30
Anneal	55 °C	1 min	30
Extend/ Ligate	65 °C	4 min	30

Figure 1. Flow scheme of the SOMA method (left). A mutagenesis primer is phosphorylated 5′ and used for a PCR reaction. Phusion polymerase amplifies the mutant strand, Taq Ligase ligates the nicks during the reaction. A DpnI digest leaves the mutagenized single stranded plasmid that is directly transformed into *E. coli* for selection and plasmid isolation. PCR condition for SOMA (right).
doi:10.1371/journal.pone.0064870.g001

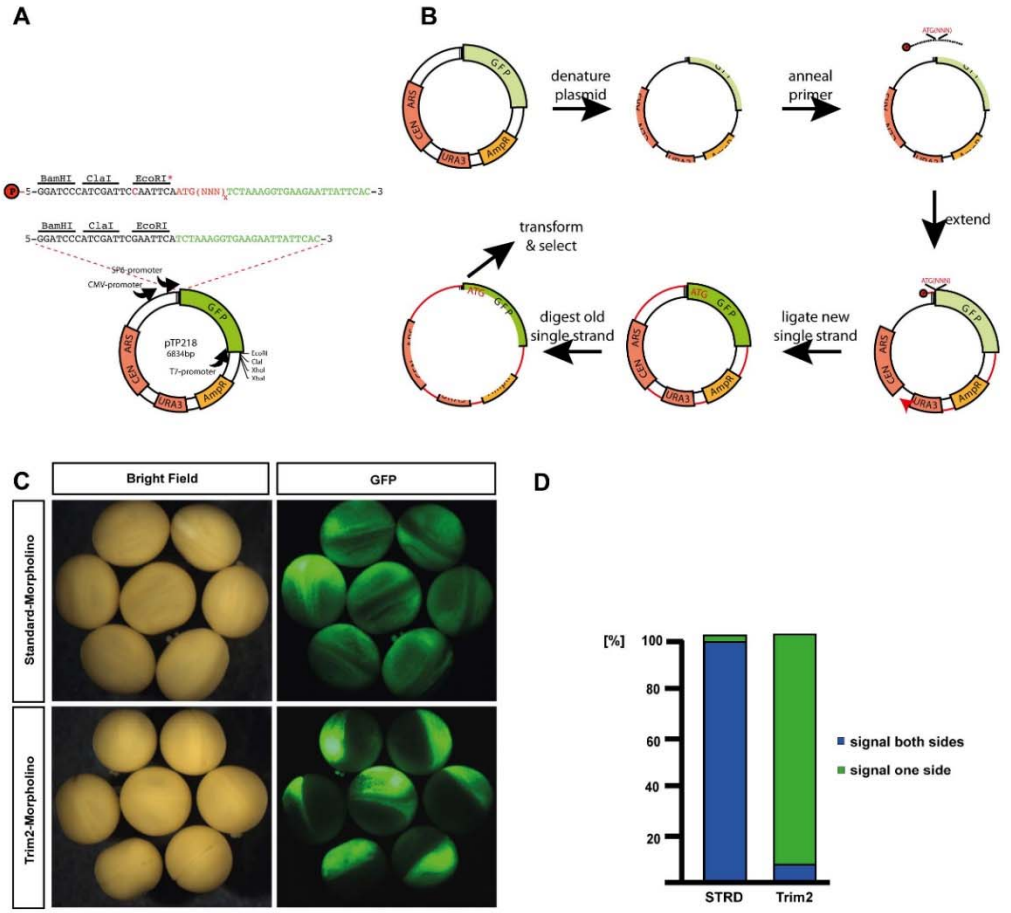

Figure 2. Standard primer for SOMA-construction of a GFP reporter (A). Phosphorylated primer (red P) with diagnostic EcoRI site (red C; EcoRI*), 23 bp of GFP (green sequence) and morpholino target sequence in frame with GFP $(NNN)_x$ including ATG (red sequence). Green fluorescent protein (GFP) gene (green); ampicillin resistance gene (Amp^R; yellow); *URA3* gene, yeast centromere (*CEN*), autonomous replication sequence (*ARS*) (red). Schematic outline of the SOMA method for production of GFP reporters (B). (1) denature pTP218; (2) 5′ phosphorylated single primer anneals; (3) primer is extended to the 5′ end; (4) nicks are ligated; (5) template strand is digested with DpnI; (6) mutated single stranded plasmid transformed into *E. coli* and positive clones identified by lack of EcoRI site. Test of TRIM2 GFP reporter construct *in vivo* (C). Synthetic reporter sense RNA injected into fertilized *Xenopus laevis* embryos at the one-cell stage; TRIM2- or Standard (STRD)-morpholino injected into one blastomere at the two-cell stage. Visualization after 1 day by brightfield or fluorescence microscopy (GFP). 99 of total 101 standard morpholino (STRD) injected embryos showed a GFP signal on both sides (98%); 249 of total 271 Trim2- morpholino injected embryos showed a GFP signal on one side (92%) (right).
doi:10.1371/journal.pone.0064870.g002

(Figure 2C; lower panel) into one of the two blastomeres. Embryos were harvested at stage 18/19 according to Nieuwkoop and Faber (1967) and photographed (Bright field, GFP). TRIM2-morpholino injected embryos show GFP signal only in one side, standard-morpholino injected ones in both sides of the embryo (Figure 2C). Figure 2D illustrates this phenotype in a bar graph. Of 101 standard morpholino injected eggs, 99 showed a GFP signal in both sides (= 98%, blue bar). Of 271 TRIM2-morpholino injected eggs, 249 showed no or little signal on the injected side (= 92%, green bar). Thus, the TRIM2-morpholino efficiently suppresses the translation of the SOMA generated GFP reporter *in vivo*. This demonstrates that pTP218 combined with SOMA can be used to produce customized GFP-reporter constructs for the assessment of morpholino-specificity *in vivo*.

Plasmid pTP218 can also be used to clone N- and C-terminal GFP-fusion products. This can be achieved by conventional cut and paste cloning or by homologous recombination cloning in *Saccharomyces cerevisiae* [15] since the plasmid has yeast replication and selection features. This allows restriction site independent, seamless and fast cloning of overlapping, multiple DNA

Table 1. Plasmids used in this study.

Plasmid	Description	Reference
pTP213	pCS2$^+$ (URA3) containing CEN/ARS	This work
pTP218	pCS2$^+$-GFP (URA3) containing CEN/ARS	This work
pTP224	pEGFP-C1 containing RMND5b (homo sapiens)	This work
pTP225	pEGFP-C1 containing RMND5a (homo sapiens)	This work
pTP233	pEGFP-C1 containing RMND5b$_{1-420}$- RMND5a$_{421-1173}$	This work
pTP234	pEGFP-C1 containing RMND5b$_{1-729}$–RMND5a$_{730-1173}$	This work
pTP157	pRS316 (URA3) containing *HAi-SSY5-GST (I378D)*	This work
pTP158	pRS316 (URA3) containing *HAi-SSY5-GST (I378S)*	This work
pTP159	pRS316 (URA3) containing *HAi-SSY5-GST (I378V)*	This work
pTP160	pRS316 (URA3) containing *HAi-SSY5-GST (I378G)*	This work
pTP165	pRS316 (URA3) containing *HAi-SSY5-GST (I378F)*	This work
pTP167	pRS316 (URA3) containing *HAi-SSY5-GST (I378V)*	This work
pTP170	pRS316 (URA3) containing *HAi-SSY5-GST (I378L)*	This work
pSH120	pRS316 (URA3) containing *HAi-SSY5-GST*	[28]
pAL001	pTP218 containing acagtggtctaggatggccagtgaagcg-GFP	This work

doi:10.1371/journal.pone.0064870.t001

fragments in a few steps [16]. Since pTP218 (Table 1) is a pCS2$^+$ derivative, it contains a functional SP6 promoter, which allows *in vitro* RNA synthesis e.g. for *in vitro* transcription/translation assays and it can be used for transient expression in various cell lines [17].

Restriction-site Independent Cloning

The ability to rapidly and precisely assemble diverse genetic elements is critical for many fields of modern biology, but perhaps particularly so for the advancement of synthetic biology. There is, despite the dropping prices of synthetic genes, a high demand for methods that allow the restriction-site-independent cloning for the production of recombinant hybrid proteins with novel functions. A vast repertoire of such methods can be found in the literature [18,19,20,21,22,23] and each method comes with beneficial and less beneficial properties. A SOMA-based method combined with a regular PCR amplification can be used for restriction-site independent, seamless protein fusions. This allows fast and reliable hybrid gene construction. Briefly, the DNA fragment to be cloned is converted into a PCR product with appropriate plasmid homology at its ends, effectively turning it into a megaprimer that can be introduced into the vector.

In Figure 3A we show a schematic representation of the two human 'Required for Meiotic Nuclear Division 5 Homolog' isoforms RMND5a (hRMD5a) and RMND5b (hRMD5b) and their protein domains. The similarity of both isoforms is not only reflected in their domain distribution but also on the amino acid residue level with 70% identical residues. We have fused both proteins to the C-terminus of GFP and examined their localization after transfection of HEK293 cells (Fig. 3C). Despite strong identity, both isoforms localize very differently in cells. RMND5a is distributed in the cytosol and in the nucleus of the cell (upper panel, left), whereas RMND5b is mostly present in the cytosol in vesicular structures (upper panel, right). To identify sequence elements responsible for the altered localization, we made several hybrid RMND5 fusion proteins using a SOMA-like method (Fig. 3B). The produced fusion proteins are schematically illustrated in Fig. 3C (upper panel) with RMND5a (hRMD5a; blue bar), RMND5b (hRMD5b; grey bar) and several hybrid proteins thereof. The length of RMND5b fragments in the hybrid proteins is depicted in numbers of amino acids (e.g. hRMD5b 1-140). The SOMA-based method is outlined in Figure 3B. Briefly, several N-terminal RMND5b fragments were PCR-amplified. Primer pairs were chosen to contain 25 bp of homologous region to the RMND5a replacement site (TP231fwd; TP233rev; TP234rev; see Table 2). The resulting PCR products were phosphorylated and used as megaprimers for mutagenesis with a plasmid encoding RMND5a as a template. This specific application exhibited a success rate between 10% and 40%. A similar method dubbed "overlap extension PCR" has been described recently [19]. We find that our modified SOMA-based protocol can be applied for cloning purposes in a similar fashion with high success rates.

Generation of a Gene Library with Randomized Site-directed Mutations using SOMA

Understanding protease specificity is a challenging task. Standard nomenclature defines the first amino acids of the C-terminal cleavage fragment as P1'–P4', the last ones of the N-terminal fragment as P1–P4 [24]. Often proteases accept several amino acids at these positions and their determination requires laborious screening methods [25]. SOMA can be used to generate semi-random mutagenized gene libraries, which have the potential to greatly facilitate such screens. Experimentally derived information regarding protease cleavage sites can be applied to predict novel protease substrates by *in silico* approaches [26].

The activity of the *S. cerevisiae* Ssy5 protease is regulated in response to the availability of extracellular amino acids [27]. During its maturation, Ssy5 cleaves itself between alanine381 and alanine382 (Figure 4A, scissors). This is a requisite event for subsequent amino acid induced activation of the endoproteolytic activity of Ssy5 by proteolytic removal of the inhibitory N-terminal domain [28]. The transcription factors Stp1 and Stp2 are the only other known substrates of Ssy5, however, the cleavage site in these substrates is not known. We noted a highly conserved isoleucine (I; yellow) at position 378 of Ssy5 (Figure 4A). Based on the proximity of a conserved residue to the autolytic processing site (P4' position), we applied SOMA to produce a gene library randomly mutagenized specifically at codon I378.

Briefly, a SSY5 specific primer with three consecutive random basepairs (NNN) at the codon I378 was synthesized and employed for SOMA using a template plasmid encoding inactive *ssy5*-I378D (Figure 4A; D378Xprimer). After *E. coli* transformation, ~1000 colonies were collected from the selection media and incubated for an hour at 37°C in LB medium before plasmids were isolated. These were subsequently used as a gene library and directly transformed into a *ssy5Δ* deletion strain. Plasmids carrying mutant alleles of SSY5 with restored activity were selected by their capacity to grow on YPD+MM [28]. Sixteen plasmids were isolated and sequenced as described in the Methods section. A list of the recovered and active mutations, including their codons, amino acid substitutions and occurrence, is shown in Figure 4 (lower panel); seven D378I (wild type), four D378L, three D378V and two D378F substitutions were recovered.

We conclude that SOMA works well to generate a gene library with a randomized codon. In principle it is possible to extend the DNA sequence targeted for mutagenesis but at the cost of coverage. Similarly, multiple mutagenic primers can be employed simultaneously to randomly mutagenize several positions in the same plasmid. When combined with error-prone PCR to generate megaprimers SOMA can be used to randomly mutagenize a larger region. Such approaches will be beneficial for e.g. the develop-

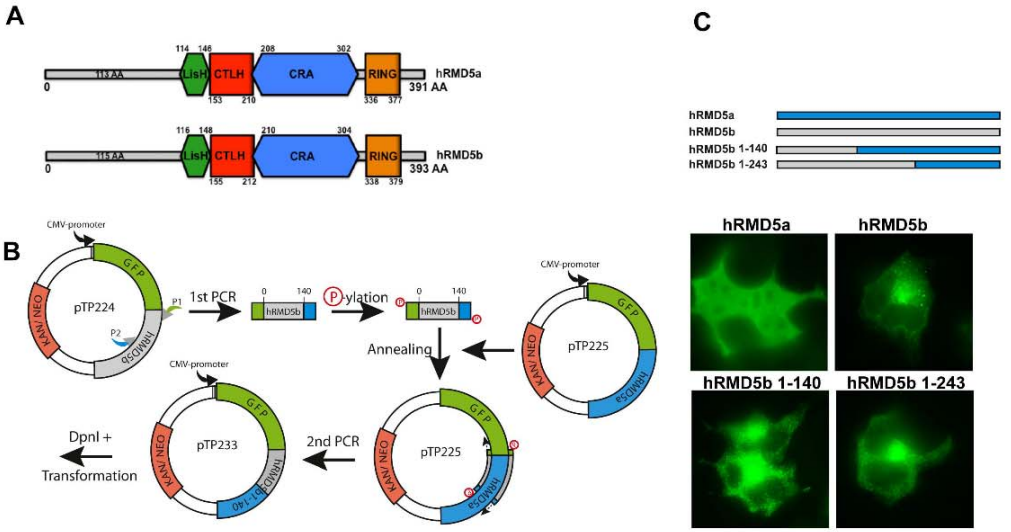

Figure 3. Restriction site independent cloning. (A) Schematic representation of two human RMND5 isoforms (hRMD5a, hRMD5b) with domains; numbers indicate amino acids. (B) Schematic outline of RMND5a/b chimera production. (1) pTP224 as template; (2) PCR with primer P1 and P2 resulting in RMND5b fragment (3) Phosphorylation of 1st PCR product. (4) 5′ phosphorylated PCR product anneals; (5) is extended to the 5′ end; (6) nicks are ligated; (7) template strand is digested with DpnI; (8) product transformed into *E. coli*. Green fluorescent protein (GFP) gene (green); Kanamycine resistance gene (Kan/Neo; orange); RMND5b (grey); RMND5a (blue) (C) Localization of hRMD5a (blue), hRMD5b (grey) and different hybrid fusion (blue/grey) in HEK293 cells. Length of RMD5b fragments indicated as numbers of amino acids (e.g. hRMD5b 1-140).
doi:10.1371/journal.pone.0064870.g003

ment of novel enzymes with for example altered activities, stability or specificity.

Taken together, with these experiments we demonstrate the broad practical utility of SOMA. The SOMA method differs from the commonly used QuikChange™ (Stratagene) method in the

Table 2. Primers used in this study.

Primer	Description	Reference
TP157fwd	gtattgtgtgaaagattacgataaaaaagctgcaagcgcagtaggcagtattccgtc	This work
TP158fwd	gtattgtgtgaaagattactctaaaaaagctgcaagcgcagtaggcagtattccgtc	This work
TP159fwd	gtattgtgtgaaagattacgttaaaaaagctgcaagcgcagtaggcagtattccgtc	This work
TP160fwd	gtattgtgtgaaagattacggtaaaaaagctgcaagcgcagtaggcagtattccgtc	This work
TP213fwd	atcggtgcgggcctcttcgctattacgccaccgaaaagtgccacctgggt	This work
TP213rev	gtccatatacgccatattgaattggctatgctccttacgcatctgtgcgg	This work
TP218fwd	ttgcaggatcccatcgattcgaattcatctaaaggtgaagaattattcac	This work
TP218rev	tacgactcactatagttctagaggctcgagctatagggagaccggcagatc	This work
AL001fwd	ggatcccatcgattccaattcacagtggtctaggatggccagtgaagcgtctaaaggtgaagaattattcac	This work
TP224fwd	catcatctcgagaagagcagtgtgcgtgcgtgg	This work
TP224rev	catcataagcttgagcagaatatgatgcgtttcccatctg	This work
TP225fwd	catcatctcgagaagatcagtgcgtgacggtg	This work
TP225fwd	catcataagcttgagtcagaaaaatatctgtttggcatctc	This work
TP231fwd	gctgtacaagtccggactcagatcacgagaagagcagtgtgcgtgcgtgg	This work
TP233rev	cttgggtctacagaaagaccagattcctgacacagctcctcggccacgc	This work
TP234rev	gaacatatggtgagttctcaatcccttgtctcaggtacaccaggctgccc	This work
D378Xfwd	gtattgtgtgaaagattacnnnaaaaaagctgcaagcgcagtaggcagtattccgtc	This work

doi:10.1371/journal.pone.0064870.t002

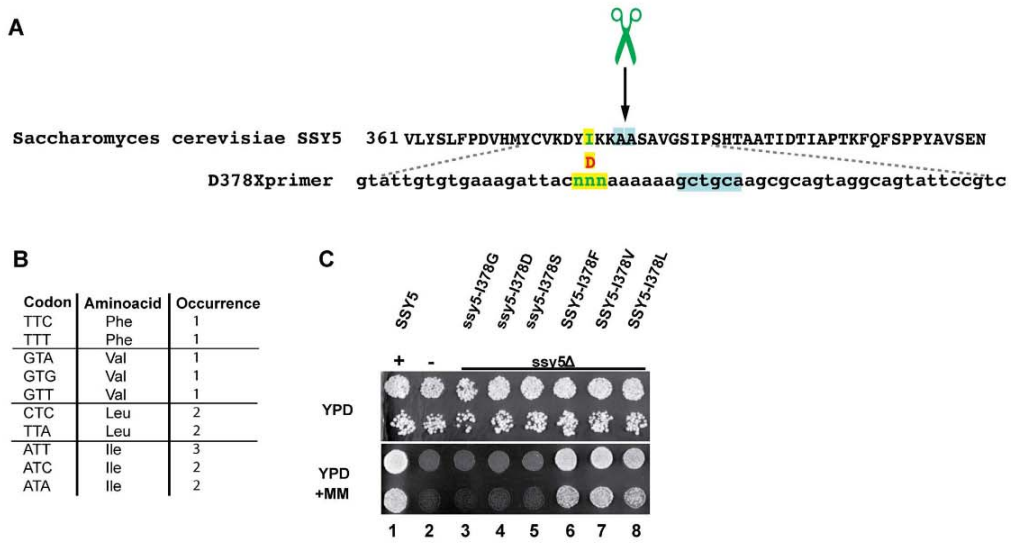

Codon	Aminoacid	Occurrence
TTC	Phe	1
TTT	Phe	1
GTA	Val	1
GTG	Val	1
GTT	Val	1
CTC	Leu	2
TTA	Leu	2
ATT	Ile	3
ATC	Ile	2
ATA	Ile	2

Figure 4. Generation of a semi-random mutagenized gene library using SOMA. (A) Ssy5 sequence with autolytic processing site (scissors) between A381 and A382 (blue). Replacement of conserved isoleucine378 (I; green) with aspartate (D; red) inactivates Ssy5. Primer D378X with random codon (NNN) theoretically capable of encoding all amino acids at position 378 (green). (B) Table with active D378 substitutions recovered in plasmids selected based on their ability to confer Ssy5-dependent growth on YPD+MM. (C) Dilutions of strain HKY77 (ssy5Δ) carrying pSH120 (SSY5; +), pRS316 (empty plasmid; -), I378G, I378D, I378S, I378F, I378V, or I378L.
doi:10.1371/journal.pone.0064870.g004

use of a single oligonucleotide and ligation of the extended product with a thermostable DNA ligase. SOMA is different to the commercially available QuikChange Multi™ (Stratagene) protocol since SOMA relies on recent advances such as state-of-the-art high speed proofreading DNA polymerase and employs a thermostable DNA ligase.

Materials and Methods

Oligonucleotides and Plasmids

Plasmids and primers used in this work are listed in Table 1 and Table 2, respectively and are available upon request. pTP213 was made by yeast homologous recombination with SalI linearized $pCS2^{+}$ and a PCR product obtained with the primers TP213fwd, TP213rev and pRS316 as a template. pTP218 was obtained by yeast homologous recombination with EcoRI/XhoI linearized pTP213 and a GFP encoding PCR fragment generated with TP218fwd, TP218rev from pYMN25. Plasmid pTP224 contains human RMND5b amplified from cDNA (clone BC009911; Open Biosystems) with TP224fwd and TP224rev, inserted via XhoI and HindIII into pEGFP-C1 (Clontech). Accordingly, pTP225 contains RMND5a amplified from cDNA (clone BC047668; Open Biosystems). Both plasmids pTP233 and pTP234 are pTP225 derivatives containing chimeric gene fusions of RMND5a and RMND5b, generated with TP231fwd and TP233rev or TP234, respectively (Figure 3 B). pAL001 is a pTP218 derivative that contains a SOMA generated insertion (Figure 2). The plasmids pTP157, pTP158, pTP159, pTP160, pTP165, pTP167 and pTP170 contain different SOMA generated point mutations at position I378 (Figure 4).

Organisms and Maintenance

Xenopus: Frogs were obtained from commercial suppliers (NASCO, USA). Production and rearing of embryos was performed as described previously [29]. Embryos were maintained at 15°C and staged according to Nieuwkoop and Faber [30]. All procedures were performed according to guidelines set by the German animal use and care laws (Tierschutzgesetz) and approved by the German state administration Saxony-Anhalt (Projekt/AZ: 42502-3-600 MLU).

Yeast: Yeast extract-peptone-dextrose (YPD) medium was prepared as described previously [31]. Sensitivity to 2-{[({[(4-methoxy-6-methyl)-1,3,5-triazin-2-yl]-amino}carbonyl)amino-]-sulfonyl}-benzoic acid (MM; 450 µg/ml) on complex medium is described elsewhere [32]. Strain HKY77 (MATa lys2Δ201 ura3-52 ssy5Δ2::hisG) is an isogenic descendant of AA255/PLY115 [33].

Cell Line: HEK293 cells were maintained in Dulbecco's modified Eagle's medium supplemented with 10% fetal calf serum (v/v). Transfections were performed using Lipofectamin 2000 (Invitrogen).

Capped mRNA and Morpholino Injections

Capped Mo-GFP m-RNA was generated using the mMESSAGE mMACHINE kit (Ambion, Austin, TX). KpnI linearized pAL001 was used as a template for SP6 transcription and 5 nl of capped mRNA (~2.5 ng) were injected into the 1-cell stage embryo. 25-mer morpholinos (MOs; Gene Tools, LLC Philomath, Oregon) were designed to target the ATG translation start site for Trim2 (NM_001092023) mRNA transcripts. A mismatch standard MO was used as control. Both were injected (2.5 pmol) into one blastomere of 2-cell stage Mo-GFP mRNA injected embryos.

Oligonucleotide Phosphorylation

Oligonucleotides were phosphorylated prior to SOMA using T4 polynucleotide kinase (NEB) according to the manufacturer. Briefly, 4 mM oligonucleotide primer was phosphorylated for 30 min at 37°C with the corresponding buffers and a final concentration of 1 mM ATP. The reaction was stopped by heat inactivation for 15 min at 65°C. Phosphorylated primers or PCR products were directly used for mutagenesis reactions.

Single Oligonucleotide Mutagenesis and Cloning Approach (SOMA)

Primers contain the mutation flanked by 20–25 bp of homologous region. Alternatively, for restriction site independent cloning, primer pairs are flanked by 20–25 bp of homologous region to the target DNA. A typical 50 µl reaction contains 0.2 mM primer, 100 ng template DNA, 1 mM NAD^+ (Sigma-Aldrich), 1 µl High-Fidelity DNA Polymerase (Finnzymes, Thermo Scientific), 1 µl Taq-Ligase (NEB), 10 µl HF-buffer (NEB) and 0,2 mM dNTPs. After an initial denaturing step (1 min at 95°C), DNA was amplified 30 cycles (95°C–1min; 55°C –1 min; 65°C –4 min). The extension time was standardly set to 4 minutes to facilitate the completion of both the polymerase extension and the ligation reaction. However, extension times for particular plasmids may have to be optimized. Afterwards 5 µl of DpnI digestion buffer was directly added (Fast Digest; Fermentas) and template DNA was DpnI digested. After purification (Qiagen PCR purification kit, Qiagen, Hilden) DNA was transformed into *E. coli*.

Plasmid Isolation from Saccharomyces Cerevisiae

A yeast colony was resuspended in 0.2 ml P1 buffer (QIAprep, Qiagen) and pretreated with Zymolyase (ZymoResearch) for 1 h at 37°C. Further steps were performed as described by the manufacturer (QIAprep, Qiagen). First 0.3 ml P2-buffer was added for cell lysis, then 0.42 ml N3-buffer was added and cell debris removed by centrifugation (10 min, 13000 rpm). The supernatant was applied to spin columns and plasmid DNA was eluted with 30 µl H_2O after washing (PB- and PE-buffer).

Acknowledgments

We thank the members of the Ljungdahl and Hollemann laboratory for constructive comments throughout the course of this work.

Author Contributions

Conceived and designed the experiments: TP CA. Performed the experiments: TP AL. Analyzed the data: TP AL TH CA PL. Contributed reagents/materials/analysis tools: PL TH. Wrote the paper: TP.

References

1. Peccoud J, Isalan M (2012) The PLOS ONE synthetic biology collection: six years and counting. PLoS One 7: e43231.
2. Pleiss J (2011) Protein design in metabolic engineering and synthetic biology. Curr Opin Biotechnol 22: 611 617.
3. Antikainen NM, Martin SF (2005) Altering protein specificity: techniques and applications. Bioorg Med Chem 13: 2701 2716.
4. Zawaira A, Pooran A, Barichievy S, Chopera D (2012) A discussion of molecular biology methods for protein engineering. Mol Biotechnol 51: 67 102.
5. Braman J, Papworth C, Greener A (1996) Site-directed mutagenesis using double-stranded plasmid DNA templates. Methods Mol Biol 57: 31 44.
6. Edelheit O, Hanukoglu A, Hanukoglu I (2009) Simple and efficient site-directed mutagenesis using two single-primer reactions in parallel to generate mutants for protein structure-function studies. BMC Biotechnol 9: 61.
7. Kirsch RD, Joly E (1998) An improved PCR-mutagenesis strategy for two-site mutagenesis or sequence swapping between related genes. Nucleic Acids Res 26: 1848 1850.
8. Zheng L, Baumann U, Reymond JL (2004) An efficient one-step site-directed and site-saturation mutagenesis protocol. Nucleic Acids Res 32: e115.
9. Hogrefe HH, Cline J, Youngblood GL, Allen RM (2002) Creating randomized amino acid libraries with the QuikChange Multi Site-Directed Mutagenesis Kit. Biotechniques 33: 1158 1160, 1162, 1164 1155.
10. Wang Y, Prosen DE, Mei L, Sullivan JC, Finney M, et al. (2004) A novel strategy to engineer DNA polymerases for enhanced processivity and improved performance in vitro. Nucleic Acids Res 32: 1197 1207.
11. Bill BR, Petzold AM, Clark KJ, Schimmenti LA, Ekker SC (2009) A primer for morpholino use in zebrafish. Zebrafish 6: 69 77.
12. Eisen JS, Smith JC (2008) Controlling morpholino experiments: don't stop making antisense. Development 135: 1735 1743.
13. Summerton J, Weller D (1997) Morpholino antisense oligomers: design, preparation, and properties. Antisense Nucleic Acid Drug Dev 7: 187 195.
14. Morcos PA (2007) Achieving targeted and quantifiable alteration of mRNA splicing with Morpholino oligos. Biochem Biophys Res Commun 358: 521 527.
15. Ma H, Kunes S, Schatz PJ, Botstein D (1987) Plasmid construction by homologous recombination in yeast. Gene 58: 201 216.
16. Benders GA, Noskov VN, Denisova EA, Lartigue C, Gibson DG, et al. (2010) Cloning whole bacterial genomes in yeast. Nucleic Acids Res 38: 2558 2569.
17. Turner DL, Weintraub H (1994) Expression of achaete-scute homolog 3 in Xenopus embryos converts ectodermal cells to a neural fate. Genes Dev 8: 1434 1447.
18. Benoit RM, Wilhelm RN, Scherer-Becker D, Ostermeier C (2006) An improved method for fast, robust, and seamless integration of DNA fragments into multiple plasmids. Protein Expr Purif 45: 66 71.
19. Bryksin AV, Matsumura I (2010) Overlap extension PCR cloning: a simple and reliable way to create recombinant plasmids. Biotechniques 48: 463 465.
20. Shuldiner AR, Tanner K, Scott LA, Moore CA, Roth J (1991) Ligase-free subcloning: a versatile method to subclone polymerase chain reaction (PCR) products in a single day. Anal Biochem 194: 9 15.
21. Zuo P, Rabie BM (2010) One-step DNA fragment assembly and circularization for gene cloning. Curr Issues Mol Biol 12: 11 16.
22. Geu-Flores F, Nour-Eldin HH, Nielsen MT, Halkier BA (2007) USER fusion: a rapid and efficient method for simultaneous fusion and cloning of multiple PCR products. Nucleic Acids Res 35: e55.
23. Zhu B, Cai G, Hall EO, Freeman GJ (2007) In-fusion assembly: seamless engineering of multidomain fusion proteins, modular vectors, and mutations. Biotechniques 43: 354 359.
24. Schechter I, Berger A (1967) On the size of the active site in proteases. I. Papain. Biochem Biophys Res Commun 27: 157 162.
25. Diamond SL (2007) Methods for mapping protease specificity. Curr Opin Chem Biol 11: 46 51.
26. Song J, Tan H, Perry AJ, Akutsu T, Webb GI, et al. (2012) PROSPER: An Integrated Feature-Based Tool for Predicting Protease Substrate Cleavage Sites. PLoS One 7: e50300.
27. Pfirrmann T, Ljungdahl PO (2012) Chapter 685 Ssy5 Peptidase: A Chymotrypsin-Like Signaling Protease in Yeast. In: Handbook of proteolytic enzymes. Academic Press: Elsevier.
28. Pfirrmann T, Heessen S, Omnus DJ, Andréasson C, Ljungdahl PO (2010) The prodomain of Ssy5 protease controls receptor-activated proteolysis of transcription factor Stp1. Mol Cell Biol 30: 3299 3309.
29. Gurdon JB (1977) Methods for nuclear transplantation in amphibia. Methods Cell Biol 16: 125 139.
30. Faber J, Nieuwkoop PD (1967) Normal Table of Xenopus Laevis (Daudin); a Systematical and Chronological Survey of the Development from Fertilized Egg Till the End of Metamorphosis.: Amsterdam: North Holland.
31. Andréasson C, Ljungdahl PO (2002) Receptor-mediated endoproteolytic activation of two transcription factors in yeast. Genes Dev 16: 3158 3172.
32. Poulsen P, Lo Leggio L, Kielland-Brandt MC (2006) Mapping of an internal protease cleavage site in the Ssy5p component of the amino acid sensor of Saccharomyces cerevisiae and functional characterization of the resulting pro- and protease domains by gain-of-function genetics. Eukaryot Cell 5: 601 608.
33. Forsberg H, Ljungdahl PO (2001) Genetic and biochemical analysis of the yeast plasma membrane Ssy1p-Ptr3p-Ssy5p sensor of extracellular amino acids. Mol Cell Biol 21: 814 826.

5 Discussion

The generation of the proper amount of neurons in the various regions of the developing vertebrate central nervous system is a complex process that involves carefully regulated spatial and temporal balance between neural progenitor cells (NPC) proliferation and differentiation. This balance is tightly regulated by the activities of numerous extracellular and intracellular molecular factors, including commitment of neural stem cells (NSCs) toward neuronal fates, specification of neuronal subtype identities, neuronal differentiation and neuronal migration. The timing of the switch of NPCs from proliferation to differentiation, as well as the sequential induction of specific NPC and neuron types, differs between central nervous system regions and vertebrate species. Accumulating evidence indicates that the ubiquitin proteasome system (UPS) plays an essential role in the proper timing of these decisions. Ubiquitin E3 ligases play a vital role in this process by targeting key factors of neurogenesis for degradation. The primary aim of the present thesis was to characterize functional interaction partners of Trim E3 ligases as well as to understand their role during the formation of the nervous system.

5.1 *Xenopus* Trim E3 ligases in early neurogenesis

The extensive research on TRIM E3 ligases in humans and lack of any data on the expressional and functional mechanism of these ligases in the vertebrates raised our interest to address this question. Trim-related cDNAs were identified in Genbank and obtained from Source BioScience (UK). Preliminary expressional analysis based on the spatio-temporal characterization using whole-mount *in situ* hybridization (WMISH) and semiquantitative-RT-PCR revealed ubiquitous expression for majority of the obtained *Xenopus* Trim E3 ligases (data not shown). However, we identified a number of cDNAs, which revealed a specific expression pattern within the neuro-ectodermal and neuronal derived structures of the early developing *Xenopus* embryo (Fig. 8). Sequence analysis of these *trim's* (*trim2, trim7, mid1, trim23, trim28, trim29,* and *trim36*) confirmed the homology towards human orthologues.

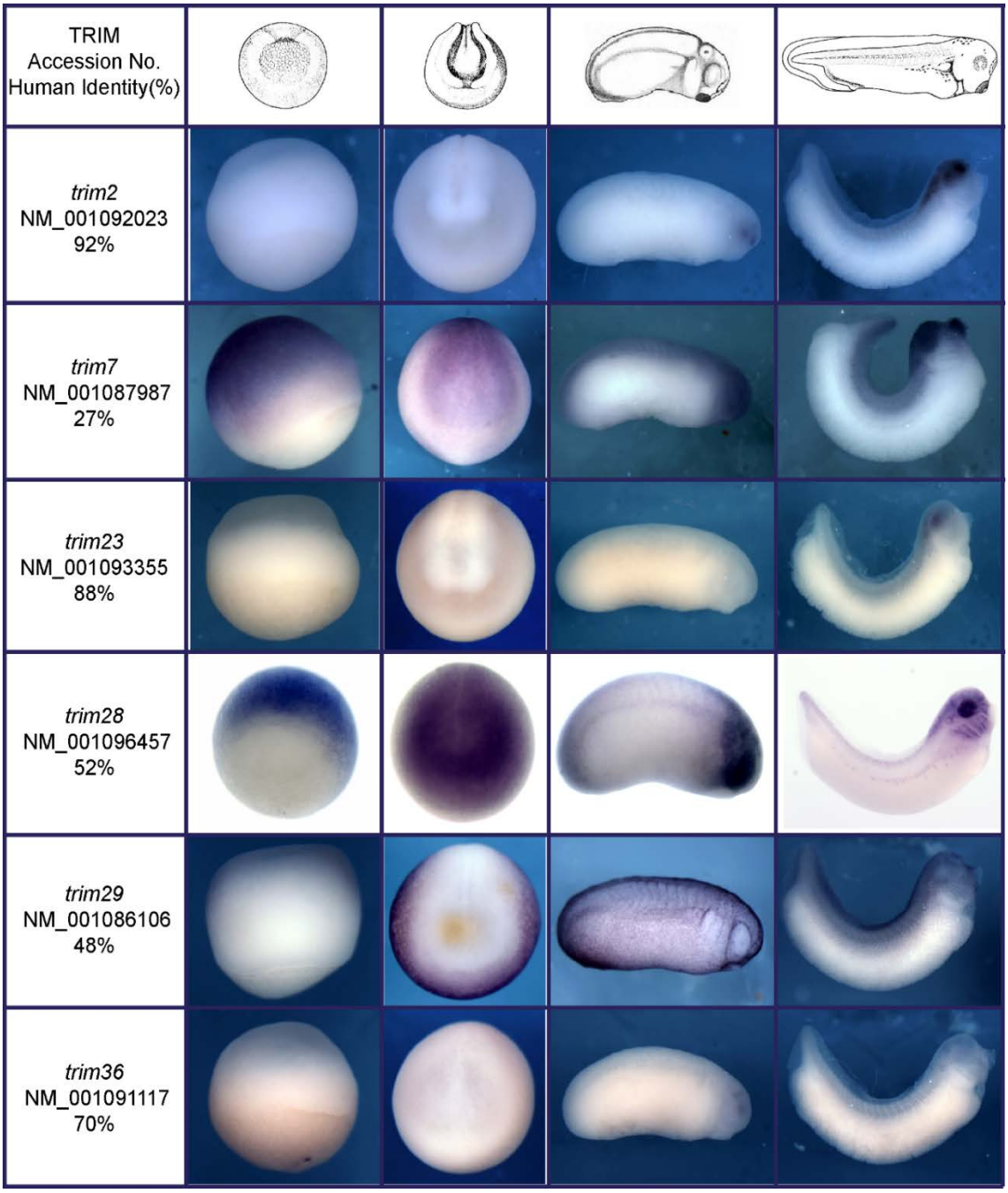

Figure 5-1. Members of the trim family of E3-ligases with distinct patterns of expression during Xenopus embryogenesis. Preliminary expression was observed in stages starting from gastrulation through to early tadpole stage. Homology towards human protein sequence is indicated in percentage

5.2 Midline1/Trim18 Ubiquitin E3 ligase during vertebrate early neurogenesis

Mid1/Trim18, was the first member of the Trim family of ubiquitin E3 ligases that had been cloned in the lab. Trim18/MID1 was first identified as the causative gene for the X-linked

OS[74]. The major activity of MID1 was associated with the ubiquitination and proteasome dependent degradation of PP2A and/or α4 protein[76]. Similarly, recent studies have revealed association of MID1 with various proteins such as elongation factor 1α (EF-1α), RACK1, Annexin A2, Nuclephosmin, Mig12 among others and is involved in mRNA transport and translation and microtubule dynamics and may cause the pathological signs affecting the patients with OS[90–92]. Though OS is a developmental disease, little is known about the role of Mid1 during early vertebrate development, which would be of high interest to understand the etiology of the disease. To address this question, we first analysed the expression of *mid1* through whole mount *in situ* hybridization (WMISH) during the early development of *Xenopus*. Early tailbud stages showed *mid1* expression in the optic vesicles overlaps with early *pax6* expression. At later stages, *mid1* expression was more confined to ventral region of the forming eye and the optic stalk, while *pax6* expression in the retina. In mouse and chick embryos, *Mid1* expression was observed in the proliferating nueroepithelium of the forebrain and the outer nuclear layer of the retina[93,94] whereas *pax6* expression is restricted to the inner nuclear layer. This expression of *mid1* in part correlated to hedgehog (hh) regulated genes *vax1* and *pax2*, important transcription factors regulating ventral *eye/eye* stalk identity[95,96]. In *Xenopus*, analysis of a similar Hedgehog dependent regulation of *mid1* revealed strong induction of *mid1* in the optic vesicle and prospective forebrain region upon misexpression of *shh*. On the other hand, it was showed that, Mid1 can function on Hh-signalling. The human Fu, known to transmit the Hh signalling in Drosophila, permits nuclear localization of the transcription factor GLI3 in a cancer cell line. Here, MID1 catalyses the ubiquitination of Fu and promotes a site-specific cleavage, which is normally needed for the nuclear localization and thus transcriptional activity of GLI3[80]. Thus, a feedback loop may exist, which regulates the balance between *mid1* and *shh* expression.

5.2.1 Mid1 modulates Pax6 protein abundance in a substrate dependent manner

Pax6, a member of the PAX gene family is an evolutionarily highly conserved transcription factor[97]. *Pax6* is one of the first eye field transcription factors (EFTFs) described in a wide area of the neural plate including the eye filed[98]. Pax6 is involved in the specification of the prospective eye and retinal field[99,100] whereby, the level and timing of Pax6 expression are tightly controlled during the formation of these structures[101–104]. Moreover, *Pax6* is an indispensable transcription factor for the proper formation of the vertebrate eye and acts cell

autonomously in the optic vesicle and lens surface ectoderm[100,104]. In humans, heterozygous mutations in PAX6 caused ocular defects, whereas the homozygous mutation resulted in anophthalmia[105]. Contrarily, transgenic mice overexpressing multiple copies of the human PAX6 gene also showed similar ocular defects as the heterozygous mice[106,107]. Similarly, both in *Xenopus* and Drosophila, overexpression of *pax6* induced the formation of ectopic eyes[108,109]. On a broader scale, Pax6 is one of the most important regulators of eye development with its function critically dependent on the spatio-temporal and quantitatively defined expression levels[101].

In *Xenopus*, *pax6* is detected in the neuroblast cells of the developing retina. In early tailbud stages, *pax6* is expressed homogenously in the optic vesicle, whereas in tadpoles expression is limited to the lens epithelium, inner nuclear layer and the ganglion cell layer[110,111]. Recently, regulation of Pax6 activity by posttranslational modification has been reported[112–114]. However, similar mechanisms leading to the development of the visual system is unknown. We addressed the question, whether Mid1 is involved in the control of Pax6 protein levels in the forming visual system. We showed that, *mid1* is expressed in the ventral region of the eye and the optic stalk, while *pax6* expression was confined to the retina, indicating spatial regionalization during the formation of the visual system. Intriguingly, this expression pattern correlated with the expression of Pax6 and Pax2 in the developing zebrafish embryos, Where Pax6 is expressed in the neural retina and pigmented epithelium, while Pax2 was observed in optic stalk[115]. Similarly, in *Pax2* and in *Pax6* mutant mice, reciprocal mutant mice, reciprocal expansion of *Pax2* and *Pax6* gene expression in the complimentary phenotypes was observed. In *Pax6* mutants, expansion of Pax2 expression at the margins of the optic cup was observed, suggesting failure to become restricted to optic cup/optic stalk boundary. Whereas, *Pax2* mutants showed Pax6 expression expanded towards the roof of diencephalon, while the primordial optic stalk acquired the fate of neural retina. These results showed that spatial specification of the *eye/eye* stalk boundary is dependent on the expression as well as reciprocal transcriptional repression of *Pax2* promoter activity by Pax6 protein and *vice versa*[116]. However, earlier it was also reported that, sonic hedgehog (Shh) both directly or indirectly induces the expression of Pax2 and inhibits the expression of Pax6, thus regulating the partition of optic primordia into optic stalk and retina[115]. In similar lines, we showed that *shh* induces *mid1* expression, whereas *pax6* expression was repressed. Interestingly, since *shh* seem to regulate both *pax2* and *mid1*,

we looked at the expression of *mid1* upon suppression of *pax2* function. We did not observe any impairment of *mid1* expression in the ventral eye or optic stalk suggesting that Mid1 acts independently to target Pax6 activity for degradation in the ventral *eye/eye* stalk region.

Thus, we wanted to test whether Mid1 can target Pax6 for degradation. In cell culture using immunofluorescence, Mid1 was mainly detected in the cytoplasm and Pax6 in the nucleus[117,118] (own data). Nevertheless, biochemical (WB) analysis of nuclear and cytoplasmic cellular fractions revealed that a minor amount of Mid1 is also present in the nucleus. Indeed, a much lower level of Pax6 protein was detected in immunoprecipitates of cell lysates co-transfected with both Pax6 and Mid1. Similarly, overexpression of Mid1 in αTN4-1 cells or in neuralized animal cap explants, led to a reduction of endogenous Pax6, while the degradation of Pax6 by the UPS was suppressed by proteasome inhibitors. These results confirmed that Mid1 indeed mediates proteasomal degradation of Pax6, acting as a Pax6 specific E3-ligase. In line with these results, Tuoc and Stoykova reported in 2008 that in the developing mice cortex, Trim11 mediates Pax6 degradation. Interestingly, Pax6 regulates *trim11* transcription, probably in a negative feed-forward loop to reduce excess Pax6 protein[119].

5.2.2 *mid1 in vivo* loss-of-function induces large eyes and Pax6 overexpression

Based on our results and to further understand the function of *mid1 in vivo*, we suppressed *mid1* function using antisense morpholino technique, which blocks the translation of the targeted mRNA. The microinjection of the *mid1*-morpholino resulted in a significant increase in the size of the embryonic eyes due to a higher rate of cell proliferation. Closer investigation of the affected eye revealed a strong enlargement of the optic vesicle with aberrant retinal folds, loss of retinal stratification and ectopic expression of *pax6*. Thus, suppression of mid1 function allows to maintain *pax6* expression in a region where normally Mid1 restricts Pax6.

Further, Pax6 was shown to be required for proliferation and retinal cell-fate determination[120,121]. In the more peripheral RPCs, Pax6 prevents activation of photoreceptor-differentiation pathway by suppressing expression of the transcription factor Crx, whereas more centrally Pax6 is dispensable for neurogenesis but is essential for their multipotency[102,120]. In chick, *Pax6* promoted the differentiation of non-photoreceptor

neurons while inhibiting the differentiation of photoreceptor cells[122]. Against this background, we investigated direct cell autonomous effects of Mid1 in retinal cells following *in vivo* lipofection experiments. Following *mid1* overexpression in the retina, an increased proportion of photoreceptor cells and a reduction in bipolar cells upon Mid1 knockdown was observed. Since, this effect could be rescued by Pax6 overexpression, the change in the proportion of retinal cell types upon Mid1 overexpression was most likely the result of a Mid1 mediated degradation of endogenous Pax6.

We conclude that, our results reveal an important aspect of Mid1 function in the eye/eye stalk regionalization during early neurogenesis. We have shown that, *mid1* is expressed in the ventral region of the eye and the optic stalk and expression of *mid1* is under the control of *shh* in a feedback dependent loop. We could show Mid1 E3 ligase dependent proteasomal degradation of Pax6 in the forming optic stalk. Thus, providing evidence that part of Mid1 function in vertebrates is the tight and specific regulation of Pax6 protein levels essential for the visual system development.

5.3 Trim2 regulates proliferation and differentiation during *Xenopus* early neural development

Trim2 was first identified in mouse brain as neural activity ring finger protein (NARF) that interacts with motor protein myosin V via the NHL domain[84]. Here, striking signals of NARF mRNA were detected in the hippocampus, cerebral frontal cortex, retina, olfactory bulb and the spinal cord[84,85]. By whole-mount *in situ* hybridization and whole-mount immunostaining approaches, we showed a strong expression of *trim2*/Trim2 in the presumptive ventral brain, the floor plate, retina, lens, otic vesicles, olfactory placodes and the spinal cord. Both, levels of *trim2* mRNA and Trim2 protein were high in committed and differentiated neuronal cell layers of the forming CNS of *Xenopus* tadpoles, highly similar to the expression of *Trim2* in adult mice. Concomitantly, *Xenopus* Trim2 amino acid sequence analysis showed 96% homology towards the human orthologues protein.

Moreover, investigation of antisense morpholino induced *trim2* loss-of-function in *Xenopus* resulted in smaller heads affecting the developing brain and eyes. Further analysis whether the small head is due to differential down regulation of precursor pool or even proneural genes, we examined the expression of panneural precursor gene *sox3* and proneural early

forebrain markers namely *fb1*, *otx2* and *pax6* at the open neural plate stage (Nieuwkoop & Faber (NF) stage 14/15). *trim2*-morphants displayed broadened expression of all these maker genes, which was presumed to be a result of impaired convergent and extension movements of cells of the neural plate and not an expansion of the neural plate itself. This assumption was strengthened by the observation of a disturbed dynamics of actin assembly/disassembly shown by the accumulation of phalloidin at early neurula (NF stage 15). The defective actin dynamics might also the cause for the neural tube closure defects and high mortality (NF stage 20) in *trim2*-morphants. Further, we counted only half the number of proliferative cells compared to the control-side. However, the number of apoptotic cells dramatically increased in all regular *trim2* territories, often showing aggregation of apoptotic cells in the presumptive brain and eye of late tailbud stages (NF stage 27). Contrarily, the *Trim2* gene trap (*Trim2*^{GT}) homozygous mice did not show any neural tube defects. However, at approximately postnatal day 50 (P50), the homozygous mice developed progressive and substantial loss of Purkinje cells (73%, differentiated neurons) due to apoptosis, which increased to 85% in the 5 month old Trim2^{GT} mice[85]. Similarly, upon analysis of *myt1*, *n-tubulin* and *nrcam* for differentiated neurons in *Xenopus trim2*-morphants, a marked reduction of differentiated neurons was observed. The reduced number of differentiated cells might be due to the high apoptosis of the precursor cells. Furthermore, in *Xenopus*, a motility-escape assay revealed loss of gross motor-sensory function in *trim2*-morphants (Movie 1 and 2, see attached CD). These observations complemented the human patient phenotype with early onset of axonal neuropathy and muscle hypotonia due to a heterozygous missense mutation in TRIM2[89] and of the Trim2^{GT} mice with juvenile onset of tremor and ataxia[85]. Thus, our findings not only complement the previous work, but provide vital evidence for a role of *trim2* function during proliferation and differentiation of neural precursor cells.

5.3.1 Pdcd6ip/Alix is an interaction partner of Trim2 involved in early neurogenesis

In general, E3 ubiquitin ligases are conceived to have more than one substrate or interaction partner. It was shown in Trim2^{GT} adult mice that, accumulation of neurofilament light chain (NEFL) in neuronal structures leads to axonopathy, progressive neurodegeneration, and juvenile onset of tremor and ataxia. Re-expression of TRIM2 prevented neurodegeneration via UbcH5a-dependent degradation of NEFL[85]. Similarly, in mouse embryonic fibroblasts,

p42/p44 MAPK-dependent ubiquitination of cell death-promoting factor Bim (Bcl-2-interacting mediator of cell death) by TRIM2 conferred neuroprotection during rapid ischemia[87]. Surprisingly, analysis of *nefl* expression in *trim2*-morphants do not show any accumulation of *nefl* in the late tadpoles, probably still too early to observe an accumulation like in adult mice. Therefore, we aimed to identify Trim2 interacting proteins during *Xenopus* development by GST pull-down based high throughput LC-MS/MS mass spectrometry. To this end, we analysis embryonic lysates of late tailbud stage embryos (NF stage 30 – 36) using Trim2-GST as a bait.

We identified Pdcd6ip/Alix (Programmed cell death 6 interacting protein/Apoptosis-linked gene-2 interacting protein X) as an interaction partner of Trim2. First isolated from *Xenopus* oocytes, the *alix* homologue Xp95 is phosphorylated by src kinases[123]. Alix is a multimodular adaptor protein involved in the sorting of cargo proteins of multivesicular bodies for incorporation into vesicles and the endo-lysosome system[124–127]. Alix plays a role in the regulation of apoptosis, cell adhesion, and cytomorphology[128,129]. Overexpression of *Alix* can promote apoptosis[130,131] or tumour cell proliferation[132], whereas a truncated form prevents apoptosis[131]. Spatial expression analysis of *alix* revealed that it correlated strongly with *trim2* during *Xenopus* development. In tadpoles, both transcripts were found in overlapping regions of the developing CNS, particularly in the retina, lens, brain, spinal cord, and the olfactory and otic placodes. Similarly, cellular expression of endogenous Alix and Trim2 as analysed in a human neuroblastoma cell line (SH-SY5Y) also revealed a highly overlapping expression within the cellular cytoplasm. Further, expression of precursor and proneural genes in *alix*-morphants showed a similar altered expression pattern and at early tail bud *alix*-morphants showed a similar loss of motor-sensory function as observed for *trim2*-morphants (Movie 4, see attached CD). Similarly, the combined suppression resulted in an almost identical phenotype, suggesting that these proteins function towards the same pathway. Moreover, loss of neural differentiation and the microcephalic-like phenotype observed in *trim2*-morphants mimicked that of *Alix* deficient mice [133]. Thus, we aimed to solve the question of an epistatic relationship or whether both act interdependently. To this end, we performed rescue experiments for co-injected morphants with synthetic *trim2* RNA or with human *ALIX* mRNA. However, we were unable to rescue morphants with either *trim2* or *ALIX* mRNA, suggesting that Trim2 and Alix interact in the same pathway in parallel. It has been reported that ALIX plays a critical role in the apoptotic pathway[134–136]

and is also involved in the regulation of the endolysosomal system[125–127,137]. *trim2*-morphants showed a significant decrease in cellular proliferation of the progenitor population, due to a high rate of apoptosis. Along similar lines, loss of neural progenitors was observed during the transient phase of apoptosis in *Alix* KO mice[133]. Numerous studies have linked Alix to the modulation of apoptosis in neurons and neurodegenerative diseases[130,131,134,138,139]. The Trim2 paralogue Trim3 was reported to localize to early endosomes[140] and from our results of TRIM2 expression in vesicular like structures, one can hypothesize that *trim2* in conjunction with *alix* might play a crucial role in the endosomal mediated apoptosis during neuronal biogenesis.

Thus, our results provide first evidence for an important function of Trim2-Alix interaction during early neurogenesis. Here, we have shown similar expression as well as loss-of function phenotypic profiles for both *trim2*- and *alix*-morphants. In both morphants apoptosis of neurogenic cells was the common phenotype. In concert, these may link developmental cues to cellular proliferation/cell survival and thus may take an important function during neuronal determination and differentiation.

6 Summary

The major focus of my work has been to elucidate the molecular mechanisms underlying the early development of nervous system in the vertebrate model organism *Xenopus laevis*. The generation of neurons and the formation of the central nervous system is tightly regulated in space and time by the activities of numerous molecular factors, beginning from neural induction, neural differentiation and migration up until adult neurogenesis. Recently, TRIM proteins have been implicated in many biological processes from cell signalling to immune response. Thus, alterations in TRIM proteins are involved in my pathological and developmental disorders including neurodegenerative diseases. In the present dissertation, I present a comprehensive analysis on the spatio-temporal expression of *Xenopus laevis* Trim protein family members. We show that majority of Trim's have ubiquitous expression with a few exceptions.

Further, for the first time we demonstrate Trim18/Mid1, identified in X-chromosome linked Opitz BBB/G (OS) syndrome, interacts with Pax6. Mid1 transcripts were observed in the neural tube, optic vesicle in the early stages, which at later stages were more defined and restricted to the ventral regions of the midbrain-hindbrain, eye, and in the optic stalk. Within the optic cup, a major territory of *mid1*, misexpression of the morphogen *shh* strongly induced *mid1* expression, whereas as *pax6* was repressed. Here, Mid1 regulates the ubiquitination and proteasomal degradation of Pax6. Concurrently, *mid1* loss-of-function showed enlarged eyes and extended expression of *pax6*. Moreover, targeted overexpression of *mid1* affected the fate of retinal precursor cells, which could be reversed by co-expression of *pax6*. These findings indicate that Mid1 mediated posttranslational modification and clearance of the excessive Pax6 protein is necessary to set proper boundaries between the eyestalk and the retina. A function that is under the regulation of sonic hedgehog to suppress the Pax6 activity and thus break autoregulation of *pax6* at defined intervals during visual system development.

Moreover, functional analysis of Trim2, another Trim protein family member showed physical interaction with Alix. Analysis *trim2*/Trim2 mRNA and protein revealed predominant expression in the developing neural system of *Xenopus laevis* embryos.

Moreover, *trim2* knock down affected neural progenitor cell survival, thereby inhibiting primary neurogenesis. Further, Alix was identified as an interaction partner in embryonic lysates of Trim2-GST pull-down led LC-MS/MS mass spectrometry screen. *alix* transcripts showed an overlapping expression similar to *trim2* during *Xenopus* neural development and in cell culture. Additionally, functional and epistatic analysis through single and co-suppression of *trim2* and alix on early neural marker genes revealed similar alterations during early neurogenesis. These findings provide evidence that Alix and Trim2 E3 ligase interact in the same pathway in parallel and are possibly involved in the timing of differentiation and determination of neural progenitors through the control of cell proliferation/apoptotic processes during early neural development.

7 Outlook

The research work presented in this thesis has opened a number of research lines that should be explored in the future. For instance, based on the expressional data analysis presented in this work both for *mid1* and *trim2*, it is of keen interest to further elucidate the molecular mechanisms underlying the development of the neural system. Towards this, one of the extensive reviews underlying the function of Mid1 in development and disease has been described by Winter J et al.[141]. Here, a functional aspect one could ask regarding the MID1 expression in neural crest cells (NCC) and its involvement in neurocristopathy of OS. MID1 expression pattern in NCC is highly conserved in human, mouse, chick and *Xenopus*[74,92,94,142]. Craniofacial dysmorphism- a condition observed in OS is caused due defective NCC formation and is linked to SHH signalling[141]. In the present work we have shown that misexpression of *shh* revealed a strong induction of *mid1* in the optic cup. It is also known from earlier research that, MID1 interacts with GLI3, an SHH effector, through FU and regulates it transcriptional activation. Therefore, future studies aimed at investigating the functional relationship between Mid1 and Shh/Gli3 in NCCs would be of immense interest/use in deciphering part of its functional role in OS.

Similarly for Trim2, apart from further elucidating the functional role between Trim2 and Alix in early neurogenesis, one could further ask its role in embryonic patterning. We have shown that *trim2* loss-of-function in *Xenopus* leads to neural tube closure defects due to inability of the cells to collectively migrate. Recently, *trim2* was identified to be enriched in the organizer around the dorsal lip of *Xenopus laevis* gastrulae[143]. It is known form earlier studies that, cells surrounding dorsal lip, the organizer are involved in patterning of the embryo. Therefore, future studies should aim at dissecting the role of *trim2* in embryonic induction and patterning.

8 Bibliography

1. Hershko, A. & Ciechanover, A. THE UBIQUITIN SYSTEM. 57 (1998).
2. Kwon, Y. T. & Ciechanover, A. The Ubiquitin Code in the Ubiquitin-Proteasome System and Autophagy. *Trends Biochem. Sci.* **42**, 873–886 (2017).
3. Pickart, C. M. & Eddins, M. J. Ubiquitin: structures, functions, mechanisms. *Biochim. Biophys. Acta BBA - Mol. Cell Res.* **1695**, 55–72 (2004).
4. Chiu, Y.-H., Sun, Q. & Chen, Z. J. E1-L2 Activates Both Ubiquitin and FAT10. *Mol. Cell* **27**, 1014–1023 (2007).
5. van Wijk, S. J. L. & Timmers, H. T. M. The family of ubiquitin-conjugating enzymes (E2s): deciding between life and death of proteins. *FASEB J.* **24**, 981–993 (2010).
6. Husnjak, K. & Dikic, I. Ubiquitin-Binding Proteins: Decoders of Ubiquitin-Mediated Cellular Functions. *Annu. Rev. Biochem.* **81**, 291–322 (2012).
7. Glickman, M. H. & Ciechanover, A. The Ubiquitin-Proteasome Proteolytic Pathway: Destruction for the Sake of Construction. *Physiol. Rev.* **82**, 373–428 (2002).
8. Mukhopadhyay, D. & Riezman, H. Proteasome-Independent Functions of Ubiquitin in Endocytosis and Signaling. *Science* **315**, 201–205 (2007).
9. Li, W. & Ye, Y. Polyubiquitin chains: functions, structures, and mechanisms. *Cell. Mol. Life Sci.* **65**, 2397–2406 (2008).
10. Ciechanover, A. N-terminal ubiquitination: more protein substrates join in. *Trends Cell Biol.* **14**, 103–106 (2004).
11. Cadwell, K. Ubiquitination on Nonlysine Residues by a Viral E3 Ubiquitin Ligase. *Science* **309**, 127–130 (2005).
12. Wang, X. *et al.* Ubiquitination of serine, threonine, or lysine residues on the cytoplasmic tail can induce ERAD of MHC-I by viral E3 ligase mK3. *J. Cell Biol.* **177**, 613–624 (2007).
13. Lee, C. S. *et al.* Loss of nuclear factor E2-related factor 1 in the brain leads to dysregulation of proteasome gene expression and neurodegeneration. *Proc. Natl. Acad. Sci.* **108**, 8408–8413 (2011).
14. Schwartz, D. C. & Hochstrasser, M. A superfamily of protein tags: ubiquitin, SUMO and related modifiers. *Trends Biochem. Sci.* **28**, 321–328 (2003).
15. Nakayama, K. I. & Nakayama, K. Ubiquitin ligases: cell-cycle control and cancer. *Nat. Rev. Cancer* **6**, 369–381 (2006).
16. Yokomizo, T. & Dzierzak, E. Fine-tuning of hematopoietic stem cell homeostasis: novel role for ubiquitin ligase. *Genes Dev.* **22**, 960–963 (2008).
17. Stegmüller, J. & Bonni, A. Destroy to create: E3 ubiquitin ligases in neurogenesis. *F1000 Biol. Rep.* (2010). doi:10.3410/B2-38
18. Liu, Y.-C. Ubiquitin Ligases and the Immune Response. *Annu. Rev. Immunol.* **22**, 81–127 (2004).
19. Weake, V. M. & Workman, J. L. Histone Ubiquitination: Triggering Gene Activity. *Mol. Cell* **29**, 653–663 (2008).
20. Acconcia, F., Sigismund, S. & Polo, S. Ubiquitin in trafficking: The network at work. *Exp. Cell Res.* **315**, 1610–1618 (2009).

21. Hampton, R. Y. & Garza, R. M. Protein Quality Control as a Strategy for Cellular Regulation: Lessons from Ubiquitin-Mediated Regulation of the Sterol Pathway. *Chem. Rev.* **109**, 1561–1574 (2009).
22. Huang, C. Roles of E3 ubiquitin ligases in cell adhesion and migration. *Cell Adhes. Migr.* **4**, 10–18 (2010).
23. Polo, S. Signaling-mediated control of ubiquitin ligases in endocytosis. *BMC Biol.* **10**, (2012).
24. Schwartz, A. L. & Ciechanover, A. Targeting Proteins for Destruction by the Ubiquitin System: Implications for Human Pathobiology. *Annu. Rev. Pharmacol. Toxicol.* **49**, 73–96 (2009).
25. Kuang, E., Qi, J. & Ronai, Z. Emerging roles of E3 ubiquitin ligases in autophagy. *Trends Biochem. Sci.* **38**, 453–460 (2013).
26. Stegmüller, J. & Bonni, A. Moving past proliferation: new roles for Cdh1–APC in postmitotic neurons. *Trends Neurosci.* **28**, 596–601 (2005).
27. Yi, J. J. & Ehlers, M. D. Emerging Roles for Ubiquitin and Protein Degradation in Neuronal Function. *Pharmacol. Rev.* **59**, 14–39 (2007).
28. Yang, Y., Kim, A. H. & Bonni, A. The dynamic ubiquitin ligase duo: Cdh1-APC and Cdc20-APC regulate neuronal morphogenesis and connectivity. *Curr. Opin. Neurobiol.* **20**, 92–99 (2010).
29. Götz, M. & Huttner, W. B. The cell biology of neurogenesis. *Nat. Rev. Mol. Cell Biol.* **6**, 777–788 (2005).
30. Metzger, M. B., Hristova, V. A. & Weissman, A. M. HECT and RING finger families of E3 ubiquitin ligases at a glance. *J. Cell Sci.* **125**, 531–537 (2012).
31. Deshaies, R. J. & Joazeiro, C. A. P. RING Domain E3 Ubiquitin Ligases. *Annu. Rev. Biochem.* **78**, 399–434 (2009).
32. Li, W. *et al.* Genome-Wide and Functional Annotation of Human E3 Ubiquitin Ligases Identifies MULAN, a Mitochondrial E3 that Regulates the Organelle's Dynamics and Signaling. *PLoS ONE* **3**, e1487 (2008).
33. Petroski, M. D. & Deshaies, R. J. Function and regulation of cullin–RING ubiquitin ligases. *Nat. Rev. Mol. Cell Biol.* **6**, 9–20 (2005).
34. Mocciaro, A. & Rape, M. Emerging regulatory mechanisms in ubiquitin-dependent cell cycle control. *J. Cell Sci.* **125**, 255–263 (2012).
35. Wilkinson, K. *et al.* The neuron-specific protein PGP 9.5 is a ubiquitin carboxyl-terminal hydrolase. *Science* **246**, 670–673 (1989).
36. Kent, C. & Clarke, P. J. The immunolocalisation of the neuroendocrine specific protein PGP9.5 during neurogenesis in the rat. *Dev. Brain Res.* **58**, 147–150 (1991).
37. Hamilton, A. M. & Zito, K. Breaking It Down: The Ubiquitin Proteasome System in Neuronal Morphogenesis. *Neural Plast.* **2013**, 1–10 (2013).
38. Saritas-Yildirim, B. & Silva, E. M. The role of targeted protein degradation in early neural development: Protein Degradation and Neurogenesis. *genesis* **52**, 287–299 (2014).
39. Blum, M. & Ott, T. Xenopus: An Undervalued Model Organism to Study and Model Human Genetic Disease. *Cells Tissues Organs* 1–11 (2018). doi:10.1159/000490898
40. Bouwmeester, T., Kim, S.-H., Sasai, Y., Lu, B. & De Robertis, E. M. Cerebus is a head-inducing secreted factor expressed in the anterior endoderm of Spemann's organizer. *Nature* **382**, (1996).
41. Piccolo, S., Sasai, Y., Lu, B. & De Robertis, E. M. Dorsoventral Patterning in Xenopus: Inhibition of Ventral Signals by Direct Binding of Chordin to BMP-4. *Cell* **86**, 589–598 (1996).

42. Zimmerman, L. B., De Jesús-Escobar, J. M. & Harland, R. M. The Spemann Organizer Signal noggin Binds and Inactivates Bone Morphogenetic Protein 4. *Cell* **86**, 599–606 (1996).
43. Harland, R. & Gerhart, J. FORMATION AND FUNCTION OF SPEMANN'S ORGANIZER. *Annu. Rev. Cell Dev. Biol.* **13**, 611–667 (1997).
44. De Robertis, E. M. & Kuroda, H. DORSAL-VENTRAL PATTERNING AND NEURAL INDUCTION IN *XENOPUS* EMBRYOS. *Annu. Rev. Cell Dev. Biol.* **20**, 285–308 (2004).
45. Gaulden, J. & Reiter, J. F. Neur-ons and neur-offs: regulators of neural induction in vertebrate embryos and embryonic stem cells. *Hum. Mol. Genet.* **17**, R60–R66 (2008).
46. Altmann, C. R. & Brivanlou, A. H. Neural patterning in the vertebrate embryo. in *International Review of Cytology* **203**, 447–482 (Elsevier, 2001).
47. Niehrs, C. On growth and form: a Cartesian coordinate system of Wnt and BMP signaling specifies bilaterian body axes. *Development* **137**, 845–857 (2010).
48. Schmidt, R., Strähle, U. & Scholpp, S. Neurogenesis in zebrafish – from embryo to adult. *Neural Develop.* **8**, 3 (2013).
49. Schroeder E., T. Neurulation in Xenopus laevis. An analysis and model based upon light and electron microscopy. *J. Embryol. Exp. Morphol.* **23**, 36 (1970).
50. Noctor, S. C., Martínez-Cerdeño, V., Ivic, L. & Kriegstein, A. R. Cortical neurons arise in symmetric and asymmetric division zones and migrate through specific phases. *Nat. Neurosci.* **7**, 136–144 (2004).
51. Taverna, E., Götz, M. & Huttner, W. B. The Cell Biology of Neurogenesis: Toward an Understanding of the Development and Evolution of the Neocortex. *Annu. Rev. Cell Dev. Biol.* **30**, 465–502 (2014).
52. Tramontin, A. D. Postnatal Development of Radial Glia and the Ventricular Zone (VZ): a Continuum of the Neural Stem Cell Compartment. *Cereb. Cortex* **13**, 580–587 (2003).
53. Miyata, T. Asymmetric production of surface-dividing and non-surface-dividing cortical progenitor cells. *Development* **131**, 3133–3145 (2004).
54. Kowalczyk, T. *et al.* Intermediate Neuronal Progenitors (Basal Progenitors) Produce Pyramidal–Projection Neurons for All Layers of Cerebral Cortex. *Cereb. Cortex* **19**, 2439–2450 (2009).
55. Yun, S. J. *et al.* Transcriptional regulatory networks associated with self-renewal and differentiation of neural stem cells. *J. Cell. Physiol.* **225**, 337–347 (2010).
56. Paridaen, J. T. & Huttner, W. B. Neurogenesis during development of the vertebrate central nervous system. *EMBO Rep.* **15**, 351–364 (2014).
57. Cremisi, F., Philpott, A. & Ohnuma, S. Cell cycle and cell fate interactions in neural development. *Curr. Opin. Neurobiol.* **13**, 26–33 (2003).
58. Ohnuma, S. & Harris, W. A. Neurogenesis and Cell Cycle. *Neuron* **40**, 199–206 (2003).
59. Salomoni, P. & Calegari, F. Cell cycle control of mammalian neural stem cells: putting a speed limit on G1. *Trends Cell Biol.* **20**, 233–243 (2010).
60. Mizuseki, K., Kishi, M., Shiota, K., Nakanishi, S. & Sasai, Y. SoxD: an Essential Mediator of Induction of Anterior Neural Tissues in Xenopus Embryos. *Neuron* **21**, 9 (1998).
61. Pevny, L. & Placzek, M. SOX genes and neural progenitor identity. *Curr. Opin. Neurobiol.* **15**, 7–13 (2005).
62. Itoh, Y. *et al.* Scratch regulates neuronal migration onset via an epithelial-mesenchymal transition–like mechanism. *Nat. Neurosci.* **16**, 416–425 (2013).

63. Zander, M. A., Cancino, G. I., Gridley, T., Kaplan, D. R. & Miller, F. D. The Snail Transcription Factor Regulates the Numbers of Neural Precursor Cells and Newborn Neurons throughout Mammalian Life. *PLoS ONE* **9**, e104767 (2014).
64. Stigloher, C., Chapouton, P., Adolf, B. & Bally-Cuif, L. Identification of neural progenitor pools by E(Spl) factors in the embryonic and adult brain. *Brain Res. Bull.* **75**, 266–273 (2008).
65. Reymond, A. The tripartite motif family identifies cell compartments. *EMBO J.* **20**, 2140–2151 (2001).
66. Torok, M. & Etkin, L. D. Two B or not two B? Overview of the rapidly expanding B-box family of proteins. *Differentiation* **67**, 63–71 (2001).
67. Short, K. M. & Cox, T. C. Subclassification of the RBCC/TRIM Superfamily Reveals a Novel Motif Necessary for Microtubule Binding. *J. Biol. Chem.* **281**, 8970–8980 (2006).
68. Ozato, K., Shin, D.-M., Chang, T.-H. & Morse, H. C. TRIM family proteins and their emerging roles in innate immunity. *Nat. Rev. Immunol.* **8**, 849–860 (2008).
69. Meroni, G. & Diez-Roux, G. TRIM/RBCC, a novel class of 'single protein RING finger' E3 ubiquitin ligases. *BioEssays* **27**, 1147–1157 (2005).
70. Borden, K. L. RING domains: master builders of molecular scaffolds? *J. Mol. Biol.* **295**, 1103–1112 (2000).
71. Metzger, M. B., Pruneda, J. N., Klevit, R. E. & Weissman, A. M. RING-type E3 ligases: Master manipulators of E2 ubiquitin-conjugating enzymes and ubiquitination. *Biochim. Biophys. Acta BBA - Mol. Cell Res.* **1843**, 47–60 (2014).
72. Tuoc, T. C. & Stoykova, A. Roles of the ubiquitin-proteosome system in neurogenesis. *Cell Cycle* **9**, 3194–3200 (2010).
73. Schwamborn, J. C., Berezikov, E. & Knoblich, J. A. The TRIM-NHL Protein TRIM32 Activates MicroRNAs and Prevents Self-Renewal in Mouse Neural Progenitors. *Cell* **136**, 913–925 (2009).
74. Quaderi, N. A. *et al.* Opitz G/BBB syndrome, a defect of midline development, is due to mutations in a ner RING finger gene on Xp22. *Nat. Genet.* **17**, 7 (1997).
75. Liu, J., Prickett, T. D., Elliott, E., Meroni, G. & Brautigan, D. L. Phosphorylation and microtubule association of the Opitz syndrome protein mid-1 is regulated by protein phosphatase 2A via binding to the regulatory subunit 4. *Proc. Natl. Acad. Sci.* **98**, 6650–6655 (2001).
76. Trockenbacher, A. *et al.* MID1, mutated in Opitz syndrome, encodes an ubiquitin ligase that targets phosphatase 2A for degradation. *Nat. Genet.* **29**, 287–294 (2001).
77. Liu, E., Knutzen, C. A., Krauss, S., Schweiger, S. & Chiang, G. G. Control of mTORC1 signaling by the Opitz syndrome protein MID1. *Proc. Natl. Acad. Sci.* **108**, 8680–8685 (2011).
78. Du, H. *et al.* The MID1 E3 Ligase Catalyzes the Polyubiquitination of Alpha4 (α4), a Regulatory Subunit of Protein Phosphatase 2A (PP2A): NOVEL INSIGHTS INTO MID1-MEDIATED REGULATION of PP2A. *J. Biol. Chem.* **288**, 21341–21350 (2013).
79. Watkins, G. R. *et al.* Monoubiquitination Promotes Calpain Cleavage of the Protein Phosphatase 2A (PP2A) Regulatory Subunit α4, Altering PP2A Stability and Microtubule-associated Protein Phosphorylation. *J. Biol. Chem.* **287**, 24207–24215 (2012).
80. Schweiger, S. *et al.* The E3 Ubiquitin Ligase MID1 Catalyzes Ubiquitination and Cleavage of Fu. *J. Biol. Chem.* **289**, 31805–31817 (2014).
81. Hettich, M. M. *et al.* The Anti-Diabetic Drug Metformin Reduces BACE1 Protein Level by Interfering with the MID1 Complex. *PLoS ONE* **9**, e102420 (2014).

82. Kickstein, E. *et al.* Biguanide metformin acts on tau phosphorylation via mTOR/protein phosphatase 2A (PP2A) signaling. *Proc. Natl. Acad. Sci.* **107**, 21830–21835 (2010).
83. Krauß, S. *et al.* Translation of HTT mRNA with expanded CAG repeats is regulated by the MID1–PP2A protein complex. *Nat. Commun.* **4**, (2013).
84. Ohkawa, N. *et al.* Molecular cloning and characterization of neural activity-related RING finger protein (NARF): a new member of the RBCC family is a candidate for the partner of myosin V. *J. Neurochem.* **78**, 75–87 (2001).
85. Balastik, M. *et al.* Deficiency in ubiquitin ligase TRIM2 causes accumulation of neurofilament light chain and neurodegeneration. *Proc. Natl. Acad. Sci.* **105**, 12016–12021 (2008).
86. Khazaei, M. R. *et al.* The E3-ubiquitin ligase TRIM2 regulates neuronal polarization: Function of TRIM2 for axon outgrowth. *J. Neurochem.* **117**, 29–37 (2011).
87. Thompson, S. *et al.* Identification of a Novel Bcl-2-interacting Mediator of Cell Death (Bim) E3 Ligase, Tripartite Motif-containing Protein 2 (TRIM2), and Its Role in Rapid Ischemic Tolerance-induced Neuroprotection. *J. Biol. Chem.* **286**, 19331–19339 (2011).
88. Schonrock, N., Humphreys, D. T., Preiss, T. & Götz, J. Target Gene Repression Mediated by miRNAs miR-181c and miR-9 Both of Which Are Down-regulated by Amyloid-β. *J. Mol. Neurosci.* **46**, 324–335 (2012).
89. Ylikallio, E. *et al.* Deficiency of the E3 ubiquitin ligase TRIM2 in early-onset axonal neuropathy. *Hum. Mol. Genet.* **22**, 2975–2983 (2013).
90. Berti, C., Fontanella, B., Ferrentino, R. & Meroni, G. Mig12, a novel Opitz syndrome gene product partner, is expressed in the embryonic ventral midline and co-operates with Mid1 to bundle and stabilize microtubules. *BMC Cell Biol.* 12 (2004).
91. Aranda-Orgillés, B. *et al.* The Opitz syndrome gene product MID1 assembles a microtubule-associated ribonucleoprotein complex. *Hum. Genet.* **123**, 163–176 (2008).
92. Suzuki, M., Hara, Y., Takagi, C., Yamamoto, T. S. & Ueno, N. MID1 and MID2 are required for Xenopus neural tube closure through the regulation of microtubule organization. *Development* 12 (2011). doi:10.1242/dev.048769
93. Dal Zotto, L. The mouse Mid1 gene: implications for the pathogenesis of Opitz syndrome and the evolution of the mammalian pseudoautosomal region. *Hum. Mol. Genet.* **7**, 489–499 (1998).
94. Richman, J. M., Fu, K. K., Cox, L. L., Sibbons, J. P. & Cox, T. C. Isolation and characterisation of the chick orthologue of the Opitz syndrome gene, Mid1, supports a conserved role in vertebrate development. *Int. J. Dev. Biol.* **46**, 8 (2002).
95. Macdonald, R. *et al.* Midline signalling is required for Pax gene regulation and patterning of the eyes. *Development* **121**, 12 (1995).
96. Hallonet, M., Hollemann, T., Pieler, T. & Gruss, P. Vax1, a novel homeobox-containing gene, directs development of the basal forebrain and visual system. *Genes Dev.* **13**, 3106–3114 (1999).
97. Walther, C. *et al.* Pax: A murine multigene family of paired box-containing genes. *Genomics* **11**, 424–434 (1991).
98. Zuber, M. E. Specification of the vertebrate eye by a network of eye field transcription factors. *Development* **130**, 5155–5167 (2003).
99. Plaza, S., Dozier, C., Turque, N. & Saule, S. Quail Pax-6 (Pax-QNR) mRNAs are expressed from two promoters used differentially during retina development and neuronal differentiation. *Mol. Cell. Biol.* **15**, 3344–3353 (1995).

100. Ashery-Padan, R. Pax6 activity in the lens primordium is required for lens formation and for correct placement of a single retina in the eye. *Genes Dev.* **14**, 2701–2711 (2000).
101. Shaham, O., Menuchin, Y., Farhy, C. & Ashery-Padan, R. Pax6: A multi-level regulator of ocular development. *Prog. Retin. Eye Res.* **31**, 351–376 (2012).
102. Oron-Karni, V. *et al.* Dual requirement for Pax6 in retinal progenitor cells. *Development* **135**, 4037–4047 (2008).
103. Farhy, C. *et al.* Pax6 Is Required for Normal Cell-Cycle Exit and the Differentiation Kinetics of Retinal Progenitor Cells. *PLoS ONE* **8**, e76489 (2013).
104. Klimova, L. & Kozmik, Z. Stage-dependent requirement of neuroretinal Pax6 for lens and retina development. *Development* **141**, 1292–1302 (2014).
105. Glaser, T. *et al.* PAX6 gene dosage effect in a family with congenital cataracts, aniridia, anophthalmia and central nervous system defects. *Nat. Genet.* **7**, 463–471 (1994).
106. Schedl, A. *et al.* Influence of PAX6 Gene Dosage on Development: Overexpression Causes Severe Eye Abnormalities. *Cell* **86**, 71–82 (1996).
107. Manuel, M., Pratt, T., Liu, M., Jeffery, G. & Price, D. J. Overexpression of Pax6 results in microphthalmia, retinal dysplasia and defective retinal ganglion cell axon guidance. *BMC Dev. Biol.* **8**, (2008).
108. Halder, G., Callaerts, P. & Gehring, W. Induction of ectopic eyes by targeted expression of the eyeless gene in Drosophila. *Science* **267**, 1788–1792 (1995).
109. Chow, R. L., Altmann, C. R., Lang, R. A. & Hemmati-Brivanlou, A. Ectopic eyes in response to Pax6. *Development* **126**, 10 (1999).
110. Hirsch, N. & Harris, W. A. Xenopus Pax-6 and retinal development. *J. Neurobiol.* **32**, 45–61 (1997).
111. Perron, M., Kanekar, S., Vetter, M. L. & Harris, W. A. The Genetic Sequence of Retinal Development in the Ciliary Margin of theXenopusEye. *Dev. Biol.* **199**, 185–200 (1998).
112. Mikkola, I., Bruun, J.-A., Bjørkøy, G., Holm, T. & Johansen, T. Phosphorylation of the Transactivation Domain of Pax6 by Extracellular Signal-regulated Kinase and p38 Mitogen-activated Protein Kinase. *J. Biol. Chem.* **274**, 15115–15126 (1999).
113. Kim, E. A. *et al.* Phosphorylation and Transactivation of Pax6 by Homeodomain-interacting Protein Kinase 2. *J. Biol. Chem.* **281**, 7489–7497 (2006).
114. Yan, Q. *et al.* Sumoylation activates the transcriptional activity of Pax-6, an important transcription factor for eye and brain development. *Proc. Natl. Acad. Sci.* **107**, 21034–21039 (2010).
115. Macdonald, R. *et al.* Midline signalling is required for Pax gene regulation and patterning of the eyes. *Development* **121**, 12 (1995).
116. Schwarz, M. *et al.* Spatial specification of mammalian eye territories by reciprocal transcriptional repression of Pax2 and Pax6. *Development* **127**, 11 (2000).
117. Xu, Z.-P. & Saunders, G. F. Transcriptional Regulation of the Human *PAX6* Gene Promoter. *J. Biol. Chem.* **272**, 3430–3436 (1997).
118. Schweiger, S. *et al.* The Opitz syndrome gene product, MID1, associates with microtubules. *Proc. Natl. Acad. Sci.* **96**, 2794–2799 (1999).
119. Tuoc, T. C. & Stoykova, A. Trim11 modulates the function of neurogenic transcription factor Pax6 through ubiquitin-proteosome system. *Genes Dev.* **22**, 1972–1986 (2008).
120. Marquardt, T. *et al.* Pax6 is required for multipotent state of retinal progenitor cells. *Cell* **105**, 13 (2001).

121. Philips, G. T. *et al.* Precocious retinal neurons: Pax6 controls timing of differentiation and determination of cell type. *Dev. Biol.* **279**, 308–321 (2005).
122. Toy, J., Norton, J. S., Jibodh, S. R. & Adler, R. Effects of Homeobox Genes on the Differentiation of Photoreceptor and Nonphotoreceptor Neurons. **43**, 8 (2002).
123. Che, S. *et al.* Identification and Cloning of Xp95, a Putative Signal Transduction Protein in *Xenopus* Oocytes. *J. Biol. Chem.* **274**, 5522–5531 (1999).
124. Katoh, K. *et al.* The ALG-2-interacting Protein Alix Associates with CHMP4b, a Human Homologue of Yeast Snf7 That Is Involved in Multivesicular Body Sorting. *J. Biol. Chem.* **278**, 39104–39113 (2003).
125. Martin-Serrano, J., Yaravoy, A., Perez-Caballero, D. & Bieniasz, P. D. Divergent retroviral late-budding domains recruit vacuolar protein sorting factors by using alternative adaptor proteins. *Proc. Natl. Acad. Sci.* **100**, 12414–12419 (2003).
126. von Schwedler, U. K. *et al.* The Protein Network of HIV Budding. *Cell* **114**, 701–713 (2003).
127. Dikic, I. ALIX-ing phospholipids with endosome biogenesis. *BioEssays* **26**, 604–607 (2004).
128. Wu, Y., Pan, S., Luo, W., Lin, S.-H. & Kuang, J. Hp95 promotes anoikis and inhibits tumorigenicity of HeLa cells. *Oncogene* **21**, 6801–6808 (2002).
129. Schmidt, M. H. H. SETA/CIN85/Ruk and its binding partner AIP1 associate with diverse cytoskeletal elements, including FAKs, and modulate cell adhesion. *J. Cell Sci.* **116**, 2845–2855 (2003).
130. Trioulier, Y. *et al.* Alix, a Protein Regulating Endosomal Trafficking, Is Involved in Neuronal Death. *J. Biol. Chem.* **279**, 2046–2052 (2004).
131. Mahul-Mellier, A.-L. Alix, Making a Link between Apoptosis-Linked Gene-2, the Endosomal Sorting Complexes Required for Transport, and Neuronal Death In Vivo. *J. Neurosci.* **26**, 542–549 (2006).
132. Zhao, C. *et al.* The role of Alix in the proliferation of human glioma cells. *Hum. Pathol.* **52**, 110–118 (2016).
133. Laporte, M. H. *et al.* Alix is required during development for normal growth of the mouse brain. *Sci. Rep.* **7**, 44767 (2017).
134. Chen, B., Borinstein, S. C., Gillis, J., Sykes, V. W. & Bogler, O. The Glioma-associated Protein SETA Interacts with AIP1/Alix and ALG-2 and Modulates Apoptosis in Astrocytes. *J. Biol. Chem.* **275**, 19275–19281 (2000).
135. Missotten, M., Nichols, A., Rieger, K. & Sadoul, R. Alix, a novel mouse protein undergoing calcium-dependent interaction with the apoptosis-linked-gene 2 (ALG-2) protein. *Cell Death Differ.* **6**, 124–129 (1999).
136. Vito, P., Pellegrini, L., Guiet, C. & D'Adamio, L. Cloning of AIP1, a Novel Protein That Associates with the Apoptosis-linked Gene ALG-2 in a Ca^{2+} -dependent Reaction. *J. Biol. Chem.* **274**, 1533–1540 (1999).
137. Strack, B., Calistri, A., Craig, S., Popova, E. & Göttlinger, H. G. AIP1/ALIX Is a Binding Partner for HIV-1 p6 and EIAV p9 Functioning in Virus Budding. *Cell* **114**, 689–699 (2003).
138. Hemming, F. ., Fraboulet, S., Blot, B. & Sadoul, R. Early increase of apoptosis-linked gene-2 interacting protein X in areas of kainate-induced neurodegeneration. *Neuroscience* **123**, 887–895 (2004).
139. Martinez, A. *et al.* Quantitative proteomic analysis of Parkin substrates in Drosophila neurons. *Mol. Neurodegener.* **12**, (2017).
140. Yan, Q. *et al.* CART: An Hrs/Actinin-4/BERP/Myosin V Protein Complex Required for Efficient Receptor Recycling. *Mol. Biol. Cell* **16**, 2470–2482 (2005).

141. Krauss, S. The MID1 protein is a central player during development and in disease. *Front. Biosci.* **21**, 664–682 (2016).
142. Pinson, L. Embryonic expression of the human MID1 gene and its mutations in Opitz syndrome. *J. Med. Genet.* **41**, 381–386 (2004).
143. Popov, I. K. *et al*. Identification of new regulators of embryonic patterning and morphogenesis in Xenopus gastrulae by RNA sequencing. *Dev. Biol.* **426**, 429–441 (2017).

Oath of Declaration

I, hereby declare under the oath and §5 of the Promotionsordnung, that this thesis is entirely my own work and has been written without the external help from other person/persons. I used only the sources mentioned and included all the citations correctly both in word and content. The thesis has not been used previously at this or any other university in order to achieve an academic degree.

Halle(Saale), January 2019 Ashwin Lokapally

List of Publications

Publications

Ashwin Lokapally, Herbert Neuhaus, Juliane Herfurth and Thomas Hollemann, Interplay of Trim2 E3 ubiquitin ligase and Alix/ESCRT complex: Control of developmental plasticity during early neurogenesis **(2019)**: Manuscript under 2nd review process

Ashwin Lokapally, Sanjeeva Metikala, Thomas Hollemann, *Xenopus laevis* neuronal cell adhesion molecule (*nrcam*): plasticity of a CAM in the developing nervous system. Development Genes and Evolution **(2017)**, 227: 61-67. https://doi.org/10.1007/s00427-016-0569-9

Thorsten Pfirrmann, Enrico Jandt, Swantje Ranft, ***Ashwin Lokapally***, Herbert Neuhaus, Muriel Perron and Thomas Hollemann, Hedgehog-dependent E3-ligase Midline1 regulates ubiquitin mediated proteasomal degradation of Pax6 during visual system development. PNAS **(2016)**, 113 (36) 10103-10108. https://doi.org/10.1073/pnas.1600770113

Ashwin Lokapally, Sanjeeva Metikala, Thomas Hollemann, Expressional characterization of mRNA (guanine-7) methyltransferase (*rnmt*) during early development of *Xenopus laevis.* International Journal of Developmental Biology **(2016)**, 60: 65-69. https://doi.org/10.1387/ijdb.150409th

Thorsten Pfirrmann, ***Ashwin Lokapally***, Claes Andréasson, Per Ljungdahl, Thomas Holleman, SOMA: A Single Oligonucleotide Mutagenesis and Cloning Approach. PLoS ONE (2013), 8(6): e64870. https://doi.org/10.1371/journal.pone.0064870